Wireless Channel Model and LDM-Based Transmission with Unequal Error Protection for Inside Train Communications

Egoitz Arruti Monasterio

Supervisor:

Mikel Mendicute Errasti

MONDRAGON
UNIBERTSITATEA

A thesis submitted for the degree of

Doctor por Mondragon Unibertsitatea

Department of Electronics and Computer Science

Mondragon Goi Eskola Politeknikoa

Mondragon Unibertsitatea

May 2017

Declaration of Originality

I hereby declare that the research recorded in this thesis and the thesis itself were developed entirely by myself at the Signal Theory and Communications Area, Department of Electronics and Computer Science, at Mondragon Unibertsitatea.

The software used to perform the simulations was developed by myself based in a previous simulator implemented by Mikel Mendicute Errasti during his PhD. I would like to thank Mikel for his support.

Egoitz Arruti Monasterio
Department of Electronics and Computer Science
Mondragon Goi Eskola Politeknikoa
Mondragon Unibertsitatea
May, 2017

Eskerrak

Orain dela urte ugari hasi nuen ibilbide honetan gente ugari ezagutu dut. Denek beraien erara eta modura erabaki bat edo beste hartzera lagundu naute. Askok, bide honetan zein bidegurutze hartu behar dudan argitu didate, eta beste batzuek aldiz, zalantza gehiago sortarazi didate galdera gehiago sortuz erantzuna aurkitzeko helburuarekin. Den denak ezin ditut hemen aipatu baina hauek dira nire memoria kaxkarrak gogoratzen dituenak bereziki:

- Denbora guzti honetan nirekin egon den eta nire atzerriko estantziak aguantatu dituen nire emazte **Izaskun Sarasola**-ri eta tesi hau aurrera joan den heinean gure bizitzan agertu diren gure seme alabei **Enetz**, **Unax** eta **June**-ri.
- Nire **aita**, **ama** eta **anai-arrebei** zer egiten nabilen ulertzen ez zuten arren.
- Tesia hasi zenetik nirekin egon diren lankide **Unai Garro**, **Eñaut Muxika**, **Ane Antia**, **Javier Oyarzun**, **Nestor Arana**, **Maitane Barretxea** eta **Aitzol Iturrospe**-ri, eta gure lankide izandakoei: **Idoia Jimenez** eta **Iker Sobron**.
- Hainbeste pintxo pote edo afari egindako unibertsitateko lagunei eta bereziki **Maria Ruiz** eta **Daniel Reguera**-ri beraien tesiko eboluzioak konpartitzeagatik.
- Edinburgon egon nintzeneko bertan egindako lagunak, paper eta garagardoak erabiliz tesia bideratzen lagundu zidatenak: **Enrique Poves**, **Harald Burchardt**, **Nikola Serafimovski**, **John Fakidis** eta **Stefan Videv**. Bereziki **John Thompson**-i emandako ahoulkuengatik.
- Oso esker berezia tesiko zuzendari izan den **Mikel Mendikute**-ri, bere laguntza gabe ez bainuen lortuko bukatzea eta denbora tarte txiki batean nire zuzendari izan zen **José María Zabalegui**-ri.

ESKERRIK ASKO BIHOTZEZ!

Acknowledgments

Many years ago I started this long journey and I met a lot of people during my travel. Every one had something to teach me, depending of his expertise and the situation. I remember with special affection as long as my bad memory can reach:

- My wife **Izaskun Sarasola** that suffered my long stay in Edimburgh and the children that appeared in our lives during this thesis **Enetz**, **Unax** and **June**.
- My **father**, **mother**, **sister** and **brother** who did not understand what I was doing.
- My colleagues who have been there from the beginning of this thesis **Unai Garro**, **Eñaut Muxika**, **Ane Antia**, **Javier Oyarzun**, **Nestor Arana**, **Maitane Barretxea** and **Aitzol Iturrospe** and the ones that now they have another challenges: **Idoia Jimenez** and **Iker Sobron**.
- All my pintxo-pote friends in the university specially to **Maria Ruiz** and **Daniel Reguera** who shared their worries about their thesis.
- My friends of Edimburgh, who oriented my thesis with papers and beers: **Enrique Poves**, **Harald Burchardt**, **Nikola Serafimovski**, **John Fakidis** and **Stefan Videv**. Special mention to **John Thompson** for his advices and support.
- A very special thank to my supervisor **Mikel Mendikute**. This thesis would not possible without his support and **José María Zabalegui** who was my supervisor during a short period of time.

MANY MANY THANKS!

Izaskun, Enetz, Unax eta Junerentzat...

Abstract

Although the deployment of wireless systems is widespread, there are still sectors where they are not used due to their lack of reliability in comparison to wired systems. Sectors like industry or vehicle communications consider their environment hostile because the wireless signals suffer a lot of interferences. One of such environments is the railway sector, where wiring removal will allow more flexibility for both control and monitoring systems.

This thesis analyzes wireless communications inside train cars, aiming at modelling their behavior and at proposing techniques to increase the reliability of the critical signals among train systems, wich can coexist with other lower priority systems. After proposing a novel model of an inside train wireless channel, a transmission system based on Layered Division Multiplexing (LDM) has been proposed which theoretically promises higher capacities than traditional TDM or FDM. This capacity gain is used to provide higher reliability to critical data using Unequal Error Protection (UEP) while maintaining the same bit rate as equivalent TDM or FDM based systems.

In the final part of the thesis, simulation results of the proposed LDM system are provided, combined with Alamouti space time coding and different coding rates. Multiantenna extensions of the proposed LDM schemes are also simulated, providing BER and throughput results. These results will be used to shed light about how to reduce BER of an inside train wireless communication system.

Resumen

Aunque el despliegue de los sistemas inalámbricos está muy extendido, aun hay sectores donde no se utiliza por la poca fiabilidad que proporcionan comparado con los sistemas cableados. Sectores como la industria o las comunicaciones vehiculares consideran el entorno donde trabajan como entorno hostil, debido a que las señales inalámbricas sufren muchas interferencias. Uno de estos entornos es el de las comunicaciones en ferrocarril donde la eliminación de cables permitiría mayor flexibilidad entre los sistemas de control y monitorización.

En esta tesis se analiza el canal de comunicación inalámbrico dentro de los trenes, con el objetivo de modelar su comportamiento y proponer técnicas que permitan aumentar la fiabilidad de la información de tipo crítico transmitida entre los sistemas del tren, repercutiendo lo menos posible en otros sistemas de menor prioridad. Tras proponer el modelo de canal inalámbrico dentro del tren, se ha propuesto un sistema de transmisión basado en Layered Division Multiplexing (LDM) que analizándolo teóricamente promete mayores capacidades que los tradicionales TDM o FDM. Esta capacidad se utilizará para obtener mayor redundancia de los datos críticos usando Unequal Error Protection (UEP) manteniendo la misma tasa de transferencia bits que los sistemas basados en TDM/FDM.

En la parte final de la tesis, se obtienen resultados de las simulaciones realizadas con el sistema LDM propuesto, combinada con codificación espacio temporal como Alamouti y diferentes ratios de codificación. También se han simulado configuraciones multiantena obteniendo resultados de BER y throughput. Estos resultados servirán para arrojar luz sobre cómo reducir el BER en las comunicaciones inalámbricas dentro de los trenes.

Laburpena

Haririk gabeko sistemak oso hedatuak dauden arren oraindik erabiltzen ez dituen sektoreak badaude ematen duten fidagarritasuna txikia delako kableatutako sistemekin alderatuz. Industria bezalako sektoreek edo ibilgailuetako komunikazioek lan egiten duten ingurua oso zaratatsua izaten da eta seinaleek interferentzia asko jasaten dituzte.

Tesi honetan tren barruko haririk gabeko komunikazio kanala aztertzen da, bere portaera aztertu eta modelatzeko asmotan. Jakintza honekin zein teknika izan daitekeen erabilgarriak aztertuko da datuen fidagarritasuna handitzeko helburuarekin, lehentasun gutxiago duten sistemetan eragin txikiena izanik. Modeloa atera ondoren proposatu den transmisio sistema Layered Division Multiplexing (LDM) izan da, non azterketa teorikoek TDM edo FDM sistemek baino kapazitate gehiago dutela frogatzen dute. Kapazitate hau sistemaren datu kritikoei erredundantzia gehiago emateko erabiliko da Unequal Error Protection (UEP) erabiliz, TDM/FDM sistemetan bidaltzen den bit tasa kopurua mantenduz.

Tesiaren azken partean, proposatutako LDM sistemaren simulazio emaitzak ematen dira, Alamouti espazio denbora kodifikazioarekin konbinatuak eta kodigo ratio desberdinekin. Antena anitzezko konfigurazioak ere simulatu dira BER eta throughput emaitzak lortuz. Emaitza hauek haririk gabeko tren barruko komunikazioetan BER-a nola gutxitu daitekeen jakiten lagunduko digute.

Contents

List of Figures

List of Tables

Acronyms

3GPP: 3rd Generation Partnership Project
AP: Access Point
ATSC 3.0: Advanced Television Systems Committee 3.0
AWGN: Additive White Gaussian Noise
BER: Bit Error Rate
BPSK: Binary Phase Shift Keying
BS: Base Station
BW: Bandwidth
CDF: Cumulative Distribution Function
COST: European Cooperation in the Field of Scientific and Technical Research
CSI: Channel State Information
DoA: Direction of Arrival
DoD: Direction of Departure
DS: Delay Spread
DSRC: Dedicated Short Range Communication
DTT: Digital Terrestrial Television
EMS: European Modeling Symposium
ETSI: European Telecommunications Standard Institute
FDM: Frequency Division Multiplexing
FSL: Free Space Losses
GBDM: Geometric Based Deterministic Model
GBSM: Geometric Based Stochastic Model
GEV: Generalized Extreme Value
HST: High Speed Train
i.i.d.: Identically Independently Distributed
IS-GBSM: Irregular Shape Geometric Based Stochastic Model
LDM: Layer Divison Multiplexing
LDPC: Low Density Parity Check

LL: Lower Layer
LN: Log Normal
LOS: Line Of Sight
LS: Least Squares
Mbps: Megabits per second
MIMO: Multiple Input Multiple Output
MISO: Multiple Input Single Output
MPC: Multipath Component
MS: Mobile Station
NGSM: Non Geometrical Stochastic Model
NLOS: No Line Of Sight
OFDM: Orthogonal Frequency Division Multiplexing
OSTBC: Orthogonal Space Time Block Coding
PL: Path loss
QoS: Quality of Service
QPSK: Quadrature Phase-Shift Keying
RS-GBSM: Regular Shape Geometric Based Stochastic Model
RT: Ray Tracing
Rx: Receiver
SCM: Spatial Channel Model
SDR: Software Defined Radio
SISO: Single Input Single Output
SNR: Signal to Noise Ratio
STBC: Space Time Block Coding
SVD: Singular Value Decomposition
TCMS: Train Control and Monitoring System
TDD: Time Division Duplex
TDM: Time Division Multiplexing
TDMA: Time Division Multiple Access
Tx: Transmitter
UEP: Unequal Error Protection
UL: Upper Layer
V2V: Vehicular to Vehicular
WINNER: Wireless World Initiative New Radio

List of Symbols

$\bar{X}_{UL}(k)$	Estimated UL symbol at k-th subcarrier
$\bar{X}_{UL}(k)$	UL symbol estimation at k-th subcarrier
ΔTh_{nc}	Non-critical data throughput difference
$\hat{H}(k)$	Channel response estimation of k-th subcarrier
$\mathbf{H}$	Channel representative $N \times M$ dimension matrix
$\mathbf{H}^H$	Conjugate transpose of matrix $\mathbf{H}$
$\mathbf{R_{SS}}$	Covariance matrix of vector $\mathbf{s}$
$\mathbf{s}$	Transmitting symbols vector
$\tilde{X}_{LL}(k)$	Regenerated LL symbol from estimated bits at k-th subcarrier
$\tilde{X}_{UL}(k)$	Regenerated UL symbol from estimated bits at k-th subcarrier
Av_{BER}	Average BER of the system
Av_{BER}^{LDM}	Average BER of the LDM system
Av_{BER}^{TDM}	Average BER of the TDM system
BER_c	BER of the critical data
BER_{nc}	BER of the non-critical data
BW	Band Width
C	Channel total capacity
C_{LL}^{LDM}	LDM capacity of the lower layer

C_{UL}^{LDM}	LDM capacity of the upper layer
C_{c}^{TDM}	TDM capacity of critical data
C_{nc}^{TDM}	TDM capacity of non-critical data
E	BER of the system
g	LDM power injection level
h_{ij}	Communication channel between i and j antenna
K_{LL}^{LDM}	Coding ratio of the LL in LDM
K_{UL}^{LDM}	Coding ratio of the UL in LDM
K_{c}^{TDM}	Coding ratio of the critical data in TDM
K_{nc}^{TDM}	Coding ratio of the non-critical data in TDM
LL	Lower layer
M	Number of transmitter antennas
N	Number of receiver antennas
$N(k)$	Noise of the subcarrier k
N_{LL}^{LDM}	Modulation order of LL in LDM
N_{UL}^{LDM}	Modulation order of UL in LDM
N_{c}^{TDM}	Modulation order of the critical data in TDM
N_{nc}^{TDM}	Modulation order of the non-critical data in TDM
$N_{UL}(k)$	Noise of the UL at subcarrier k
P_{LL}	Power of the lower layer
P_{n}	Noise power
P_{s}	Signal power
P_{UL}	Power of the upper layer
R	Total bitrate of the system
R_{LL}^{LDM}	Bit rate of LL in LDM

R_{UL}^{LDM}	Bit rate of UL in LDM
R_{c}^{TDM}	Critical data rate in TDM
R_{nc}^{TDM}	Non-critical data rate in TDM
SNR	Signal to noise ratio
T_a	Available time to transmit in a TDM system
T_c	Available time to transmit critical information
T_{nc}	Available time to transmit non-critical information
Th	Throughput
Th_{LL}^{LDM}	Throughput of the LL of LDM
Th_{nc}^{TDM}	Throughput of the non-critical data of TDM
UL	Upper layer
$unvec(\cdot)$	Inverse operation of vectorization
$vec(\cdot)$	Vectorization
$X_{LDM}(k)$	LDM symbol of k-th subcarrier
$X_{LL}(k)$	Transmitted LL symbol at k-th subcarrier
$X_{TDM}(k)$	TDM symbol of k-th subcarrier
$X_{UL}(k)$	Transmitted UL symbol at k-th subcarrier
$X_{UL}(k)$	Upper layer symbol of k-th subcarrier k
$Y(k)$	Received symbol at k-th subcarrier

Chapter 1
Introduction

1.1 Introduction and state of art

The use of wireless communications has grown in recent years. The incorporation of wireless systems at homes, offices and in public places has been made gradually and nowadays we are surrounded of wireless transmission and reception systems. The adoption of wireless systems in leisure and entertainment has evolved from the IEEE 802.11b based transmission systems that reached 11 megabits per second (Mbps) to the IEEE 802.11ac [IEEE13] standard that can reach up to 1.3 Gbps. The evolution of wireless systems in consumer markets has been lead by the demand of the end users, who want more throughput and for whom reliability of the data is not so important.

Although wireless systems implementation in our everyday life is widespread, the implementation and use of wireless systems in environments considered hostile is very limited. Traditionally, the communications deployment in a hostile environment has been done in a wired way using shielded cables, since the robustness and reliability of wireless systems in hostile environments is not guaranteed due to noise and interference [Pellegrini06].

Environments considered hostile, such as industrial or vehicle communications, have characteristics and peculiarities that home or office environment do not have, such as the presence of metallic elements or the appearance of spurious or unwanted elements in the signal due to short-term interferences. The advantages of using wireless systems in such hostile environments are the following:

- Reduction of system weight by removing interconnection wiring between different elements.
- Ease of adaptation to different locations of measurement and control systems.
- Avoidance of mechanical problems due to cables, such as the twisting of cables when moving parts are intercommunicated.

Although the advantages of wireless systems in such environments are promising, there are a number of issues that need to be addressed. The wired system is more immune to

electromagnetic interference than the wireless system thanks to its external shielding and the signal does not suffer the characteristic fading of the wireless channel.

To design robust wireless systems to be used in hostile environments, it is important to characterize the propagation medium. There are many different hostile environments that can be characterized, but two of them have special interest in the scientific community:

- Industrial environments.
- Vehicular environment.

This thesis focuses on vehicular environment, specifically on railway systems and the use of wireless schemes. The main issues that have been addressed are the proposal of a suitable wireless channel model and the design of an effective transmission scheme to reduce data error rate increasing reliability.

1.1.1 Channel models

In order to analyze the reliability of the most appropriate wireless systems, it is important to know the model of the channel over which the information will be propagated [Molisch05] [Liu12] [Unterhuber16]. An accurate channel model will allow us to know the behavior of the system and design the most appropriate transmission scheme to meet the requirements of reliability, delay or throughput. Although there are different methods of modelling the communications channel, they are commonly classified as *physical models* or *analytical models* [Ozcelik04].

The proper modeling of the channel helps us to know the propagation mode of the waves and the adverse effects that the signal will suffer. It allows us to foresee how the propagation medium will affect wireless communications and analyze the actions that need to be taken to avoid such adverse effects.

There are different ways to obtain a channel model. One of them is to perform extensive measurements to extract significant parameters of the channel, called *Channel Sounding*. Another way is to know its physical parameters of propagation and, thanks to *Ray Tracing* techniques, obtain the model. This latter technique will be used in this thesis to propose an inside train wireless channel model.

1.1.2 Wireless transmission systems

There are multiple ways to transmit different types of signals using wireless systems. In order to transmit information, the systems can use typical multiplexing schemes like Time Division Multiplexing (TDM) or Frequency Division Multiplexing (FDM). TDM divides the available time in slots in order to insert different services or users in each of them. TDM

transmission usually uses a single transmission frequency allowing other systems to use other available frequencies.FDM divides the available bandwidth for transmission into subbands or frequency slots for each user or service. Unlike TDM, they can transmit all the time necessary in the allocated bandwidth for each service.

A lot of services use a mix between TDM and FDM to transmit the information exploiting the capacity of the channel. In the railway system analyzed in this dissertation, the transmitted data can be classified as critical and non-critical data. Critical data bear essential information for the correct operation of the train while non-critical data is less sensible to information loss. In this thesis we want to analyze the performance of the TDM/FDM transmission schemes and analyze alternative schemes that help to improve the reliability of the critical data sent in a wireless intravehicular system.

Alternative schemes as Layered Division Multiplexing (LDM) [Zhang16] have recently been proposed to be used in other scenarios, such as Digital Terrestrial Television (DTT). In DTT, LDM is proposed to send fixed television services along with mobile services. In the railway scenario considered in this thesis, LDM will be used with Unequal Error Protection (UEP) which implies that resources available to protect data are not equally distributed among each bit stream. Critical data will use the available resources obtained with LDM to ensure reliability, while the maximum data throughput will be maintained as in TDM or FDM. As it will be proven in this thesis, using this scheme allows lower bit error rates (BER) than those obtained with TDM and FDM using the same bit rate of transmission.

1.2 Motivation and hypothesis

As discussed earlier, the use of wireless systems in industrial and vehicular environments has become particularly important in recent years. The advantages that wireless systems provide are weight reduction, flexibility and ubiquity but they incur in disadvantages like the high bit error rates of wireless systems compared to existing wired systems. This reduces the reliability and the use of wireless systems in these environments has limited use.

Vehicular communications, specifically intravehicular communications, are a special case to study. The use of wireless systems in trains would reduce the weight of the wiring in trains and give mobility to the systems. There are a lot of different channel models in the literature, but inside train carriage channel models have not been analyzed extensively because with the use of wired systems, it was not necessary. But with the proposal of replacing wired systems by wireless ones, a good inside train wireless channel model is required.

Two types of data will share the wireless system as mentioned before, having the critical data need priority than the non-critical one. In this thesis we want to improve the performance of the critical data without penalizing the non-critical data. As seen in literature, LDM is only used in DTT systems and not in railway systems, so it could be a candidate

to be used in railway systems. The hypothesis of this thesis is the following: LDM together with other techniques could be used to obtain reliability of critical data coexisting with non-critical data.

1.3 Objectives

The main objective of this thesis is to propose an alternative technique to improve the reliability of the critical data of an inside train wireless system, while it coexists with other non-critical systems, as well as to prove its performance in a realistic channel model. To achieve the objective, secondary objectives have been defined:

- To obtain a realistic inside train wireless channel model.
- To analyze different techniques to handle different types of data in a wireless system.
- To design a realistic simulator to prove the proposed model and techniques.

1.4 Methodology

The methodology to achieve the proposed objectives has been the following:

- To obtain the channel model, literature has been analyzed to find a suitable model or methodology. The obtained channel model has been introduced in a simulator to obtain results. The results have been compared with measurements done in real train measurements campaigns to validate it.
- The proposed alternative technique has been selected after literature review. To prove its viability, a mathematical analysis has been done. Using a simple simulator based in gaussian channel model, the proposed technique has been validated.
- To validate and to prove the proposed transmission technique with the inside train channel model, a complete simulator has been developed.

1.5 Structure of the thesis

This thesis proposes a novel inside train wireless channel model and a transmission scheme to be used in intravehicular systems. The proposed scheme allows very high reliability of critical control data even in environments where the signal to noise ratio (SNR) is around 0 dB and also allows the simultaneous transmission of non-critical information of multimedia.

The work done during the thesis has been divided in the following parts or chapters:

- **Chapter 2**. A state of the art of wireless channel models has be done, focusing on the intra-vehicular wireless channel of a train. Several channel models have been compared and evaluated as candidate models for the considered intravehicular scenario.

- **Chapter 3**. A novel channel model, based on ray-tracing is proposed based in Chapter 2, with the special characteristics of the considered intra-vehicular scenario: the control systems are in low SNR environments (metal boxes near power systems, systems placed near metal...) that makes wireless transmission more difficult while monitoring and multimedia systems are in high SNR places. A mathematical model has been proposed to be used in a future simulator. This simulator will allow to validate the schemes analyzed in the next chapter.

- **Chapter 4**. Analyzing the characteristics of the transmission systems and the channel model proposed, a new transmission scheme based in LDM has been proposed. This transmission scheme provides higher reliability of control data than traditional TDM or FDM systems. The capacity increase of this scheme is theoretically analyzed, as well as its capacity in order to increase reliability of critical data using UEP techniques.

- **Chapter 5**. A simulator has been implemented using the model proposed in Chapter 3. In addition to LDM, the possibility of transmitting using TDM/FDM has been implemented. In this chapter, only SISO systems have been simulated to obtain BER and throughput results using different UEP rates.

- **Chapter 6**. After simulating SISO systems in Chapter 5, multiantenna configurations have been simulated in this last chapter. As the previous chapter, BER and throughput simulation results are obtained to evaluate the reliability level introduced by multiantenna systems.

1.6 Contributions of the thesis

The main contributions of this thesis are the following:

- **Chapter 3:** After the analysis of different models of the literature, an inside train wireless channel, based on the Winner methodology and fed with data from a ray-tracing simulation, has been proposed. The proposed novel model has been published in [Arruti13].

- **Chapter 4:** An LDM-based system has been proposed to transmit critical and non-critical data in the considered scenario. Although LDM has been proposed for DTT scenarios in [Zhang14], it has been adapted to intra-vehicular wireless communications in this thesis. Furthermore, simulation results proving the benefits of the proposed

LDM scheme have been provided. The results of the simulations and the conclusions obtained have been accepted for publication in [Arruti17a].

- **Chapter 5:** The performance of the proposed LDM scheme has been evaluated and compared with TDM and FDM, using a more realistic simulator than in Chapter 4. Different channel models including the model proposed in this thesis have been simulated using SISO systems. The results and conclusions of this chapter have been accepted in [Arruti17b].

- **Chapter 6:** The proposed LDM system has been extended to a multiantenna scenario. Simulation results of multiantenna configurations and general overview of the thesis have been submitted to "Vehicular Communications" journal of Elsevier editorial.

Chapter 2

Wireless channel models and systems in vehicular environments

2.1 Introduction

The understanding of the transmission channel is of great importance to properly simulate the communication system. The results of the simulation at system or link level depend directly on the used channel model. Hence, the design of realistic channel models is a prerequisite to create efficient wireless system architectures [El-Sallabi06]. Nowadays there are channel models used to simulate at system or link level, that will be analyzed in this chapter. Using these models it can be analyzed how to exploit the channel capacity to achieve higher throughput, to obtain extra redundancy to ensure the reliability of the transmitted data or to assess the bit error rate (BER) of the system. The analyzed environments are hostile environments, particularly in the industrial and vehicular sectors. The review of channel models to characterize different environments, specifically in hostile environments is analyzed in this chapter.

2.2 Wireless channel models

2.2.1 Communication scenarios of interest

The analyzed scenarios in this review are two:

1. Industrial environment.
2. Vehicular environment.

A wired shielded communication system is usually used in these kind of environments to avoid interference and electromagnetic noise sources. The use of a wireless communication system will allow a more flexible deployment of communications. The wireless communication system needs to ensure the same reliability level as the wired one required by these kind of applications.

Figure 2.1: Example of a industrial environment [Karedal07].

2.2.1.1 Industrial environment

The industrial environment is characterized by the existence of electromagnetic impulses generated by the elements of the plant, and that can interfere in the wireless system. This environment is usually composed by metallic structures that can lead to very dispersive multipath channels with large temporal dispersion [Ouyang08].

It is well known that in the industrial environment there is a lot of multipath [Karedal07] that systems like Multiple Input Multiple Output (MIMO) systems could exploit to obtain larger capacities. It is also proved that in a multipath environment the channel behaves like a Rayleigh channel, even having direct line of sight (LOS) [Ouyang08], [Karedal07]. This is due the large number of energy received thanks to the scattered rays in the metallic structures, that make that the direct ray is less significative compared with the sum of scattered rays.

2.2.1.2 Vehicular environment

There is a lot of work published in the field of vehicular wireless communications. The intervehicular wireless communication systems are designed to provide security applications and they are based in the IEEE 802.11p standard [IEEE10]. The radio technology of IEEE 802.11p is directly derived from 802.11a standard, with some modifications to adapt it to the vehicular environment. It has 75 MHz bandwidth from 5.85 Ghz to 5.925 Ghz. This band is part of the intelligent transport system band dedicated to short range communication (DSRC) in USA. Some non critical security applications like V2V (Vehicular to Vehicular) notification of dangerous areas could be done using IEEE 802.11 a/b/g standard or other wireless technologies.

Inside the vehicular environment there is an specific railway system area. The growth of railway transport systems and specially of the high speed trains has increased the interest of using wireless communication systems [Unterhuber16]. There are several studies that classify

the different group of channels in a railway system. In [Ai12] the different environments where a high speed train (HST) can travel are classified, describing the effects that can be observed in each one. The considered scenarios are:

Viaducts: The viaduct is one of the most typical cases of a HST environment. Viaduct is long structure similar to a bridge that allows a HST to avoid valley or irregular areas. This kind of structures are necessary to maintain the flatness of the area required by HST.

Field cuts: In some sections it is necessary to cut the field. This way, HST will travel inside a V shape cut and it is commonly used to travel through valleys.

Tunnels: A tunnel is an artificial underground passage that allows the train to go through mountains.

Station: A station is a place where HST stop to pick up or leave passengers. Commonly it is a platform near the railway with facilities associated to passengers.

Combined scenarios: These scenarios are combination of the previous scenarios. Due the complexity of the system, there are places where a new scenario is obtained combining two or more of the previous scenarios.

Inside train compartment: This scenario is the scenario to provide personal communications to the passengers with high Quality of Service (QoS). This last scenario is the more interesting one to us and where this thesis will be focused.

Table 2.1 shows typical characteristics of these scenarios.

Scenario	Definition	LOS/NLOS	Speed(km/h)	Channel behaviour
S1	Viaduct	LOS	0-350	Rice
S2	Cuts	LOS	0-350	Rice
S3	Tunnel	LOS	0-250	Rice
S4	Station	LOS/NLOS	0-80	Rice/Rayleigh
S5	Combined	LOS	0-250	Rice
S6	Compartment	LOS/NLOS	0-5	Rice/Rayleigh

Table 2.1: Scenario classification in HST.

The main prerequisite to design broadband wireless transmitter and receivers, is the knowledge of the propagation characteristics of the radio channel [Liu12]. A realistic and reliable channel model is the starting point to design a reliable communication system. There is a lot of broadband urban measure campaigns to know and to model an urban scenario. Nevertheless, train radio channels specially in the band of 2 GHz have not been studied widely [Liu12]. In the Table 2.2 there is a mention to the most interesting publications.

	Measure campaign	Description
Power Signal measures in field	The measures were done in the train line Ning-Qi, in China, in the band of 800 MHz.[Li08]	The measures cover some scenarios like plain terrains, urban scenarios and tunnels.
	Train to train collision detection system measures at 400 MHz.[Garcia08]	Pathloss, doppler frequency and delay dispersion were obtained in three scenarios (train station, loading docks, bridges and tunnels).
	Measures inside a moving train at 320 MHz in India.[Prasad10] [Prasad09]	Pathloss models were defined in scenarios with low multipath.
	Obtained signal power samples at 930 MHz based in GSM-Railways in China. [Gao10] [Wei10][He11]	Proposals of pathloss models in a viaduct and in and scenario with U shape. The fading depth and K Ricean factor were parameterized.
Channel impulse response measures	A ray tracing approximation is presented to obtain a tunnel model[Cichon95] [Cichon96].	Channel impulse response are obtained for inside tunnels stations.
	Measures in Germany with the campaign RUSK [Medav08][Pekka07b].	It were obtained: pathloss, fading factor, K factor and other parameters related with delay dispersion.
	Measures done with Propsound equipment in 2.5 GHz in Taiwan [Parviainen08].	Investigated parameters were: delay dispersion, maximum delay, arrival angles and departure angles, and angle dispersion.
	Measures done with Propsound equipment in 2.35 GHz in China, inside a train carriage [Dong10].	Obtained empiric pathloss models, angular dispersion and Ricean K factor.

Table 2.2: Channel measurements campaigns done in HST.

Although there are a lot of measure campaigns around HSTs, there are few broadband channel research studies inside train carriages [Dong10]. 3GPP (3rd Generation Partnership Project) defines a channel model for HST [3GPPUE12] [3GPPBS12]. This channel model is a single ray model without fading. It mainly focuses on the Doppler effect and how it affects the efficiency of the system, without analyzing other characteristics of the channel.

In a railway system a new train-ground communication model is being considered. The model considered until now consists of a Base Station (BS) like in Figure 2.2. In this configuration there is a BS in ground and the mobile receivers are inside the train, receiving the signal directly from the BS [Barazzetta16].

In new trains, specially in HST, train body structure acts like a shielding structure that stops signals from BS outside the train [Dong10]. For this reason, the model described before is not valid and it is necessary to use a new ground to train alternative. The use of retransmitters inside trains is currently being discussed [Berisha16], where the scenario used until now is now divided in two subscenarios. The first scenario is the scenario from BS to

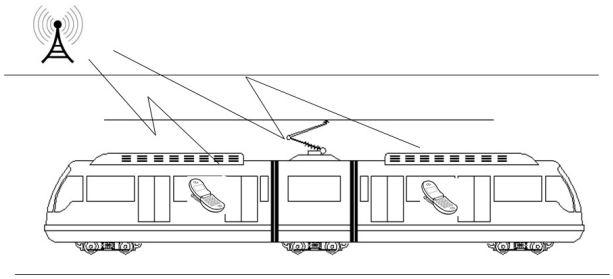

Figure 2.2: Direct signal receiving from a BS to mobile receivers inside train.

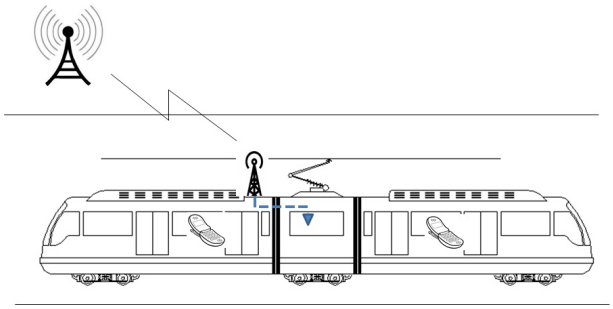

Figure 2.3: BS to repeater transmission, and retransmission to end devices.

the receiver in the train, and the second scenario is between the repeater inside train and the final users. This new model can be observed in Figure 2.3.

In this case, the channel between the BS and the train and the inside train carriage channel need to be analyzed. It is proposed that the last one could follow a classic indoor channel model [Ai12] but in measure campaigns was proved that it has different characteristics [Dong10] that do not follow the indoor scenarios analyzed until now. This scenarios, characterized by multiple reflections due the train material and geometry, fulfill some characteristics described in the literature, confirmed with the measurements. This characteristics are the following:

- Due the high number of reflected rays due the metallic environment, Rayleigh fading is the predominant one, even when there is LOS. The effect of the dominant ray is negligible versus the sum of reflected rays that receiver receives [Ouyang08].
- Due the metallic body of the carriage, all the system acts like a waveguide, making that the pathloss is lower than free space losses [Kita09].

2.2.2 Channel models

To design a communication system that fulfills the reliability levels that the transmission system needs, it is mandatory to perform the necessary measurements and obtain the channel model [Molisch05] [Liu12]. A radio signal received from a communication channel usually depends on three factors [Yannick04]:

1. The location of transmitter and receiver antennas ($\vec{r}$).
2. The time t that corresponds to the temporal variability.
3. The delay τ of the different paths of the electromagnetic waves that arrive to the receiver.

The characterization of a wireless channel will be explained from the point of view of propagation in terms of bidirectional channel response for better understanding.

2.2.2.1 Bidirectional propagation

In a wireless communication the radio propagation mechanism can be defined as the impulsional channel response between the transmitter location $\mathbf{r}_{Tx}$ and the receiver location $\mathbf{r}_{Rx}$. This impulse response is the contribution of all receiving paths, or multipath components (MPCs). Without considering factors like polarization moment, the temporal and angular dispersion of a time invariant channel, the channel is defined by its *double-directional channel impulse response* [Steinbauer01] [Steinbauer98] [Steinbauer00]:

$$h(\mathbf{r}_{Tx}, \mathbf{r}_{Rx}, \tau, \phi, \psi) = \sum_{l=1}^{L} h_l(\mathbf{r}_{Tx}, \mathbf{r}_{Rx}, \tau, \phi, \psi), \tag{2.1}$$

where

- τ is the time delay.
- ϕ is the direction of departure (DoD) of the ray at the transmitter.
- ψ is the direction of arrival (DoA) of the ray at the receiver.
- L is the total number of MPCs.

For plane waves the contribution of the l-th MPC l, $h_l(\mathbf{r}_{Tx}, \mathbf{r}_{Rx}, \tau, \phi, \psi)$ is

$$h_l(\mathbf{r}_{Tx}, \mathbf{r}_{Rx}, \tau, \phi, \psi) = a_l \delta(\tau - \tau_l)\delta(\phi - \phi_l)\delta(\psi - \psi_l), \tag{2.2}$$

where

- a_l is the complex amplitude of the component l.
- τ_l is the delay of the component l.
- ϕ_l is the DoD of the component l.
- ψ_l is the DoA of the component l.

For time-varying channels, the parameters of MPC of Equation 2.2 $(a_l, \tau_l, \phi_l, \psi_l)$, transmitter and receiver locations and the MPC numbers (L) can vary with time (t). The Equation 2.1 can be replaced by a general time varying bidirectional channel response equation as follows:

$$h(\mathbf{r}_{Tx}, \mathbf{r}_{Rx}, t, \tau, \phi, \psi) = \sum_{l=1}^{L} h_l(\mathbf{r}_{Tx}, \mathbf{r}_{Rx}, t, \tau, \phi, \psi). \tag{2.3}$$

2.2.3 Channel model classification

There are different ways to classify channel models depending on their characteristics. One could be depending on the type of channel, for example according to the bandwidth (*narrowband channel (flat fading)* vs. *broadband channels (frequency selective fading)*), or depending on the time variation (*time varying channels* vs. *time static channels*). Narrowband channels can be perfectly characterized thanks to the spatial configuration, whereas in a broadband channel it is necessary to know the behavior model of multipath components.

However the fundamental classification is done in terms of *physical models* and *analytical models* [Ozcelik04], as shown in Figure 2.4 where starting from single antenna configuration, multiantenna (MIMO) models can be obtained.

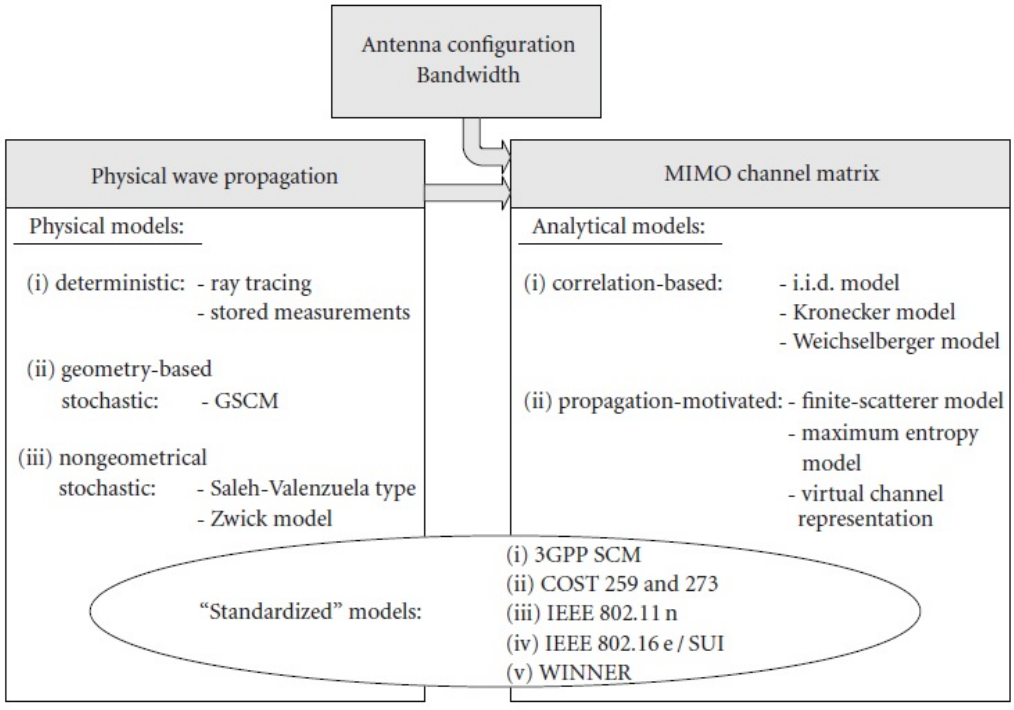

Figure 2.4: Channel classification and channel models [Ozcelik04].

The physical models characterize a channel in terms of electromagnetic propagation by

describing the bi-directional behavior of the waves between the transmitter and the receiver. This model explicitly describes propagation parameters such as complex amplitude, DoD, DoA and MPC delays of the rays. The most sophisticated models incorporate the variations suffered during time and the polarizations of the antennas. Also, within this classification, the physical models can be divided into *deterministic*, *stochastic based on geometry* and *stochastic not based on geometry*.

In contrast to physical models, analytic models characterize the channel's impulse response in a mathematical/statistical way without explicitly taking into account wave propagation. The impulse responses of each pair of transmitting and receiving antennas are collected in a channel matrix, which represents a MIMO channel. The analytic models can be divided also into *models extracted from propagation* and *models based on correlation*. These two models will be analyzed in Chapter 2.2.3.2.

2.2.3.1 Physical models

2.2.3.1.1 GBDM - Geometric Based Deterministic Model

Physical propagation models are called deterministic when they reproduce the process of actual physical propagation in a given environment. In urban scenarios, the geometric and electromagnetic characteristics of the environment, as well as the properties of the link, can be measured and stored so that the propagation process can be afterwards simulated using computer programs. Objects such as buildings, cars or trees can be represented by polygonal objects. The deterministic models are very precise, and very reliable. However, they can only represent the behavior in the environment for which they are designed. Hence, different environments must be designed to represent different situations. Due to the high precision offered by these models, they are used to replace measurements campaigns in those cases where it is not possible to perform in an extensive way.

One of the most appropriate methods to have a deterministic model are *ray tracing* (RT) tools. RT models use the theory of geometric optics to treat reflection, transmission and refraction of the objects that make up the physical model. Geometric optics are based on ray approximation, assuming that the wavelength is sufficiently small in relation to the object with which it is interacting. This assumption is valid in many environments, which allows to express the electromagnetic field in terms of a series of rays, each of which corresponds to a ray that linearly connects the two terminals, thanks to diffractions and refractions in objects. A typical example of GBDM can be seen in Figure 2.5.

2.2.3.1.2 GBSM - Geometric Based Stochastic Model

GBSM models are based on a predefined stochastic distribution of the elements that produce reflection, applying the fundamental laws of propagation. These models can be adapted easily to different scenarios by changing the profile of the region that produces

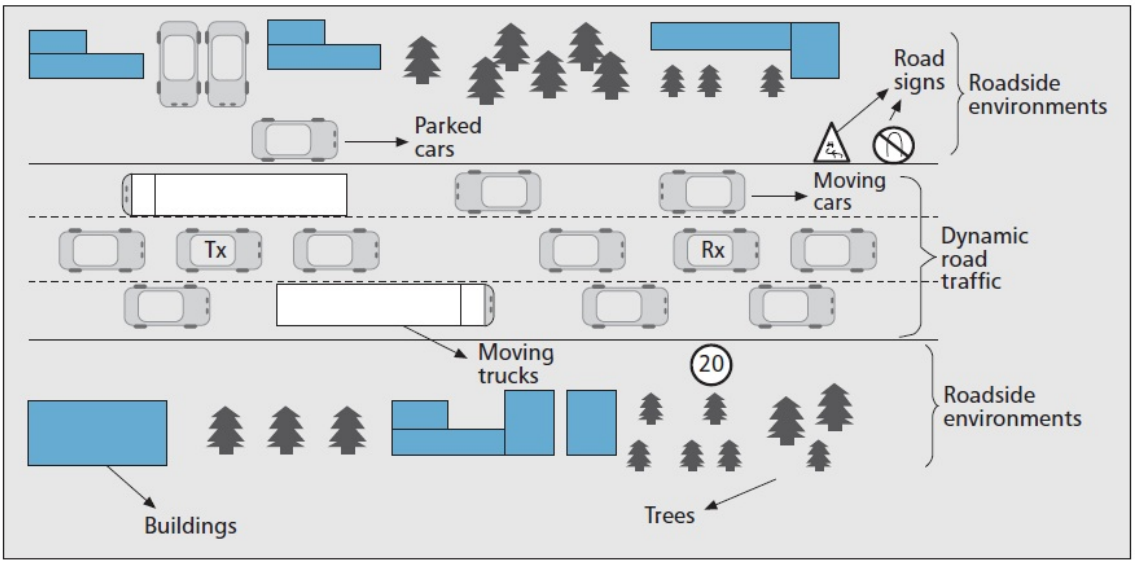

Figure 2.5: A typical V2V environment and its description using GBDM [Maurer08].

reflections. The GBSM models can be classified as regular shape (RS-GBSM) or irregular shape (IS-GBSM), depending on whether the reflecting elements are in regular regions such as a ring, two rings or ellipses, or on irregular forms. In general, RS-GBSM is used for theoretical analysis of channel statistics. To ensure and help mathematical processing, RS-GBSM assumes that all reflective elements are located in regular profiles. There are some two-ring RS-GBSM proposals in [Akki86]. An example of this model is found in Figure 2.6.

On the other hand, IS-GBSM tries to reproduce the environment surrounding the transmitter and receiver in a more accurate way as seen in Figure 2.7. IS-GBSM places the reflective elements in random locations with some statistical distribution. This way, IS-GBSM are considered as a great simplification of the GBDM model, making it valid for different scenarios by modeling and adjusting the statistics of the reflective elements.

2.2.3.1.3 NGSM - Non-Geometrical Stochastic Model

Non-geometrical stochastic models describe the paths between the transmitter and the receiver using only statistical parameters, without any reference to the physical geometry of the environment. There are two kinds of NGSM in the literature. The first uses MPC clusters and it is called the extended Saleh-Valenzuela model, since it generalizes the temporal cluster model presented in [Saleh87]. The second model called the Zwick model, treats MPCs individually. The main features of both models are summarized below:

- Saleh-Valenzuela extended model: Saleh and Valenzuela proposed to model MPC clusters in the delay domain using an exponential double-fall process [Saleh87]. The Saleh-Valenzuela model uses an exponential fall profile to control the power of a multipath cluster. MPCs inside individual clusters are characterized by a second exponential profile with a more steep fall. This model has been extended to the spatial domain

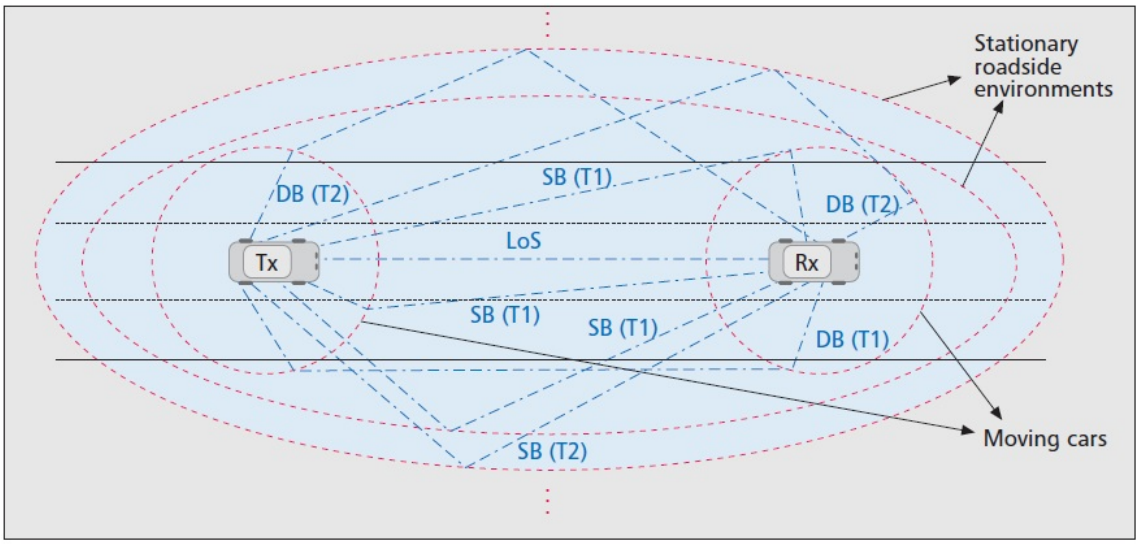

Figure 2.6: Geometrical description using RS-GBSM of the V2V model of the Figure 2.5 [Wang09].

in [Spencer00] [Wallace02]. As a particularly relevant case, a MIMO Saleh-Valenzuela model is proposed in [Wallace02].

- Zwick Model: In [Zwick02] it is argued that for indoor channels, multipath grouping and fading do not occur if the sampling frequency is large enough. Thus, in the Zwick model, MPCs are generated independently (without clustering) and without amplitude fading. However, phase changes of MPCs are included in the model via geometric considerations in function of the movement of the receiver, transmitter and reflective elements.

2.2.3.2 Analytical models

2.2.3.2.1 Correlation based analytical models

Several narrow-band analytic models are based on *complex multivariant Gaussian distribution* of the MIMO channel coefficients (usually Rayleigh or Ricean). The channel matrix can be divided into a stochastic part with zero mean $\mathbf{H}_s$ and a deterministic part $\mathbf{H}_d$ as seen in the following equation:

$$\mathbf{H} = \sqrt{\frac{1}{1+K}}\mathbf{H}_s + \sqrt{\frac{K}{1+K}}\mathbf{H}_d, \tag{2.4}$$

where $K \geq 0$ is the Rice factor. The matrix $\mathbf{H}_d$ includes the LOS component and other contributions not arising from fading. In next lines, the focus will be in the NLOS component characterized by $\mathbf{H}_s$, which is considered Gaussian. For simplicity, it will be assumed that $K = 0$, that is, $\mathbf{H} = \mathbf{H}_s$. In its most general form $\mathbf{h} = vec\{\mathbf{H}\}$ is the complex multivariant

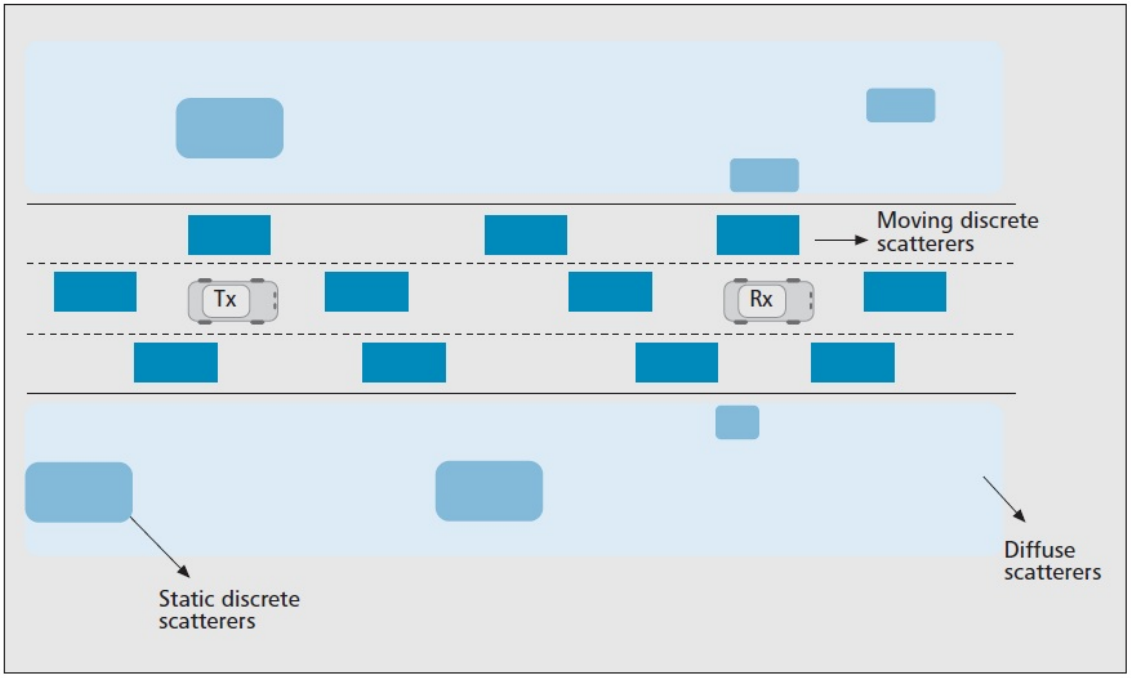

Figure 2.7: Geometric description using IS-GBSM of the V2V model of the figure 2.5 [Wang09].

Gaussian distribution with zero mean where $vec\{\cdot\}$, the vectorization of $\mathbf{H}$, is given by Equation 2.5:

$$f(\mathbf{h}) = \frac{1}{\pi^{NM} det\{\mathbf{R_H}\}} \exp(-\mathbf{h}^H \mathbf{R_H}^{-1} \mathbf{h}). \tag{2.5}$$

Matrix $\mathbf{R_H} = E\{\mathbf{h}\mathbf{h}^\mathbf{H}\}$ of dimensions $NM \times NM$ is known as the *total correlation matrix* [Shiu00] [Kermoal02] and describes the spatial statistics of the MIMO channel. This matrix contains the correlations of all elements of the channel matrix. MIMO channel realizations with the distribution of Equation 2.5 can be obtained with Equation 2.6:

$$\mathbf{H} = unvec\{\mathbf{h}\}, \text{ with } \mathbf{h} = \mathbf{R_H^{1/2}} \mathbf{g}, \tag{2.6}$$

where function $unvec\{\cdot\}$ is the inverse operator of $vec\{\cdot\}$, $\mathbf{R_H}^{1/2}$ is the square root of an arbitrary matrix (that is, any matrix satisfying $\mathbf{R_H}^{1/2} \mathbf{R_H}^{H/2} = \mathbf{R_H}$), and $\mathbf{g}$ is a vector of length NM with identically independently distributed (i.i.d.) Gaussian elements of zero mean and unit variance. To use Equation 2.6, the complete specification of $\mathbf{R_H}$ is usually required, which implies $(NM)^2$ real parameters. To reduce this large number of parameters, several models have been proposed which impose a particular structure of the MIMO correlation matrix [Weichselberger03].

2.2.3.2.1.1 Identically independently distributed model (i.i.d.)

The simplest MIMO analytical model is the i.i.d. or canonical model. Here $\mathbf{R_H}$ =

$\rho^2\mathbf{I}$, that is, all elements of the MIMO channel matrix $\mathbf{H}$ are completely uncorrelated (and thus are statistically independent) and have ρ^2 variance. This physically corresponds to environments where there is a lot of reflection and where MPCs are independently and uniformly distributed in all directions. The i.i.d model depends on a single parameter (the channel power ρ^2) and is used for theoretical considerations of MIMO systems.

2.2.3.2.1.2 Kronecker model

The Kronecker model was used in [Chuah98] [Chizhik00] [Shiu00] for capacity analysis before being proposed in [Kermoal02] in the framework of the European project SATURN (Smart Antenna Technology in Universal bRoadband wireless Networks) [SATURN]. This model assumes that the spatial correlation of the transmitter and the receiver is detachable, which means that it can be described by a Kronecker product of two partial correlation matrices:

$$\mathbf{R_H} = \mathbf{R_{Tx}} \otimes \mathbf{R_{Rx}}, \tag{2.7}$$

where the correlation matrices of the transmitter and the receiver are given by

$$\mathbf{R_{Tx}} = E\{\mathbf{H}^H\mathbf{H}\},\ \mathbf{R_{Rx}} = E\{\mathbf{H}\mathbf{H}^H\}. \tag{2.8}$$

Combining Equation 2.8 and Equation 2.6 the Kronecker model can be simplified leading in Equation 2.9.

$$\mathbf{h} = (\mathbf{R_{Tx}} \otimes \mathbf{R_{Rx}})^{1/2})\mathbf{g} \Longleftrightarrow \mathbf{H} = \mathbf{R_{Rx}}^{1/2}\mathbf{G}\mathbf{R_{Tx}}^{1/2}, \tag{2.9}$$

where $\mathbf{G} = unvec(\mathbf{g})$ is an i.i.d. MIMO channel matrix of variance one. The model requires the definition of the correlation matrices of the transmitter and receiver. The number of parameters to be defined is reduced to $N^2 + M^2$.

The biggest constraint of the Kronecker model is that it treats DoD and DoA angles independently. This uncorrelation is not true for the MIMO systems where there is only one reflection in the signal.

Even with this restriction, the model has been extensively used for the theoretical analysis of MIMO systems and simulations. The model allows the optimization of the transmitter array and the receiver array independently. For this simplicity the Kronecker model is very popular.

2.2.3.2.1.3 Weichselberger model

The Weichselberger model attempts to correct the constraint of the Kronecker model which assumes that the DoD and DoA are uncorrelated. The definition of this model is

based on the singular value decomposition (SVD) of the correlation matrices in transmission and reception:

$$\mathbf{R}_{Tx} = \mathbf{U}_{Tx}\mathbf{\Lambda}_{Tx}\mathbf{U}_{Tx}^{H}, \tag{2.10}$$

$$\mathbf{R}_{Rx} = \mathbf{U}_{Rx}\mathbf{\Lambda}_{Rx}\mathbf{U}_{Rx}^{H}, \tag{2.11}$$

where $\mathbf{U}_{Tx}$ and $\mathbf{U}_{Rx}$ are unitary matrices whose columns are the eigenvalues of $\mathbf{R}_{Tx}$ and $\mathbf{R}_{Rx}$ respectively, while $\mathbf{\Lambda}_{Tx}$ and $\mathbf{\Lambda}_{Rx}$ are diagonal matrices with their own eigenvalues. The model is given by

$$\mathbf{H} = \mathbf{U}_{\mathbf{Rx}}(\Omega \odot \mathbf{G})\mathbf{U}_{Tx}^{T}, \tag{2.12}$$

where $\mathbf{G}$ is a $N \times M$ MIMO matrix, $\odot$ is the Schur-Hadamard product (element-wise multiplication), and Ω is the coupling matrix of dimensions $N \times M$ (real and non-negative values) whose elements determine the average coupling power between the values of the eigenvalues of the transmitter and the receiver. It can be deduced that the Kronecker model is a special case of Weichselberger when the coupling matrix is of rank one ($\Omega = \lambda_{Rx}\lambda_{Tx}^{T}$), where λ_{Tx} and λ_{Rx} are vectors containing the eigenvalues of the correlation matrices of the transmitter and the receiver.

The Weichselberger model needs to know the eigenvalues of the transmitter and the receiver ($\mathbf{U}_{Tx}$ and $\mathbf{U}_{Rx}$) and the coupling matrix Ω. This condition requires to define $N(N-1) + M(M-1) + NM$ real parameters.

2.2.3.2.2 Analytical models based on propagation

2.2.3.2.2.1 Finite reflecting elements model

This model assumes that there is a finite number of reflecting or dispersing elements and that the propagation can be modeled by a finite number P of multipaths. For each of the p paths, there will be an azimuth exit angle (DoD_{az}) (ϕ_p), an azimuth arrival angle (DoA_{az}) (ψ_p), a complex amplitude (ξ_p) and a specific delay (τ_p). The model allows the integration of a single rebound or the incorporation of multiple rebounds. The model also allows to separate paths with the same DoD and different DoAs or viceversa, called subpaths.

If all the parameters are known, the matrix $\mathbf{H}$ of the MIMO channel for a narrowband case, ignoring delays (τ_p) can be expressed as:

$$\mathbf{H} = \sum_{p=1}^{P} \xi_p \psi(\psi_p)\phi^{\mathbf{T}}(\phi_p) = \mathbf{\Psi\Xi\Phi^{T}}, \tag{2.13}$$

where $\mathbf{\Phi} = [\phi(\phi_1)...\phi(\phi_P)]$, $\mathbf{\Psi} = [\psi(psi_1)...\psi(\psi_P)]$, $\phi^{\mathbf{T}}(\phi_p)$ and $\psi(\psi_p)$ are the direction vectors

of the transmitter and the receiver corresponding to the pth MPC, and $\mathbf{\Xi} = diag(\xi_1, ..., \xi_p)$ is a diagonal matrix containing all the amplitudes of the different MPCs. The direction matrices contain the geometry, direction and coupling of the elements of the antenna array. In broadband systems the delay must also be incorporated. Given the system bandwidth ($B = 1/T_s$) limitation within the channel, the channel representation as a function of delays (τ) is solved using $\mathbf{H}(\tau) = \sum_{l=-\infty}^{\infty} \mathbf{H}_l \delta(\tau - lT_S)$, with

$$\mathbf{H}_l = \sum_{p=1}^{P} \xi_p sinc(\tau_p - lT_S)\psi(\psi_p)\phi^{\mathbf{T}}(\phi_p) = \mathbf{\Psi}(\mathbf{\Xi} \odot \mathbf{T_l})\mathbf{\Phi^T}, \tag{2.14}$$

where ($sinc(x) = sin(\pi x)/(\pi x)$) y $\mathbf{T_l}$ is a diagonal matrix with the elements ($sinc(\tau_p - lT_S)$), $p = 1, ..., P$.

This model is compatible with other standard models such as 3GPP [3GPP03] or Winner [Pekka07b] which define the statistical distributions of MPC parameters.

2.2.3.2.2.2 Virtual channel representation

A MIMO channel model can be represented by a virtual representation of the channel [Sayeed02]:

$$\mathbf{H} = \mathbf{F_n}(\mathbf{\Omega} \odot \mathbf{G})\mathbf{F_m^H}, \tag{2.15}$$

where $\mathbf{F_m}$ and $\mathbf{F_n}$ matrices contain the direction vectors of M transmitter virtual scatterers and N receiver virtual scatterers, $\mathbf{G}$ is a gaussian i.i.d. array of mean zero and $n \times m$ dimension, and $\mathbf{\Omega}$ is a $N \times M$ array which characterizes the coupling between each pair of virtual scatterers. $\Omega \odot G$ represents the propagation environment between the transmitter and receiver virtual scatterers.

2.2.4 Standardized models

Standardized models approved by many institutions are widely used to define new radiofrequency communication systems.

2.2.4.1 COST 259/273

"COST" is the abbreviation for *European Cooperation in the field of Scientific and Technical Research*. The COST 259 initiative is about "Personal Flexible Wireless Communications" (1996-2000) and the COST 273 initiative is entitled "Towards Multimedia Broadband Networks" (2001-2005). These two initiatives developed channel models that included directional characteristics of the antennas and made them suitable for simulating intelligent antennas and MIMO systems. They are the most standardized general models and were not designed with a specific system in mind.

2.2.4.1.1 COST 259

The COST 259 directional channel model is a physical model that gives the delay dispersion and angles in the base station (BS) and in the mobile station (MS) for different radio environments. It is considered the first model that includes the relationship between distance, delay dispersion, angular dispersion and other parameters between BS and MS. It is considered general because it is defined for 13 different radio environments (typical urban, bad urban, open courtyard, inside offices, corridors, etc), which includes models of macrocells, microcells and picocells.

Each radio environment is described by external parameters (positions, frequency, mean altitudes of BS and MS) and by global parameters, which are set by different probability densities depending on the environment. The global parameters are fixed using terms of geometric properties and stochastic criteria.

This model has two major constraints. On one hand, it is assumed that the dispersing elements are stationary, so that the channel variations are given only by the movement of the MS. This is not true, for example in indoor scenarios, where there are people moving. On the other hand, the attenuations of the delays are modeled as complex Gaussian random variables. This requires a large number of MPCs within each delay slot, which is not true in some situations.

2.2.4.1.2 COST 273

The COST 273 model is very similar to COST 259, with the following main differences:

1. It includes some interesting radio channel scenarios for MIMO.
2. It updates some parameters, thanks to new measurements.
3. It uses the same approximation for macro, micro and picocell models. The approximation is similar to COST 259.
4. The DoA and DoD distribution model is different compared with COST 259. A cluster is divided in two representations of itself: one relative to BS and another one related to MS. These two representations join one of the delays of the cluster, allowing to assure realistic delays. These delays are obtained from measurement campaigns.

2.2.4.2 3GPP SCM

The spatial channel model or SCM [3GPP03] was developed by 3GPP/3GPP2 to be a common reference for evaluating different MIMO concepts in outdoor environments at a central frequency of 2 GHz and a bandwidth of 5 MHz. The SCM consists of two parts:

1. Calibration Model: The calibration model is a very simplified channel model that allows to verify the correct implementation of the simulation. This calibration model should not be used to simulate algorithms or systems.

2. Simulation model: This is the SCM used to assess system performance. The model is a physical model and distinguishes between three different environments: urban macrocell, suburban macrocell and urban microcell. The model structure and the simulation methodology are identical for all environments, but parameters such as angular scattering or delay dispersion are different.

The model uses both geometric and statistical components. For a single link between MS and BS, the position within a cell, the orientation of the antenna array and the direction of movement within the cell are randomly chosen. From the MS position the pathloss can be determined, which is determined by the Hata model of COST 231 for macrocells and by the Walfish-Ikegami model of COST 231 for microcells. The number of paths with different delay is defined as 6, but their delays and average powers are stochastically generated from a probability density function.

Each delay shows a different angular dispersion in the BS and MS. The dispersion of each delay is represented by a number of subpaths with the same delay, but different DoA and DoDs. Physically this means that each path is composed of a cluster of 20 rays, each one with different directions, but reaching the receiver at the same instant of time. The modeling of the angular dispersion is as follows: the mean of DoD and DoA is defined by the position of the MS and the orientation of the array of antennas. The mean of the delays is chosen randomly from a Gaussian distribution centered at the mean of DoD and DoA. The variance of this dispersion is one of the parameters defined in the model. The 20 rays have different phases, which are defined in the 3GPP standard. Adding all subpaths gives Rayleigh or Rice fading.

A simulation with SCM is usually carried out simulating sequences of time, which are short periods of time. The period is short enough so that the simulation parameters such as angular scattering, temporal scattering and signal fading can be assumed constant. During simulation these parameters are chosen from a given distribution. The positions of the MS are changed randomly in each simulation sequence.

In addition to who has been described above, the model can include other characteristics such as the polarization model, clusters of far scatterers, the effect of LOS and the modification of the angular distribution in the MS, such as in urban canyons scenarios.

2.2.4.3 IEEE 802.11n

The IEEE 802.11 TG model [Erceg09] was developed for indoor scenarios at 2 GHz and at 5 GHz, with special focus on MIMO WLAN networks. Measurements on these two frequencies

were combined to generate a single model (in fact, only pathloss depends on frequency). Scenarios such as small and large offices, residential homes and open spaces were investigated for both LOS and NLOS. The TGn channel model specifies six environments labeled from A to F, which basically correspond to the single antenna WLAN models presented in [Medbo99] and [Medbo98a]. For each of these environments, the TGn model specifies the corresponding parameters.

The TGn 802.11 model is a physical model, using a non-geometric stochastic approximation, very similar to the 3GPP/3GPP2 model. The directional impulse response is described by a sum of clusters, each of which consists of up to 18 delay instants, separated by at least 10ns. At each moment, a DoA and a Laplacian power in Azimuth are assigned, with an angular dispersion between 20° and 40° (the DoD is very similar). The number of clusters varies between 2 and 6 (based on measurements) and the delay dispersion varies between 0 (flat fading) and 150 ns.

For each time instant, each MIMO channel delay is modeled using Equation (2.4). A Kronecker model is chosen for the Rayleigh fading part. The correlation matrices of the transmitter and the receiver are determined by the power spectrum in azimuth and by the geometry of the array. The time domain variations of the model are simulated by moving the dispersers.

2.2.4.4 Winner model

Winner (Wireless World Initiative New Radio) is a consortium of 41 partners coordinated by the Nokia-Siemens network. This consortium has developed 17 different scenario models thanks to extensive campaigns of measurements made with channel analyzers. The scenarios are classified into 4 large environments (A to D), which are divided into subenvironments and probability distribution functions are obtained for each scenario. It defines a number of clusters that have the same delay, but different DoD and DoA like previous models. Large-scale parameters are obtained and thanks to them, low-level elements are modeled. The steps to obtain the parameters of the different models are described in the Figure 2.8. This process starts with an extensive measurement campaign, and in a second step the parameters necessary for the channel generation can be modeled. These channel parameters are integrated with the characteristics of antenna arrays in transmission and reception to obtain the MIMO channel to be used in simulations.

To obtain the simulation model from the parameters obtained from the measurements, the methodology described in Figure 2.9 is followed. It starts from the definition of the chosen scenario and the high-level parameters of that scenario. Thus, low-level characteristics are then obtained to create the channel impulse response following general equation:

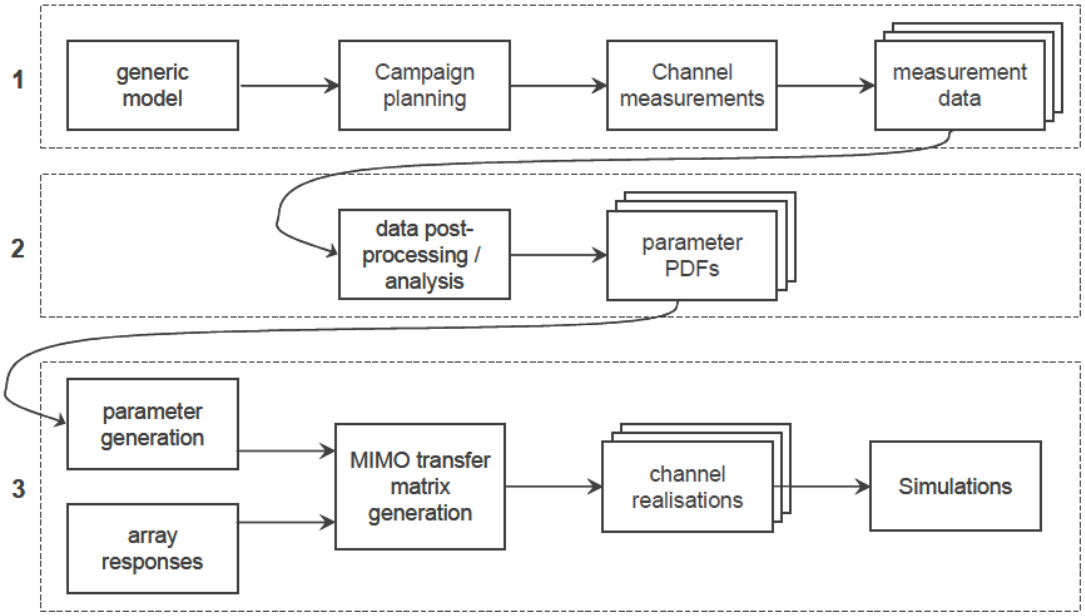

Figure 2.8: Steps to obtain Winner model parameters [Pekka07a].

$$\mathbf{H}_{u,s,n}(t) = \sqrt{P_n} \sum_{m=1}^{M} \begin{bmatrix} F_{rx,u,V}(\phi_{n,m}) \\ F_{rx,u,H}(\phi_{n,m}) \end{bmatrix}^T \begin{bmatrix} \exp(j\Phi_{n,m}^{vv}) & \sqrt{\kappa_{n,m}}\exp(j\Phi_{n,m}^{vh}) \\ \sqrt{\kappa_{n,m}}\exp(j\Phi_{n,m}^{hv}) & \exp(j\Phi_{n,m}^{hh}) \end{bmatrix} \begin{bmatrix} F_{tx,s,V}(\varphi_{n,m}) \\ F_{tx,s,H}(\varphi_{n,m}) \end{bmatrix} \exp(j2\pi\lambda_0^{-1}\bar{r}_s\bar{\Phi}_{n,m})\exp(j2\pi\lambda_0^{-1}\bar{r}_u\bar{\Psi}_{n,m})\exp(j2\pi\upsilon_{n,m}t), \tag{2.16}$$

where the scalar product $\bar{r}_s\bar{\Phi}_{n,m}$ is calculated as

$$\bar{r}_s\bar{\Phi}_{n,m} = x_s\cos\gamma_{n,m}\cos\phi_{n,m} + y_s\cos\gamma_{n,m}sin\phi_{n,m} + z_s sin\gamma_{n,m}, \tag{2.17}$$

and

- $\bar{r}_s$ is the position vector of the s-th element of the transmitter array.
- $\bar{\Phi}_{n,m}$ is the departure angle vector of the n,m-th ray.
- x_s, y_s, z_s are the components x, y, z of $\bar{r}_s$.
- $\phi_{n,m}$ is the angle in azimuth of the n,m-th ray.
- $\gamma_{n,m}$ is the elevation angle of n,m.
- $\bar{r}_u\bar{\Psi}_{n,m}$ is the scalar product of the u-th element of the and the arrival angle n,m.

Equation 2.16 provides the elements of Equation 2.2. As mentioned before, all parameters of the Equation 2.16 are computed thanks to distribution functions obtained in measurement

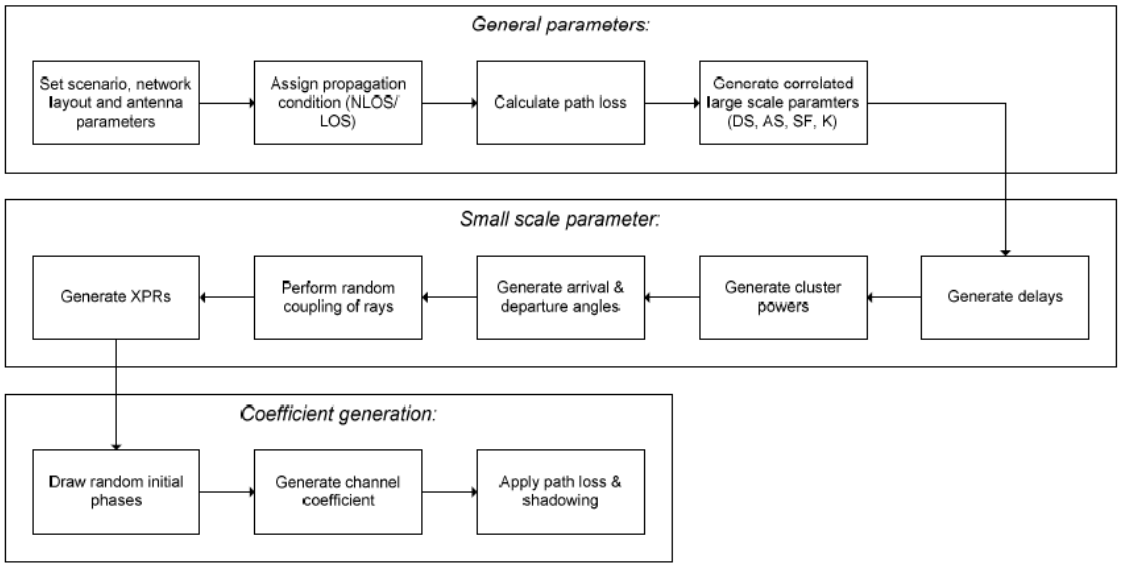

Figure 2.9: Model generation to be used in simulators [Pekka07a]

.

campaigns. These measurement campaigns have been carried out in the scenarios of Table 2.3 [Baum05].

2.2.4.5 HiperLAN 2

HiperLAN (High Performance Radio LAN) is an European alternative for the IEEE 802.11 standard defined by the European Telecommunications Standard Institute (ETSI). HiperLAN 2 is the second version of the HiperLAN standard. HiperLAN 2 standard was presented on February 2000 as a fast wireless connection for many networks, like UMTS backbone network, ATM and IP networks. Operation frequency of HiperLAN 2 is 5 GHz and in Europe the lower band is from 5.15 to 5.35 GHz for indoor use and the upper band is from 5.47 to 5.725 GHz for both indoor and outdoor use. HiperLAN 2 can transmit up to 54 Mbps and uses OFDM. The medium access makes use of time division duplex and dynamic time division multiple access (TDD/TDMA). The main features of the HiperLAN 2 are described in [Haider02]. The access points (AP) use a link adaptation scheme using various modulation schemes. Seven physical layers are defined of which the first six are mandatory and the last one is optional [ETSI02]. The physical layers are summarized in Table 2.4.

To simulate systems throughput, HiperLAN 2 describes different types of environment. The different channel models are described in detail in [Medbo98b] where tap number, delay, the average relative power, Rice factor and doppler spectrum are defined. There are five channel models identified from A to E that are summarized in Table 2.5.

Scenario	**Definition**	**LOS/NLOS**	**Speed (km/h)**	**Distance range**
A1 Indoor	Indoor, small office or residential	LOS/NLOS	0-5	3-100 m
A2 Indoor	From indoor to outdoor	NLOS	0-5	
B1 Hotspot	Typical urban microcell	LOS/NLOS	0-70	20-400 m
B2 Hotspot	Typical hostile urban environment	NLOS	0-70	
B3 Hotspot	Indoor	LOS	0-5	
B4 Hotspot	From outdoor to indoor	NLOS	0-5	
B5a Hotspot	LOS en enlaces de tejado a tejado	LOS	0	30 m - 8 km
B5b Hotspot	LOS en enlaces a nivel de calle	LOS	0	
B5c Hotspot	LOS link from roof to street level	LOS	0	20-400 m
B5d Hotspot	NLOS link from roof to street level	NLOS	0	35-3000 m
C1 Metropolitan	Suburban	LOS/NLOS	0-70	35-3000 m
C2 Metropolitan	Typical urban macrocell	LOS/NLOS	0-70	35-3000 m
C3 Metropolitan	Hostile urban	NLOS	0-70	
C4 Metropolitan	From outdoor to indoor	NLOS	0-70	
C5 Metropolitan	LOS link	LOS	0	
D1 Rural	Rural macrocell	LOS/NLOS	0-200	35 m - 10 km
D2 Rural	Mobile links with LOS	LOS	0-300	

Table 2.3: Measured and modelled scenarios in Winner.

Mode	Modulation	Code rate	Bit rate	Bytes/symbol
1	BPSK	1/2	6Mbps	3.0
2	BPSK	3/4	9Mbps	4.5
3	QPSK	1/2	12Mbps	6.0
4	QPSK	3/4	18Mbps	9.0
5	16QAM	9/16	27Mbps	13.5
6	16QAM	3/4	36Mbps	18.0
7	64QAM	3/4	54Mbps	27.0

Table 2.4: Physical layer modes of HiperLAN 2 [Haider02].

Channel model	r.m.s delay spread	Rice factor on first tap	Environment
A	50 ns	-	Office NLOS
B	100 ns	-	Open space / Office NLOS
C	150 ns	-	Large open space NLOS
D	140 ns	-	Large open space LOS
E	250 ns	-	Large open space NLOS

Table 2.5: Channel models used in HiperLAN 2.

2.3 Wireless systems

2.3.1 Multiantenna systems

In wireless communication systems it is possible to use different antenna configurations, depending of the number of transmit antennas and the number of receive antennas. Such systems can exploit the space diversity if they are using more than one antenna to transmit or receive and are defined as space-time systems. Depending of the antenna configuration they are classified as SISO, SIMO, MISO or MIMO. These configurations will be explained in next sections.

2.3.1.1 SISO

In traditional wireless communication systems, single input single output (SISO) is a well-known wireless configuration where a single antenna is used to transmit information and uses a single antenna to receive (Figure 2.10a). The system is defined by Equation 2.18,

$$y = h_{11}s + n, \tag{2.18}$$

where y is the received symbol, h_{11} is the channel response between antennas, s is the transmitted symbol and n is the additive noise. The capacity of a SISO system, defined as the maximum achievable error-free data rate was first derived by Claude Shannon in 1948

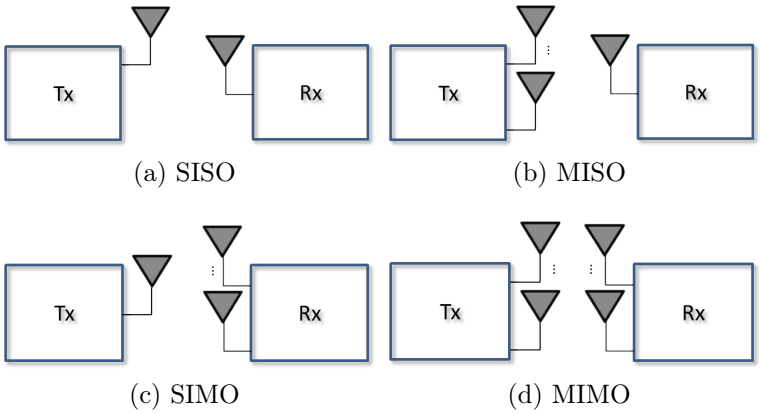

(a) SISO (b) MISO

(c) SIMO (d) MIMO

Figure 2.10: Antenna configuration in space-time systems.

[Shannon48]. The capacity for an Additive White Gaussian Noise (AWGN) is given by:

$$C_{SISO} = \log_2(1+\rho) \text{ bps/Hz}, \tag{2.19}$$

where $\rho = E_s/N_0$ is the signal to noise ratio (SNR) of the wireless system.

2.3.1.2 MIMO

Multiple Input Multiple Output (MIMO) systems use M_T antennas to transmit and M_R antennas to receive as it can be seen in Figure 2.10d. MIMO systems are defined by Equation 2.20.

$$\mathbf{y} = \mathbf{H}\mathbf{s} + \mathbf{n}, \tag{2.20}$$

with

$$\mathbf{y} = \begin{pmatrix} y_1 \\ y_2 \\ \vdots \\ y_{M_R} \end{pmatrix}, \tag{2.21}$$

$$\mathbf{H} = \begin{pmatrix} h_{11} & h_{12} & \dots & h_{1M_T} \\ h_{21} & h_{22} & \dots & h_{2M_T} \\ \vdots & \vdots & \ddots & \vdots \\ h_{M_R1} & h_{M_R2} & \dots & h_{M_RM_T} \end{pmatrix}, \tag{2.22}$$

$$\mathbf{s} = \begin{pmatrix} s_1 \\ s_2 \\ \vdots \\ s_{M_T} \end{pmatrix}, \tag{2.23}$$

$$\mathbf{n} = \begin{pmatrix} n_1 \\ n_2 \\ \vdots \\ n_{M_R} \end{pmatrix}, \tag{2.24}$$

where $\mathbf{y}$ is a $M_R \times 1$ matrix containing the received symbols in each antenna, $\mathbf{H}$ is a $M_R \times M_T$ matrix containing the channel response of each pair of transmit-receive antenna, $\mathbf{s}$ is a $M_T \times 1$ matrix with the symbols transmitted from each antenna and $\mathbf{n}$ is a $M_R \times 1$ matrix with the additive noise of each receive antenna.

The capacity of a MIMO system is defined as [Foschini98], [Telatar99]:

$$C = \max_{f(\mathbf{s})} I(\mathbf{s};\mathbf{y}), \tag{2.25}$$

where $f(\mathbf{s})$ is the probability distribution of vector $\mathbf{s}$ and $I(\mathbf{s};\mathbf{y})$ is the mutual information between vectors $\mathbf{s}$ and $\mathbf{y}$. $I(\mathbf{s};\mathbf{y})$ is defined in Equation 2.26:

$$I(\mathbf{s};\mathbf{y}) = H(\mathbf{y}) - H(\mathbf{y}|\mathbf{s}), \tag{2.26}$$

where $H(\mathbf{y})$ is the differential entropy of vector $\mathbf{y}$ and $H(\mathbf{y}|\mathbf{s})$ is the conditional differential entropy of vector $\mathbf{y}$, knowing vector $\mathbf{s}$. Since vectors $\mathbf{s}$ and $\mathbf{n}$ are independent, Equation 2.26 is simplified as:

$$I(\mathbf{s};\mathbf{y}) = H(\mathbf{y}) - H(\mathbf{n}). \tag{2.27}$$

To maximize $I(\mathbf{s};\mathbf{y})$ reduces to maximizing $H(\mathbf{y})$, which happens when $\mathbf{s}$ is a Zero Mean Circularly Symmetric Complex Gaussian (ZMCSCG) vector characterized by its covariance matrix $\mathbf{R_{ss}}$. The differential entropies $\mathbf{H}(\mathbf{y})$ and $\mathbf{H}(\mathbf{n})$ are given as [Paulraj03]:

$$H(\mathbf{y}) = \log_2(\det(\pi e \mathbf{R_{yy}})) \text{ bps/Hz}, \tag{2.28}$$

$$H(\mathbf{n}) = \log_2(\det(\pi e \sigma^{\mathbf{2}} \mathbf{I}_{M_R})) \text{ bps/Hz}. \tag{2.29}$$

$I(\mathbf{s};\mathbf{y})$ is reduced to:

$$I(\mathbf{s};\mathbf{y}) = \log_2 \ \det\left(\mathbf{I}_{M_R} + \frac{E_S}{M_T N_0} \mathbf{H R_{SS} H^H}\right) \text{ bps/Hz}. \tag{2.30}$$

Therefore the capacity of MIMO from Equation 2.25 is given by

$$C = \max_{Tr(\mathbf{R_{ss}})=M_T} \log_2 \det\left(\mathbf{I}_{M_R} + \frac{E_S}{M_T N_0}\mathbf{H}\mathbf{R_{SS}}\mathbf{H^H}\right) \text{ bps/Hz.} \tag{2.31}$$

If there is no knowledge of the channel at the transmitter, the transmitted signals are independent and with the same power, i.e., $\mathbf{R_{SS}} = \mathbf{I_M}$ and the capacity is now:

$$C = \log_2 \det\left(\mathbf{I}_{M_R} + \frac{\rho}{M_T}\mathbf{H}\mathbf{H^H}\right) \text{ bps/Hz.} \tag{2.32}$$

After the singular value decomposition of $\mathbf{HH^H}$, the capacity of Equation 2.31 can be expressed as

$$C = \sum_{i=1}^{r} \log_2\left(1 + \frac{E_S}{M_T N_0}\lambda_i\right) \text{ bps/Hz,} \tag{2.33}$$

where r is the rank of the channel and $\lambda_i (i = 1, 2, \ldots, r)$ are the positive eigenvalues of $\mathbf{HH^H}$. Capacity of the MIMO channel is expressed as a sum of r SISO channels, each having a gain of λ_i and transmit power E_S/M_T.

Orthogonal channel matrices ($\mathbf{HH^H} = \alpha\mathbf{I}_M$) maximize the capacity [Paulraj03] and if the elements of $\mathbf{H}$ satisfy $\|\mathbf{H}_{i,j}\|^2 = 1$ and a full-rank MIMO channel is considered with $M_T = M_R = M$ then the MIMO channel capacity becomes

$$C = M \log_2\left(1 + \frac{E_S}{N_0}\right) \text{ bps/Hz.} \tag{2.34}$$

2.3.1.3 SIMO

In a SIMO system there are $M_T = 1$ transmit antennas and M_R receive antennas as it can be seen in Figure 2.10c. The channel matrix is a column matrix as seen in Equation 2.35:

$$\mathbf{H} = \begin{pmatrix} h_1 \\ h_2 \\ \vdots \\ h_{M_R} \end{pmatrix}. \tag{2.35}$$

In SIMO, $M_R > M_T$ and if the channel is unknown to the transmitter Equation 2.31 becomes

$$C = \log_2 \det\left(\mathbf{I}_{M_T} + \frac{E_S}{M_T N_0}\mathbf{H}^H\mathbf{H}\right) \text{ bps/Hz.} \tag{2.36}$$

Now $\mathbf{H}^H\mathbf{H} = \sum_{i=1}^{M_R} |h_i|^2$ and $M_T = 1$. Hence,

$$C = \log_2 \ \det\left(1 + \sum_{i=1}^{M_R} |h_i|^2 \frac{E_S}{N_0}\right) \ \text{bps/Hz}, \tag{2.37}$$

and if $|h_1|^2 = |h_2|^2 = \ldots = |h_{M_R}|^2 = 1$ the channel capacity when the channel is unknown at the transmitter is:

$$C = \log_2 \ \det\left(1 + M_R \frac{E_S}{N_0}\right) \ \text{bps/Hz}. \tag{2.38}$$

2.3.1.4 MISO

In MISO channels $M_R = 1$ and there are M_T transmit antennas. Now $M_T > M_R$ and Equation 2.31 is used as it is. The system can be seen in Figure 2.10b and the channel matrix is a row matrix as seen in Equation 2.39:

$$\mathbf{H} = (h_1 \ h_2 \ldots h_{M_T}). \tag{2.39}$$

As $\mathbf{H}\mathbf{H}^H = \sum_{j=1}^{M_T} |h_j|^2$ and from Equation 2.31 it becomes:

$$C = \log_2 \left(1 + \sum_{j=1}^{M_T} |h_j|^2 \frac{E_S}{M_T N_0}\right) \ \text{bps/Hz}. \tag{2.40}$$

If the channel coefficients are equal and normalized as $\sum_{j=1}^{M_T} |h_j|^2 = M_T$ then the MISO capacity becomes:

$$C = \log_2 \left(1 + \frac{E_S}{N_0}\right) \ \text{bps/Hz}. \tag{2.41}$$

It can be seen that Equation 2.41 is the same as for SISO case, i.e, the capacity does not increase with the number of antennas. This is the case when the channel is unknown at the transmitter. If the channel is known at the transmitter, the transmitter can weight the transmission with weights depending in the channel coefficients, so there is a coherent combining at the receiver (MISO case). Knowing the channel at the transmitter the capacity is:

$$C = \log_2 \left(1 + \sum_{j=1}^{M_T} |h_j|^2 \frac{E_S}{N_0}\right) \ \text{bps/Hz}. \tag{2.42}$$

If the channel coefficients are equal and normalized as $\sum_{j=1}^{M_T} |h_j|^2 = M_T$ the capacity becomes:

$$C = \log_2 \left(1 + M_T \frac{E_S}{N_0}\right) \ \text{bps/Hz}. \tag{2.43}$$

2.3.1.5 Random Channels

The capacity described in Section 2.3.1.1, 2.3.1.2, 2.3.1.3 and 2.3.1.4 are obtained using deterministic channels. In the case when **H** is chosen randomly from a known distribution and the channel is unknown at the transmitter but the receiver has perfect knowledge of the channel, the obtained capacity and data rate is also random for each channel realization. In this case, the cumulative distribution function (CDF) is used to know the channel performance. Two values are used in this case: Ergodic Capacity and Outage Capacity.

The ergodic capacity assumes an independent channel realization for each channel use and represents the ensemble average of information rate over the distribution of elements of **H**. The ergodic capacity can be expressed as:

$$C = E\left[\log_2 \ \det\left(\mathbf{I}_{M_R} + \frac{E_S}{M_T N_0}\mathbf{H}\mathbf{R_{SS}}\mathbf{H^H}\right)\right] \ \text{bps/Hz}. \tag{2.44}$$

The outage capacity quantifies the capacity that can be guaranteed with a certain level of reliability [Paulraj03]. Capacity $C_{out,g}$ is defined as the information rate that is guaranteed for $(100 - g\%)$ of the channel realizations, i.e., $P(C \leq C_{out,g}) = g\%$ [Biglieri98].

2.3.2 Space-Time Block Coding

Space-time block coding (STBC) is a transmit diversity technique used in MIMO systems. The first STBC was the Alamouti code [Alamouti98]. Alamouti is a scheme for a 2 x 2 system that has a full diversity gain with a maximum likelihood decoding algorithm. This algorithm can be extended to other $M_T \times M_R$ systems. The main premise in such systems is that we have perfect knowledge at the receiver and that the data streams are independent.

2.3.2.1 Alamouti Space-Time Code

In this scheme the information bits are modulated first and after the modulator the encoder takes a block of two modulated symbols s_1 and s_2 in each encoding operation and sends it to the transmit antennas, according to the code matrix,

$$\mathbf{S} = \begin{bmatrix} s_1 & -s_2^* \\ s_2 & s_1^* \end{bmatrix}. \tag{2.45}$$

In Equation 2.45, first column is the first transmission period and the second column represents the second transmission period. The first row are the symbols transmitted from the first antenna and the second row are the symbols transmitted from the second antenna as seen in Figure 2.11.

This way, the system is transmitting both in space and time (two antennas during two intervals), that is, it is space-time coding. The sequence of Equation 2.45 is orthogonal, i.e.,

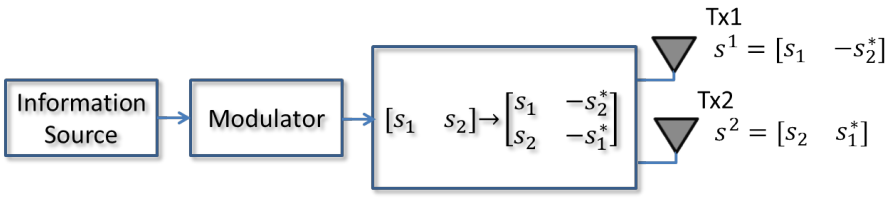

Figure 2.11: Block diagram of a Alamouti space-time encoder.

the inner product of s_1 and s_2 is zero:

$$s_1 s_2 = s_1 s_2^* - s_2^* s_1 = 0. \tag{2.46}$$

Assuming that the channel remains constant and the fading is frequency-flat, the received signal for each symbol time indexes 1 and 2 is given by:

$$r_1 = \sqrt{\frac{E_S}{2}} h_1 s_1 + \sqrt{\frac{E_S}{2}} h_2 s_2 + n_1, \tag{2.47}$$

$$r_2 = -\sqrt{\frac{E_S}{2}} h_1 s_2^* + \sqrt{\frac{E_S}{2}} h_2 s_1^* + n_2, \tag{2.48}$$

where h_1 and h_2 are the complex channel gains from transmit antenna 1 and 2 to the receive antenna. The receiver receives:

$$\mathbf{y} = \sqrt{\frac{E_S}{2}} \begin{bmatrix} h_1 & h_2 \\ h_2^* & -h_1^* \end{bmatrix} \begin{bmatrix} s_1 \\ s_2 \end{bmatrix} + \begin{bmatrix} n_1 \\ n_2^* \end{bmatrix} = \begin{bmatrix} r_1 \\ r_2^* \end{bmatrix}. \tag{2.49}$$

Rearranging Equation 2.49, the signals after passing through channel are

$$\begin{aligned} r_1 &= h_1 s_1 + h_2 s_2 + n_1 \\ r_2 &= -h_1 s_2^* + h_2 s_1^* + n_2. \end{aligned} \tag{2.50}$$

2.3.2.2 Maximum Likelihood Decoding

The receiver has perfect channel state information (CSI) and h_1 and h_2 are recovered perfectly at the receiver. The combiner of Figure 2.12 combines the received signals as:

$$\begin{aligned} \tilde{s}_1 &= h_1^* r_1 + h_2 r_2^* = \left(|h_1|^2 + |h_2^2|\right) s_1 + h_1^* n_1 + h_2 n_2^*, \\ \tilde{s}_2 &= h_2^* r_2 - h_1 r_2^* = \left(|h_1|^2 + |h_2^2|\right) s_2 - h_1^* n_2^* + h_2^* n_1, \end{aligned} \tag{2.51}$$

and the maximum likelihood detector uses it minimizing the following decision metric:

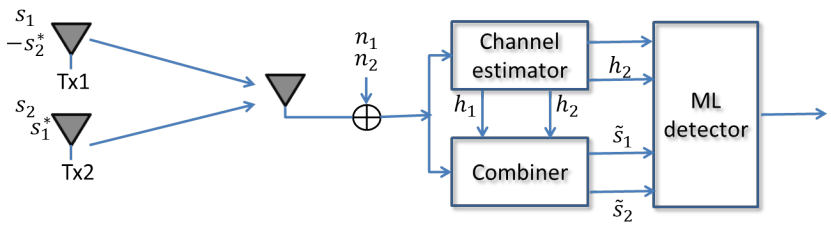

Figure 2.12: Alamouti diversity scheme.

$$|r_1 - h_1 s_1 - h_2 s_2|^2 + |r_2 + h_1 s_2^* - h_2 s_1^*|^2, \tag{2.52}$$

over all possible values of s_1 and s_2.

2.3.2.3 General STBC Schemes

The Alamouti scheme is used in a 2×2 scheme but it can be extended to be used in larger orthogonal space-time block coding (OSTBC). These codes can be designed for any number of transmit antennas with a code rate of 1, provided that only real constellations are used [Jankiraman04]. For example in a $M_T = 4$ system, the orthogonal code is

$$\mathbf{S}_{STBC} = \begin{bmatrix} s_1 & -s_2 & -s_3 & -s_4 \\ s_1 & -s_2 & -s_3 & -s_4 \\ s_2 & s_1 & s_4 & -s_3 \\ s_3 & -s_4 & s_1 & s_2 \\ s_4 & s_3 & -s_2 & s_1 \end{bmatrix}, \tag{2.53}$$

where it uses 4 time slots (columns) to send 4 symbols, so the code rate is 1.

In the case of complex constellations, orthogonal designs with code rate of 1 only exist for $M_T = 2$. STBC codes exist for code rates of 1/2 with any number of transmit antennas. Following the same example of $M_T = 4$, the code used with these complex symbols is

$$\mathbf{S}_{STBC} = \begin{bmatrix} s_1 & -s_2 & -s_3 & -s_4 & s_1^* & -s_2^* & -s_3^* & -s_4^* \\ s_2 & s_1 & s_4 & -s_3 & s_2^* & s_1^* & s_4^* & -s_3^* \\ s_3 & -s_4 & s_1 & s_2 & s_3^* & -s_4^* & s_1^* & s_2^* \\ s_4 & s_3 & -s_2 & s_1 & s_4^* & s_3^* & -s_2^* & s_1^* \end{bmatrix}. \tag{2.54}$$

Note that with this scheme is necessary to use 8 time slots to send 4 symbols, so the code rate is 1/2 .

2.4 Chapter summary

There are several models and techniques described in the literature to simulate and assess wireless channels. A description of the available models had been done in this chapter, remarking their characteristics, advantages and weak points. Two scenarios have been considered: industrial and vehicular environment. Physical, analytical and standardized models have been described and reviewed as the basis of Chapter 3. Wireless systems, such as multiantenna schemes and space-time block coding have also been analyzed for their use in Chapters 5 and 6.

Chapter 3

Wireless channel model for inside train carriage communications

3.1 Introduction

As mentioned in Chapter 2, it is important to know the environment where the wireless system will be used in order to design new transmission methods. With this knowledge, a channel model can be generated and used to simulate and evaluate the performance of the transmission scheme before testing it in a real environment. This chapter focus on an inside train carriage wireless scenario and novel channel model is proposed, which will be later used in simulations of Chapter 5 and 6.

3.2 Target scenario

The channel to study in this research project is a wireless channel inside train carriages. There is not to much references of this kind of wireless channel in the literature. In [Unterhuber16], a survey of channel measurements and models is done and a study of propagation characteristics for a wireless communication system within a high-speed train is carried out in [Kita09]. This study together with [Dong10] and [Chiu10] are the starting points of the work described in this chapter.

The analyzed environment is composed mainly of metallic material which generates multiple propagation paths from transmitter to receiver thanks to reflections in the metal. The elements inside the car cause the shadowing of the signal. In [Kita09] the authors state that this metallic environment creates a waveguide effect of the propagation, making the pathloss (PL) lower than in a free space environment, and very different from the ITU-R P.1238-5 recommendation for office environments, proving that inside train wireless channel is very different from these typical channel models. Propagation losses of the ITU-R recommendation P.1238-5 are given by Equation 3.1.

$$L_{total} = 20\log_{10} f + N\log_{10} d + L_f(n) - 28 \ \ (dB), \tag{3.1}$$

where

- N is the pathloss coefficient due the distance.
- f is the frequency in MHz.
- d separation between emitter and receiver in meters ($d > 1m$).
- L_f is the penetration loss factor in ground (dB).
- n number of floors between transmitter and receiver ($n \geq 1$).

The coefficients to be used in the Equation 3.1 from recommendation P.1238-5 are in Table 3.1.

Frequency	**Residential building**	**Office building**	**Commercial building**
900 MHz	-	33	20
1,2-1,3 GHz	-	32	22
1,8-2 GHz	28	30	22
4 GHz	-	28	22
5,2 GHz	-	31	-
60 GHz	-	22	17
70 GHz	-	22	-

Table 3.1: Pathloss coefficient N according to [ITU-R07].

The comparison of Free Space Losses (FSL) in an office environment following the ITU recommendation and the PL obtained by measurements in a train car can be observed in Figure 3.1. It shows that the measured environment does not match with the expected free space losses, nor with the pathlosses expected inside an office.

As mentioned before, the measurements made in [Dong10] has been the starting point. In [Dong10] the PL and the delay spread (DS) inside train carriages are obtained. The DS is defined as the square root of the second central moment and is calculated as follows:

$$\sigma_\tau = \sqrt{\overline{\tau^2} - (\overline{\tau})^2}, \tag{3.2}$$

where

$$\overline{\tau} = \frac{\sum_\tau |h_\tau|^2 \tau}{\sum_\tau |h_\tau|^2}, \tag{3.3}$$

and

$$\overline{\tau^2} = \frac{\sum_\tau |h_\tau|^2 \tau^2}{\sum_\tau |h_\tau|^2}, \tag{3.4}$$

where h_τ is the channel response in the instant τ.

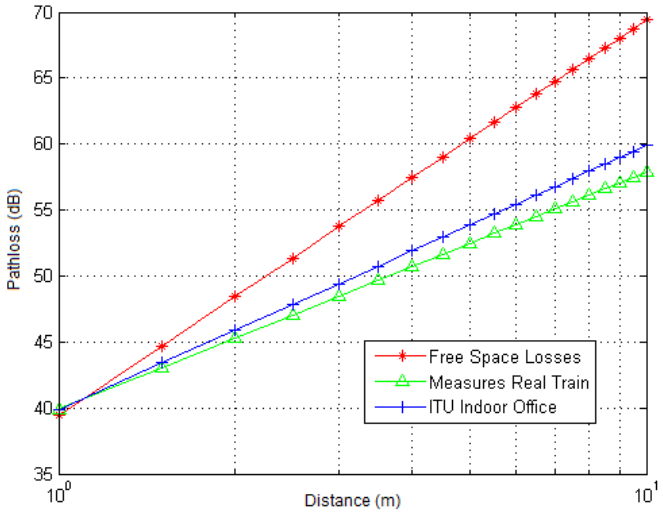

Figure 3.1: Comparison of PL: train, free space and office.

These two values (PL and DS) are the reference values to obtain the results of this work.

3.3 Ray-Tracing Simulation

The channel model proposed in this chapter has been developed using a deterministic physical model. The most relevant dimensions and characteristics of a train are determined by its geometry. Dimensions, walls, fixed objects and their characteristics are preset and the variance factor of the system is given by people moving inside the train and external fluctuations due to electromagnetic noises or possible couplings of energy from outside to inside or vice versa [Kita09]. The first design has been based on the geometry of a train as proposed in [Dong10] and sketched in Figure 3.2.

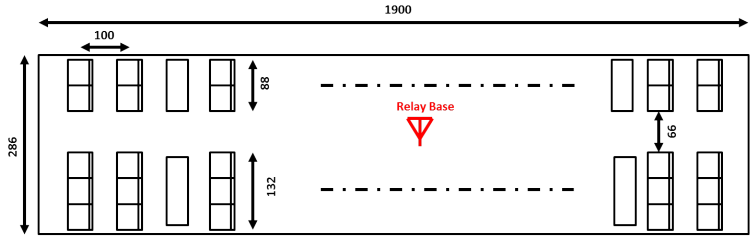

Figure 3.2: Train plant diagram used to generate the model (distances in cm.)

The geometry and the elements of the scenario must be defined to create the model. The

train carriage will be defined as a high conductivity metal structure (iron) with conductivity $\sigma = 10^7$ and electrical permittivity $\varepsilon_r = 1$. Furniture elements are designed with a low conductivity material ($\sigma \approx 0$) and electrical permittivity $\varepsilon_r = 3.2$. The proposed model approaches the structure used in [Chiu10]. In this case the structure is a passenger cabin of a medium-sized aircraft, which is almost the same dimensions as the considered train carriage.

Using the RT EM.CUBE simulation software of EMAG Technologies [Emag17], the structure under study is generated. The input of the simulator is the geometry of the environment to be simulated, as well as some parameters such as frequency (2.35 GHz), antenna polarity (vertical), antenna type (omnidirectional), emission power (30 dBm) and the locations of the transmitters and receivers. In Figure 3.3 a cut of the model created in the software of the RT simulator can be observed. The green points are the receivers distributed throughout the train at a height of 0.8 meters from the floor. This height is taken as the average height of a receiver placed on a table or being used by a seated person. The blue dot near the ceiling represents the omnidirectional access point transmitter. The light blue structures represent the furniture, that is, the obstacles that the rays will find in their paths.

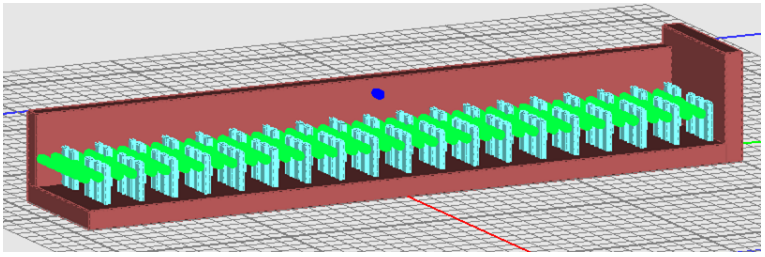

Figure 3.3: 3D model of a train carriage.

The RT simulation outputs all the necessary data to obtain the values, both at system level and at link level. The values returned by the software for each emitter-receiver pair n, m are:

- Number of different paths of the rays.
- Delay of each path.
- Power received from each different ray in each receiver (in function of the polarity).
- Departure angle of each ray.
- Arrival angle of each ray.

In Figure 3.4 a detailed screenshot of the simulation can be observed. The purple lines are the representations of the different paths that are following the rays bouncing on walls and objects. These rays are attenuated and blocked by the furniture of the train. It can be

observed that the propagation above the furniture is greater than in the lower part of the car due to the shadowing created by the furniture.

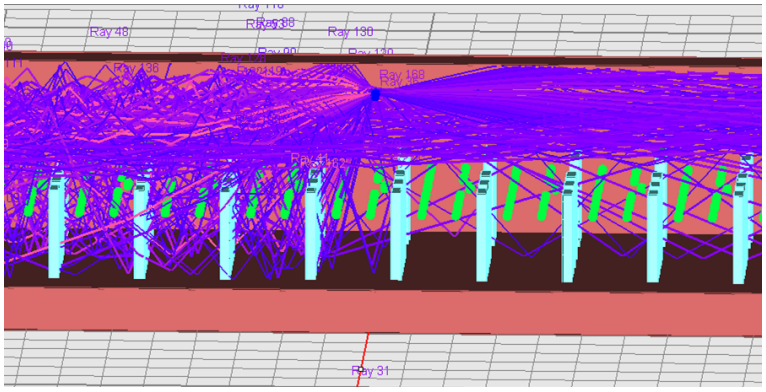

Figure 3.4: Screenshoot of the simulator and ray representation.

The advantages of this geometry-based modeling is the accuracy of the resulting model, which is conditioned by the precision when defining the real environment geometry inside the simulator. Factors not introduced into the simulator will cause a deviation from the actual system.

The output of the RT simulator generates all the detailed information for each ray. Processing this link information using Equation 2.16, responses between each transmitter and receiver can be obtained. The simulator also provides information of the delays of each ray. The DS of the system, which is shown in Figure 3.5 can be obtained using Equation 3.2. It can be observed that the mean of the DS is 32 ns.

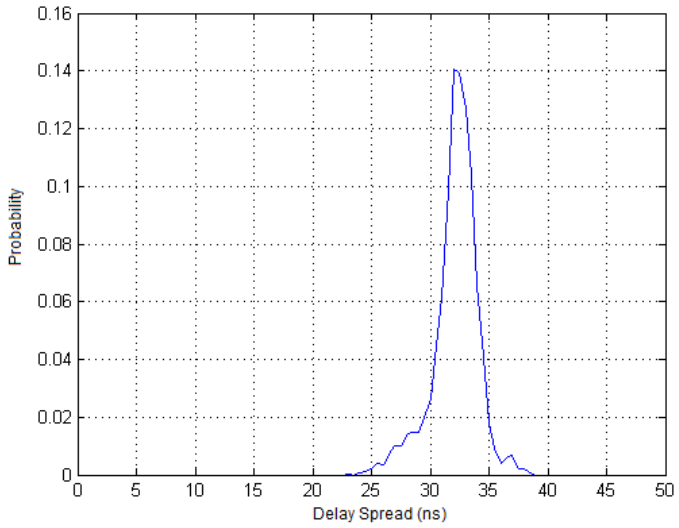

Figure 3.5: Delay Spread of the simulated system using Ray Tracing.

The obtained PL with the RT simulator can be observed in Figure 3.6. The pathloss curve is obtained using the least-squares approximation. The obtained line can be observed

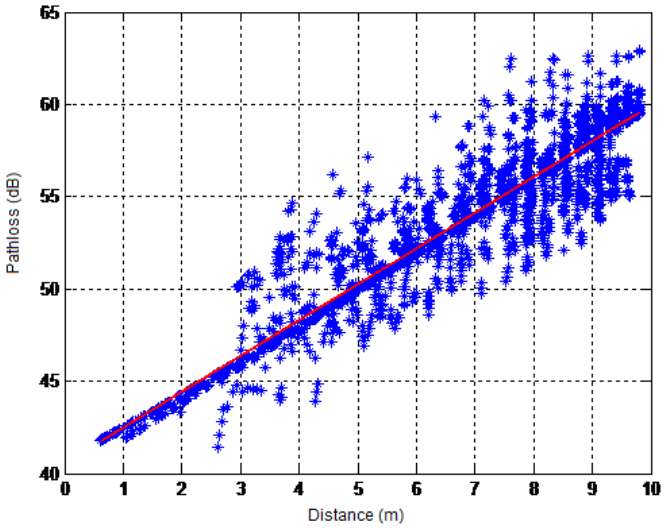

Figure 3.6: Simulated PL using Ray Tracing and Least Squares (LS) approximation.

in red in Figure 3.6 and follows Equation 3.5.

$$PL_{RT} = 40.56 + 19.39\log_{10}(d) \text{ dB}. \tag{3.5}$$

It can be observed that the resulting model is very similar to PL measured in [Dong10]. The comparison between PL of the RT simulator and the PL obtained with measurements are in Figure 3.7 and in Table 3.2. Analyzing the DS, differences can be observed with respect to the measurements done. The RT model obtains a lower dispersion of the DS, but the mean is very close to the measurements. The comparison between the two DS (RT and measurements) can be seen in Figure 3.8. It can be observed that the measured DS has greater dispersion than the obtained using simulation. This deviation is caused by the material and the characteristics of the objects used in the RT simulator.

	Measured PL in [Dong10]	**PL using RT**
Line	$39.9 + 18\log_{10}(d)$	$40.56 + 19.39\log_{10}(d)$
Shadow Fading	LN $\sigma = 2.3$	LN $\sigma = 2.208$

Table 3.2: Comparison between measured PL and obtained PL using RT.

3.4 D2b Winner model

The models defined in Winner also define the channel model inside a train carriage. The channel model is the D2b channel model (indoor train model) and is applicable within high-speed train cars. The transmitter is assumed to be on the roof in the center of the car, and

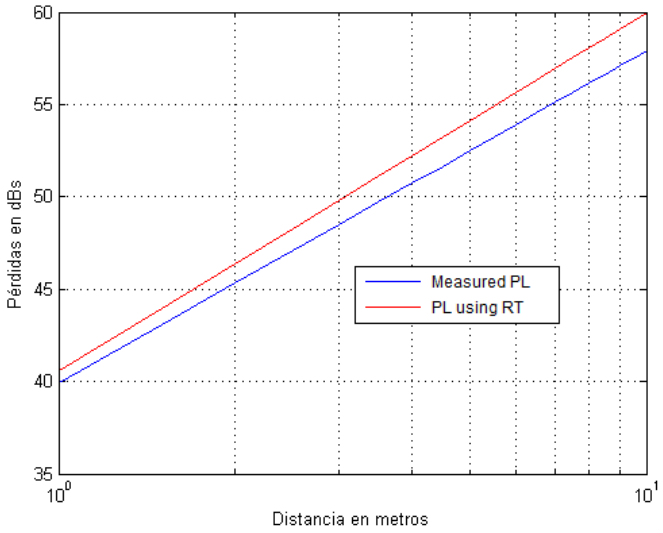

Figure 3.7: Comparison between PL using RT simulator and measurements.

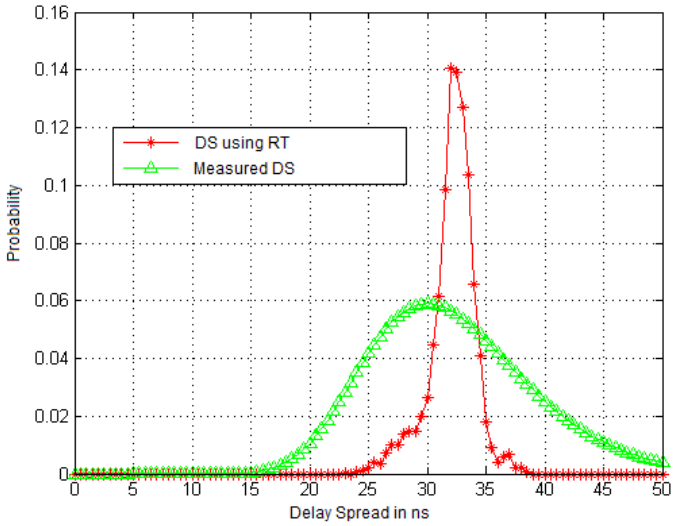

Figure 3.8: Comparison of obtained Delay Spread using RT and the measurements.

there is a high density of furniture (chairs and tables), as in the scenario simulated using RT. In this scenario, NLOS is assumed due the density of furniture. It is also assumed that the crystals are reflective, that is, the rays inside the train do not exit and re-enter the train, they stay inside. The modeled scenario is the one represented as D2b in Figure 3.9. The assumption that the scenario is NLOS can be considered adequate by two reasons. The first reason is the density of furniture, which blocks the direct ray between transmitter and receivers. The second reason is that even having LOS, the rays arriving to receiver due the reflections in the metallic environment are so many and of such power that the LOS is negligible in proportion. This statement was postulated and proven in [Ouyang08].

Winner models this scenario in the same way as the A1 NLOS scenario, that is, as an

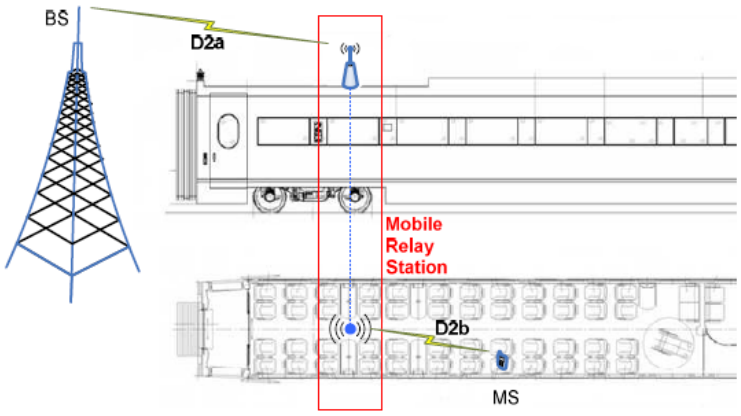

Figure 3.9: D2b propagation scenario inside a train carriage [Pekka07b].

office scenario with no direct line of sight. Within the office models, the model used is the model of a corridor without direct line of sight. The PL of the A1 NLOS Winner model is given by Equation 3.6.

$$PL_{Winn} = 43.4 + 36.8\log_{10}(d) + 20\log_{10}\frac{f_c[GHz]}{5.0} \quad \text{(dB)} \quad \sigma = 3.5 \quad \text{(dB)}. \tag{3.6}$$

Using the parameters provided by the Winner model, the link-level parameters of an A1 NLOS environment are obtained. The method described in 2.2.4.4 and summarized in the Figure 2.9 has been followed to obtain the parameters. The DS curve obtained with these parameters is plotted in Figure 3.10.

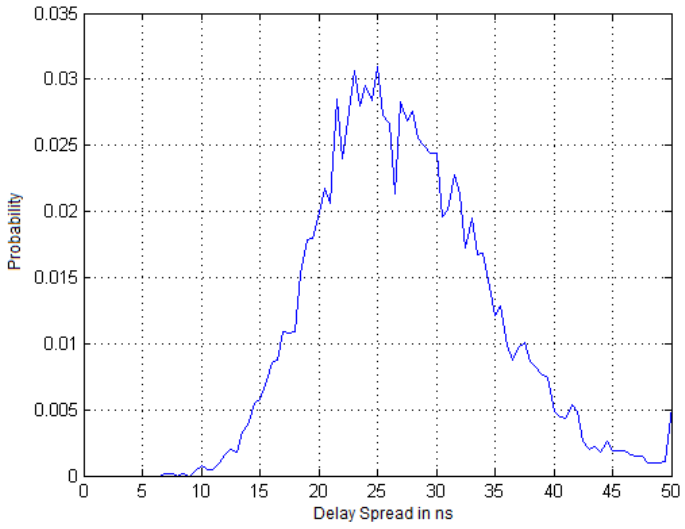

Figure 3.10: Delay Spread of the A1 NLOS Winner model.

It can be seen that the total DS dispersion of the Winner model is larger than that measured in [Dong10]. The mean value of DS is 26 ns who differs from the measurements and simulation. In Section 3.5 the three models (Winner D2b, RT and measurement-based)

will be compared.

3.5 Comparison between different models

The PL and DS from the RT simulation, from the D2b model proposed by Winner and from the measurements obtained in a real car have been obtained so far. In Figure 3.11 PL curves of each model can be observed as comparison.

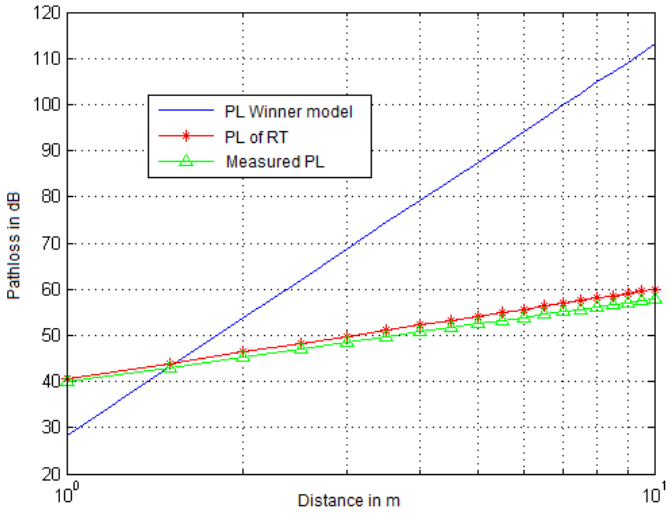

Figure 3.11: Comparison of the 3 PL: Winner D2b, RT and measurements.

It can be observed that the curve provided by the D2b Winner model, which assumes that a train carriage is equal to an indoor model without direct line of sight, could be questioned. The PL curve proposed by Winner is far from the other two curves.

Analyzing the DS, the probability densities of the DS of the three models is plotted in Figure 3.12. In this case the statement that a train carriage model is similar to an indoor NLOS model can also be questioned.

The DS of the three models follows a lognormal curve. In Table 3.3 DS of the three models is shown as a comparison.

	D2b Winner model	**Ray Tracing model**	**Measures**
Mean	26 ns	32 ns	30 ns
mean μ	3.27695	3.4677	3.45
estandar dev. σ	0.265496	0.063279	0.22

Table 3.3: Comparison of DS of the three models.

In [Chiu10] there is a second reference to check the measurements. In this case, the measurements were made inside an airplane passenger cabin. The measurements, structures

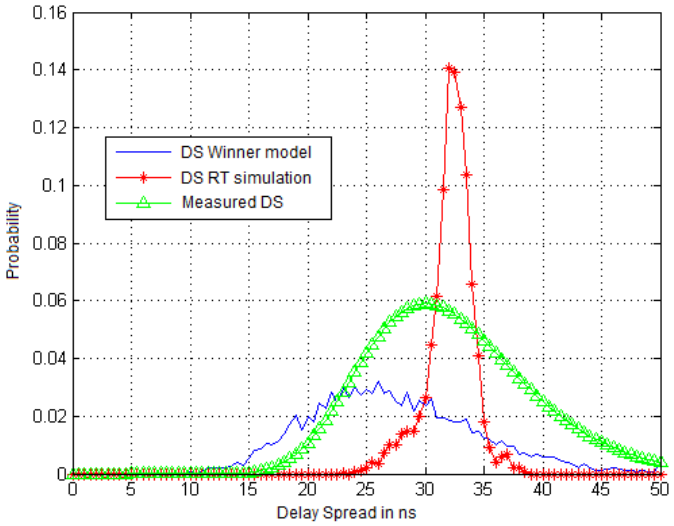

Figure 3.12: DS comparison of the 3 models: Winner, RT and measurements.

and density of furniture, are very similar to the scenario analyzed in this work. In this measurement campaign, it is determined that the DS average is between 29 and 32.3 ns, depending on the receiver power threshold. These data is very similar to that obtained in [Dong10] and the Ray Tracing simulator, far from the values provided by Winner. With these results it can be concluded that the general D2b model of Winner is not suitable for the considered simulated scenario. For this reason new improved values will be obtained to fit better the simulation model to the real scenarios.

3.6 Proposed Winner model for inside carriage wireless communications

The results obtained with the scenario simulated with ray tracing software differ from the model proposed by Winner and is different in some details of the measurements made in [Dong10]. These differences could be due to a mismatch in materials and density used in the actual measurements and in the simulation.

Based on the scenario simulated with RT, the probability distributions of the proposed scenario will be obtained in this section. Using these probability distributions the proposed scenario can be treated as a Winner model, so it allows to simulate it according to the generation methodology described in Figure 2.9, which is described in [Pekka07a].

Thanks to the output values of the RT simulator the distribution probabilities of the different parameters of the Winner model have been analyzed. The Section 3.6.1 will explain the obtained distributions and compare them with those proposed by Winner for the D2b scenario. PL, DS and capacity parameters of the resulting new model will be compared with

the values returned by the RT software.

3.6.1 Parameters of the proposed Winner model

The methodology described in Figure 2.9 will be followed to generate the new Winner model. The distribution of each parameter will be obtained and compared with the one proposed by the D2b Winner model. The most representative parameters of the generated model will be compared with the results obtained with the simulator to validate the model. The following parameters will be defined:

A. Path loss estimation

PL as a function of distance follows the general equation:

$$PL = A + B\log_{10}(d) \quad \text{dB}. \tag{3.7}$$

In Table 3.4, values of A and B of D2b model and the new model are compared.

Model	**D2b Winner model**	**Proposed Winner model**
A	39.42	40.56
B	30	19.39

Table 3.4: A and B values of the path loss.

Resulting values of PL using RT simulation and the line obtained using minimum square approximation are shown in the Figure 3.13.

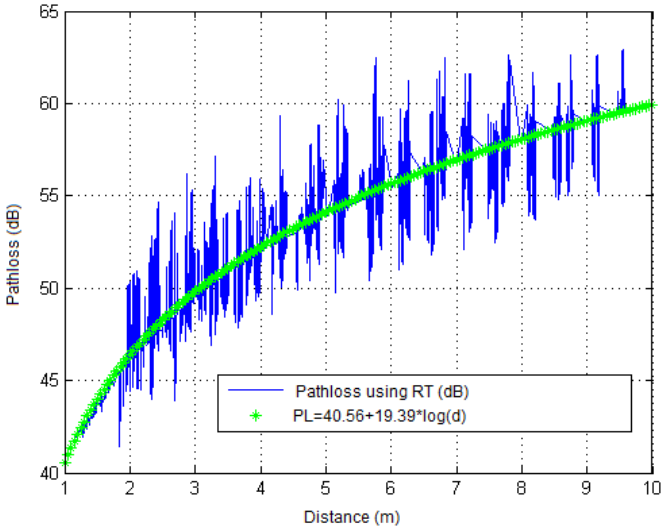

Figure 3.13: Resulting path loss using RT and the model.

B. Number of paths estimation

The Winner model proposes clustering different multipaths in order to have a defined number of paths and multipaths per cluster. The model proposed in this chapter, instead of doing so, it will provide a paths number probability distribution between the transmitter i and the receiver j. This adds complexity to the system but gives more flexibility to the model obtaining all the different delays between each pair of antennas.

The Winner model defines 16 clusters and 20 subpaths per cluster, i.e., a total of 320 fixed paths. In the proposed new model the number of paths between a transmitter antenna and a receiver antenna is modeled as a Rayleigh distribution with $\sigma = 226.159$. The number of paths of the two models is summarized in Table 3.5.

Model	**D2b Winner model**	**New proposed Winner model**
Path numbers	Fixed 320 paths	Rayleigh $\sigma = 226.159$

Table 3.5: Number of paths between a Tx antenna i and a Rx antenna j.

C. Shadowing

The shadowing follows a lognormal (LN) distribution in the D2b Winner model. The simulated shadowing with ray tracing, can fit a LN distribution using least squares approximation but with different values. Values of the D2b model and the new proposed model are in Table 3.6.

Model	**D2b Winner model**	**Proposed Winner model**
LN shadowing	4 dB	2.208 dB

Table 3.6: Shadowing values.

D. Delay generation

The delays of the D2b Winner model are generated following Equation 3.8.

$$\tau'_n = -r_\tau \sigma_\tau ln(X_n), \tag{3.8}$$

where r_τ is the proportionality factor, σ_τ is the DS and $X_n \sim \mathrm{U}(0,1)$, where U(0,1) is the uniforme distribution between 0 and 1. After analyzing the simulation results an using LS fitting, the new proposed model fits better with a Generalized Extreme Value (GEV) distribution like Equation 3.9:

$$f_{GEV}(x|k,\mu,\sigma) = \frac{1}{\sigma}\exp\left(-\left(1+k\frac{(x-\mu)}{\sigma}\right)^{-\frac{1}{k}}\right)\left(1+k\frac{(x-\mu)}{\sigma}\right)^{-1-\frac{1}{k}}. \tag{3.9}$$

The values of k, σ and μ of the GEV distribution are in Table 3.7.

Model	**Delay distribution** (τ_n)
D2b Winner model	$\tau_n = -r_\tau \sigma_\tau ln(X_n) \quad r_\tau = 2.4$ y $\sigma_\tau = 28.5$
Proposed Winner model	GEV con $k = -0.735465$, $\sigma = 35.2042$ y $\mu = 81.4635$

Table 3.7: Delay distribution of the models.

E. Exponential profile of the delay

The Winner D2b model follows a classical exponential profile. The proposed model also follows this exponential profile but with another value of K_p in the Equation 3.10.

$$P_n = \exp\left(-K_p \tau_n\right), \tag{3.10}$$

where values of K_p factor are described in Table 3.8.

Model	**D2b Winner model**	**Proposed Winner model**
$\mathbf{K_p}$	0.0205	0.045

Table 3.8: Exponential factor value.

F. Fast fading generation

The fast fading follows a LN distribution in both models. The values used to generate the LN distribution are summarized in Table 3.9.

Model	**D2b Winner model**	**Proposed new Winner model**
Fast fading	3 dB	2.582 dB

Table 3.9: Fast fading values.

G. Angle generation

The departure and arrival angle of the rays approach to a random distribution both in transmitter and receiver. This is due to the high reflectivity of the materials near the transmitter and receivers, receiving rays from any angle. The approximation is a Gaussian distribution where the σ variance is sufficiently large. This hypothesis will be demonstrated obtaining the channel capacity through simulations and comparing the channel capacity obtained using RT. The angle generation process for model D2b and the new model are summarized in Table 3.10.

Model	D2b Winner model	Proposed new Winner model
Angles	Process described in page 39 in [Pekka07a]	U(0,2π)

Table 3.10: Departure and arrival angle generation.

3.6.2 Comparison and validation of the proposed model

To verify that the proposed novel Winner model in the Chapter 3.6.1 and the results obtained by RT agree, the most significant parameters will be obtained. The resulting model can be used to generate a bidirectional propagation model as described in 2.2.2.1 between one transmitter and one receiver. To exploit the spatial diversity that a reflective scenario like the simulated case can have, the use of multiantenna systems will be analyzed in simulations of Chapter 5 and 6 so a 4x4 MIMO channel model will be generated and simulated using Winner model (Equation 2.16) and compared with RT as an example. The analyzed parameters are power received at the receivers, delay spread and the capacity of the 4x4 MIMO system.

A. Signal power at the receivers

The signal power received at the receivers is shown in Figure 3.14. The power received according to ray tracing simulations is shown in blue (with an offset of -15 dB for better viewing) and in red, the power received thanks to the Winner model created in this chapter.

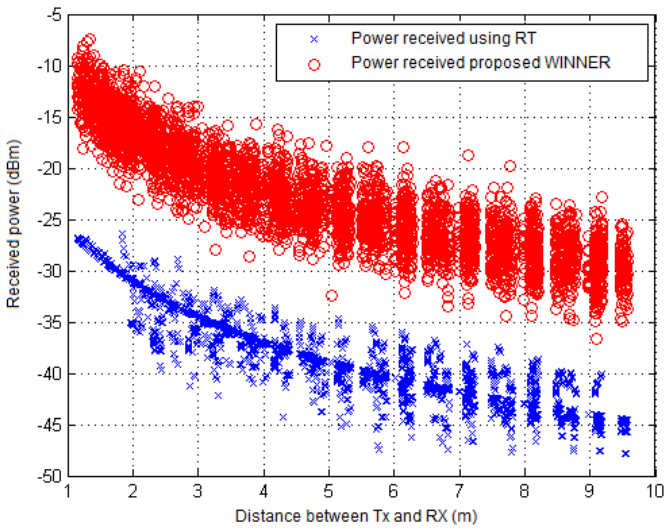

Figure 3.14: Comparison of the received power using RT and the proposed model (-15 dB power offset in RT power for better viewing).

In that figure it can be seen that the exponential power profile of the RT simulator and the profile obtained using the novel Winner model follows the same behaviour, with a exponential power profile and a similar fast fading. RT simulation has less simulated points

than the Winner model so the point cloud is less dense.

The Cumulative Distribution Function (CDF) of the powers is plotted in Figure 3.15; RT simulation is in blue and the proposed model is red. It can be seen than two curves are very similar.

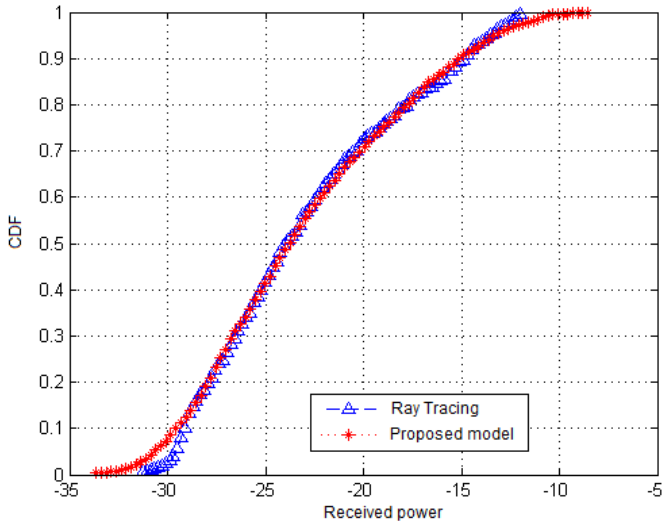

Figure 3.15: Comparison of the CDF of the received power using RT and the proposed model.

B. Delay spread

DS is a good indicator to know if the system is behaving as expected [Hoppe07]. DS of RT simulator in blue and proposed model in red are plotted in the Figure 3.16.

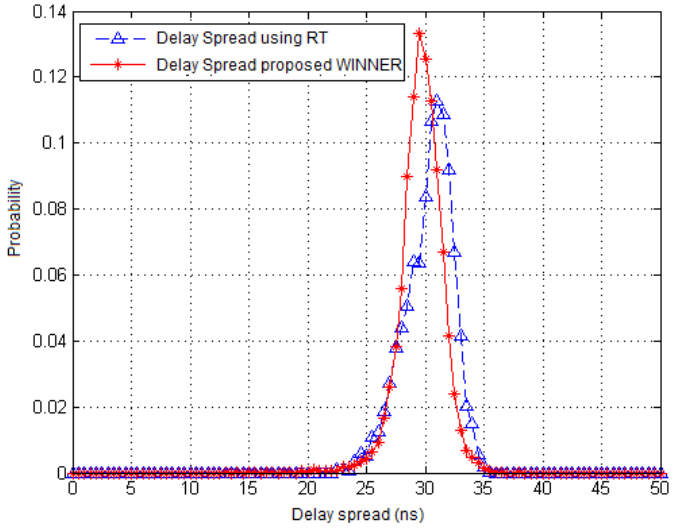

Figure 3.16: Comparison of the DS of the simulation and the proposed model.

CDF of the DS of the RT simulation and the proposed model are shown in Figure 3.17. Both curves are very similar each other validating our model.

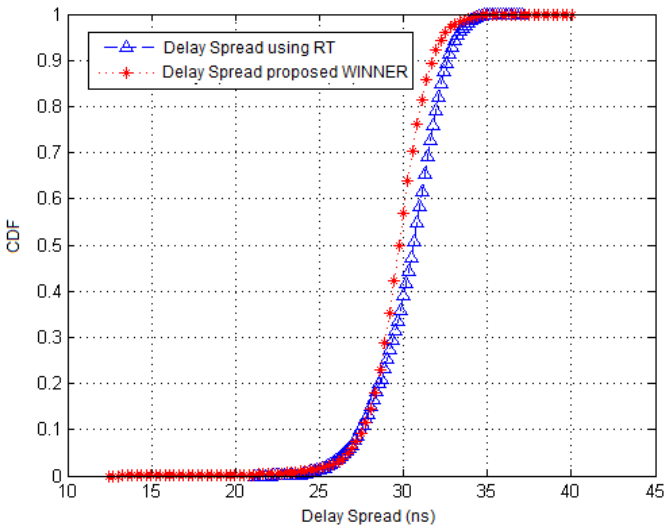

Figure 3.17: DS CDF comparison between RT simulation and proposed model.

C. MIMO channel capacity

In order to validate the rest of parameters, MIMO channel capacity will be obtained and compared. A 4x4 MIMO system is selected to validate the capacity, with 4 transmit antennas and 4 receive antennas. The MIMO capacity is obtained following Equation 3.11.

$$C = \log_2 \ \det\left(\mathbf{I} + \frac{\rho}{M}\mathbf{H}\mathbf{H}^{\mathbf{H}}\right), \tag{3.11}$$

where $\mathbf{H}$ is the $N \times M$ MIMO channel matrix, N is the number of antennas at the receiver and M is the number of antennas at the transmitter, while ρ is the signal to noise ratio.

The capacity curves of the system vs distance and the CDF of capacity are plotted in Figures 3.18 and 3.19. The obtained capacities in both models are very close validating the parameters modeled in this chapter.

The proposed new model follows the same behavior as the RT simulations validating that the RT simulation and the new proposed Winner model are equivalent. The new proposed Winner channel model will be used in this research work in future simulations generated with Matlab to evaluate the performance of the proposed schemes.

3.7 Chapter summary

Following the analysis of wireless models of Chapter 2 and after describing different ways to model a wireless channel, the Winner methodology is chosen to propose a novel train

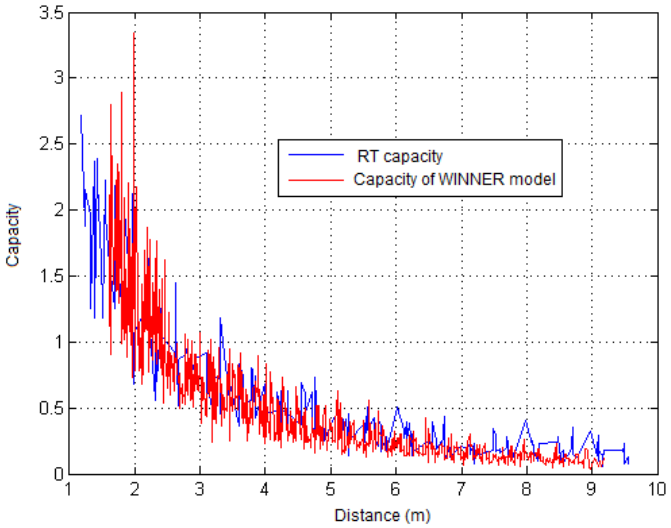

Figure 3.18: System capacity as a function of the distance.

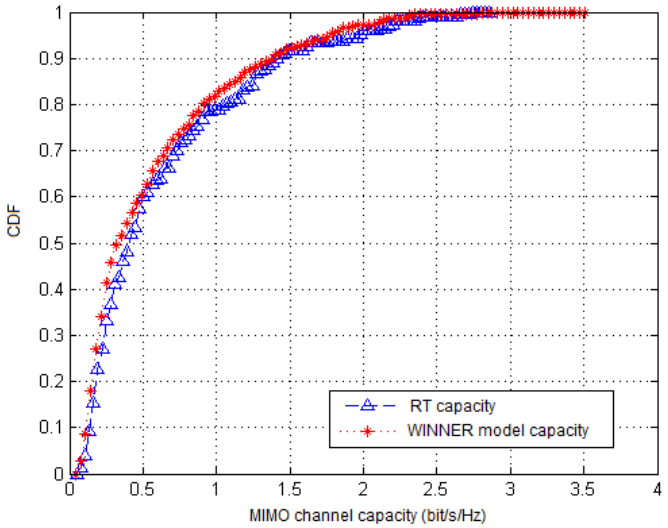

Figure 3.19: CDF of capacities of the proposed model and the RT simulation.

carriage wireless channel model. Winner models consider most of the typical wireless channel scenarios but comparing with an empirical channel model of a train carriage [Dong10] there are significant differences between the proposed D2b Winner model and measurements. A physical simulation based on Ray Tracing has been done with the aim to obtain a more accurate model compared with the empirical data. Based on the empirical measurements, the physical dimensions and parameters of the propagation environment of a train carriage, a mathematical model has been proposed based on the Winner model. The obtained novel Winner model to be used inside train carriages has led to the publication [Arruti13].

Chapter 4

Unequal Error Protection using LDM in time critical applications

4.1 Introduction

Layered Division Multiplexing (LDM) technology [Zhang16] is a non-orthogonal multiplexing technology that differs from traditional time division multiplexing (TDM) or frequency division multiplexing (FDM). An LDM based system uses a layer-based system to simultaneously transmit different signals using the same time, number of antennas or frequency.

LDM can support N different layers to transmit N different information frames in the same time or frequency slot. This type of technology is being adopted as one of the technology enablers for the new generation of digital terrestrial television transmission system called Advanced Television Systems Committee 3.0 (ATSC 3.0) [Zhang14].

As mentioned before, LDM is based on transmitting information in different layers where the signals may have different transmission powers and modulation schemes, with different level of reliability depending on the service they are distributing. An example of a two-layer LDM transmissions is shown in Figure 4.1 where a QPSK modulation is represented over BPSK and QPSK in Figure 4.1a and 4.1b respectively.

The use of several layers to transmit information sharing the same time and bandwidth was introduced by [Bergmans74] as a superposition encoding, although the computational power needed to make successive cancellations made its implementation impossible. Thanks to the advances in processing cores, the implementation of such systems can be carried out nowadays.

The goal of this chapter is to analyze the viability of an LDM based transmission system to increase the throughput and reliability of the communications in railway scenarios. Extra protection can be added to the system using Unequal Error Protection (UEP) in different layers. The scenario to be analyzed is a vehicular environment, specifically targeted at an implementation of a reliable wireless Train Control and Monitoring System (TCMS). There are two types of data in a TCMS system; the train control data, considered to be

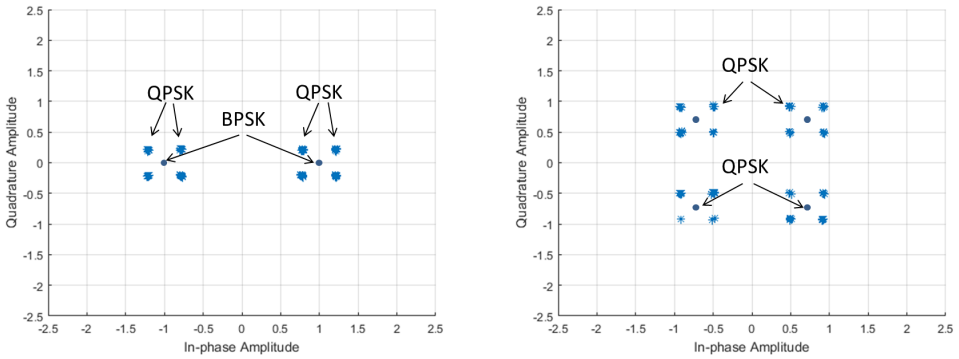

(a) QPSK over BPSK (b) QPSK over QPSK

Figure 4.1: LDM scheme examples.

critical, and the monitoring data, which is less sensitive to the packet losses. Sometimes this monitoring data can coexist with multimedia information for the passengers. The control information is considered critical because it transmits sensor and actuator information of the train. The viability of replacing current TDM and FDM systems by an LDM system will be analyzed, maintaining the control data error rate below a certain threshold to ensure vehicle reliability while non-critical information (monitoring and multimedia) is transmitted targeting a determined throughput according to the service to be transmitted.

4.2 Layered Division Multiplexing - LDM

As mentioned in Section 4.1, two types of data will be considered in the proposed intra-vehicular wireless system: critical and non-critical. Traditional systems use TDM or FDM to transmit different streams, where each type of information uses a slot of time or a frequency band. In an LDM system, the different types of data could occupy all available bandwidth (BW) and full available time to transmit but using different layers. For simplicity, the LDM system will be compared with TDM, since the comparison with FDM is identical.

The analyzed wireless channel is a dispersive channel, so an Orthogonal Frequency Division Multiplexing (OFDM) based transmission is chosen. It will be assumed that the TDM system and the LDM system will use an OFDM system with K subchannels, where S subchannels transmit signal.

An LDM signal is generated as an overlay of two signal layers. If the k-th subcarrier is considered, the generated LDM signal will be [Zhang16]

$$X_{LDM}(k) = X_{UL}(k) + g \cdot X_{LL}(k), \tag{4.1}$$

where $X_{UL}(k)$ is the upper layer (UL) symbol, $X_{LL}(k)$ is the lower layer (LL) symbol and $X_{LDM}(k)$ is the generated LDM symbol. The power of the LL relative to the power of the

UL is defined by the constant g, which is defined as the injection level. Varying injection level g, power of different layers that compose the LDM symbol can be assigned. The g value is a real value that fulfills $0 \leq g \leq 1$. It is clear that if the injection level is $g = 0$, LL symbol is ignored and an LDM system becomes a single layer scheme.

The transmitted symbols will propagate through a channel whose response for the k-th subcarrier will be $H(k)$ and the received symbol for the k-th subcarrier will be

$$Y(k) = X_{LDM}(k) \cdot H(k) + N(k). \tag{4.2}$$

Combining Equation 4.1 with Equation 4.2, the received symbol in the receiver is expressed as:

$$Y(k) = X_{UL}(k) \cdot H(k) + g \cdot X_{LL}(k) \cdot H(k) + N(k), \tag{4.3}$$

where $Y(k)$ is the received symbol, $X_{UL}(k)$ is the UL symbol, $X_{LL}(k)$ is the LL symbol, $H(k)$ is the channel response and $N(k)$ is the channel noise, all referred to the k-th subcarrier.

The receiver can receive and decode both the UL and LL, depending on the information is awaiting. Critical information is transmitted in the UL so the receivers who expect to receive critical information will decode the UL and ignore the non-critical information contained in the LL.

In order to decode the UL, the receiver processes the information received in $Y(k)$ (Equation 4.3) considering the information received in the LL as an extra noise that is added to the channel's noise. The symbol received at the UL is shown in Equation 4.4.

$$Y(k) = X_{UL}(k) \cdot H(k) + N_{UL}(k), \tag{4.4}$$

where,

$$N_{UL}(k) = g \cdot X_{LL}(k) \cdot H(k) + N(k). \tag{4.5}$$

That way the UL receiver can be as simple as a low-cost zero-forcing receiver that needs to estimate the $X_{UL}(k)$ symbol using Equation 4.6.

$$\bar{X}_{UL}(k) = \frac{Y(k)}{\hat{H}(k)}, \tag{4.6}$$

where $\hat{H}(k)$ is the estimated channel response and $\bar{X}_{UL}(k)$ is the estimated UL symbol at the receiver.

The LL receiver needs to perform more complex operations than the UL receiver to decode the LL. The LL receiver must perform signal cancellation after estimating the transmitted UL symbol $\bar{X}_{UL}(k)$ using Equation 4.6. In the LL receiver the detection of the UL symbol

is obtained by doing the equalization, demodulation, deinterleaving and decoding of the channel, obtaining a very precise bit level decoding. The receiver then needs to perform the inverse operation to regenerate the transmitted UL symbol ($\tilde{X}_{UL}(k)$), that is, perform the channel coding, interleaving and modulation. The complexity of the detection of the UL symbol increases the complexity of the LL receiver but a more reliable estimation of the UL symbol is obtained, which will allow a more reliable detection of the LL symbol. The UL symbol estimation can be done doing a regular symbol detection without a bit level decoding, simplifying the process, but the reliability of the detected symbol UL and thus the following LL symbol is lower.

After estimating $\tilde{X}_{UL}(k)$, the estimation of the LL symbol is carried out as

$$\bar{X}_{LL}(k) = \frac{1}{g} \cdot \frac{\left(Y(k) - \tilde{X}_{UL}(k) \cdot \hat{H}(k)\right)}{\hat{H}(k)}, \tag{4.7}$$

where $\tilde{X}_{UL}(k)$ is the regenerated UL symbol on the receiver and $\bar{X}_{LL}(k)$ is the estimated LL symbol.

As can be seen in Equation 4.6, one of the advantages of LDM systems is that the UL receiver can be a standard receiver that estimates the channel response $\hat{H}(k)$ and decodes the received symbol. This receiver will treat the information from the LL as interference. The disadvantage is that the received noise is increased, reducing the signal to noise ratio (SNR).

The LL receiver must be a more complete and complex receiver. This receiver must decode and regenerate the UL symbol before decoding the LL symbol as it can be seen in Equation 4.7, increasing the complexity of the receiver. If the UL is not decoded correctly, this erroneous symbol will generate an interlayer error that will affect the detection of the LL symbol.

In the case of critical and non-critical information traffic (control and multimedia), the simplest receiver (UL) can be used as a low-cost receiver used in critical sensors, whereas the LL can be used for more complex multimedia or monitoring receivers.

4.3 Capacity comparison between LDM and TDM/FDM

The use of LDM instead of the traditional TDM/FDM systems is proposed after analyzing the theoretical capacity of LDM. The capacity of a two-layer system such as the one proposed in this thesis, i.e., the capacity of UL with critical information C_{UL}^{LDM} and the capacity of LL with non-critical information C_{UL}^{LDM} are calculated using Equation 4.8 and Equation 4.9 [Zhang16] where expectation is taken over $|H|^2$.

$$C_{UL}^{LDM} = E\left[\log_2\left(1 + \frac{P_{UL}\cdot|H|^2}{P_{LL}\cdot|H|^2 + P_n}\right)\right], \tag{4.8}$$

$$C_{LL}^{LDM} = E\left[\log_2\left(1 + \frac{P_{LL}\cdot|H|^2}{P_n}\right)\right], \tag{4.9}$$

where C_{UL}^{LDM} is the theoretical capacity of the UL in LDM, C_{LL}^{LDM} is the theoretical capacity of the LL in LDM, P_{UL} is the power of the UL, P_{LL} is the power of the LL, H is the channel response and P_n is the noise power.

It can be observed that the capacities of UL and LL have a non-linear dependence with the power level assigned to each layer.

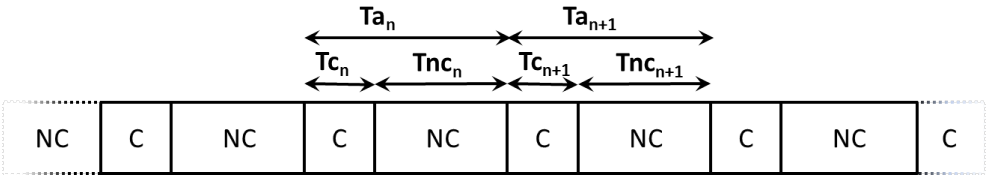

Figure 4.2: Time division in TDM system.

In a TDM or FDM system channel capacity of a particular service is directly proportional to the time or frequency reserved for that service. If a TDM system is used to transmit critical information shared with non-critical one, transmission time is divide in time slots, where every n time slot, critical data will allocate T_c time to send data and T_{nc} time will be allocated to transmit non-critical data as seen in Figure 4.2. Following this notation the capacity to send critical data in TDM is given by Equation 4.10.

$$C_c^{TDM} = C\cdot\frac{T_c}{T_a}, \tag{4.10}$$

where C is the total channel capacity and $T_a = T_c + T_{nc}$ is total time duration. Following the same criteria the time slot assigned to send non-critical information is T_{nc} and the capacity is

$$C_{nc}^{TDM} = C\cdot\frac{T_{nc}}{T_a}. \tag{4.11}$$

In Equations 4.10 and 4.11, C is the total channel capacity where in a selective channel is [King14]

$$C = E\left[\log_2\left(1 + \frac{P_s\cdot|H|^2}{P_n}\right)\right], \tag{4.12}$$

where P_s is the signal total power, P_n is the noise power and H is the channel response.

Capacity relation between two layers in a TDM system is directly proportional to the time reserved to transmit the information of each layer or the power associated to each layer

as shown in Equations 4.10 and 4.11. The capacity of the two layers in an LDM system does not follow a linear relationship as in TDM as it can be seen in Equation 4.8 and Equation 4.9. A comparison of the capacity of a TDM system versus an LDM system has been plotted in Figure 4.3.

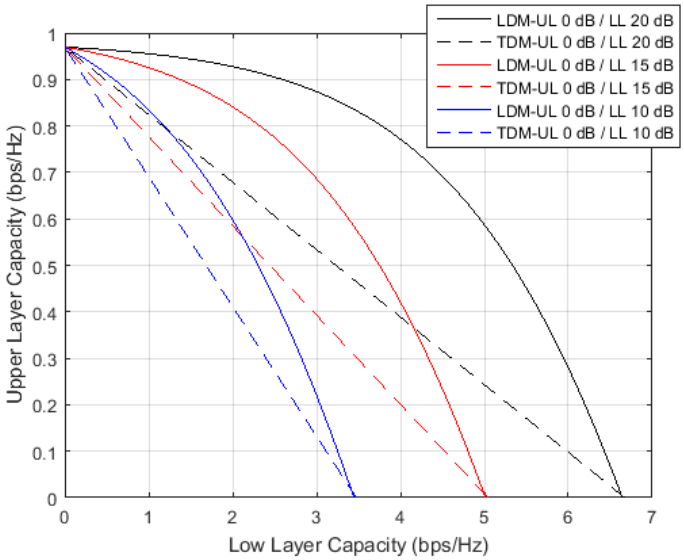

Figure 4.3: LL vs UL capacity using ideal codification over a gaussian channel. SNR of the UL is fixed to 0 dB and SNR of the LL varies from 20 to 10 dB.

Three possible scenarios have been considered in Figure 4.3. In the three possible scenarios, the UL receiver or the critical data receiver is located at a position where its SNR is 0 dB. This assumption assumes that the receiver is in a hostile localization where the signal reception is weak or has lot of interference, without the possibility to use antennas to provide gain to the received signal. SNR of the LL receiver or non-critical data receiver is 20, 15 and 10 dB in the three different scenarios. The non-critical receiver is located in a place with higher SNR than the critical receiver or has the opportunity to use antennas to provide gain to the received signal. The points located to the left of the figure are the points where there is only UL transmission. On the other hand, the points that are totally to the left are the points where there is only LL transmission.

In terms of capacity, the LDM system always outperforms the TDM system so it can be assumed that it is a good candidate to improve the overall performance of the proposed transmission system. Another characteristics that can be observed in an LDM system is that the capacity compared with TDM increases with the difference of SNR between the two layers [Gómez-Barquero15]. Looking at Figure 4.3, in the LL curve with SNR of 10 dB, it can be seen that, for a capacity of 0.5 bps/Hz of the UL, a capacity of 1.6 bps/Hz is reached for the LL in a TDM system and 2.2 bps/Hz in an LDM system, obtaining 0.6 bps/Hz more in terms of capacity. Analyzing the curve of the LL for SNR 15 dBs at the same point, it can be seen that the capacity gain is 1.2 bps/Hz, while it increases to 2.2 bps/Hz in the

curve of 20 dBs. However in [Gadkari99] the authors prove that an LDM system does not always outperform a TDM system in an actual implementation. Moreover the authors show that in the presence of suboptimal channel coding TDM may be more efficient than LDM, so selection of suitable channel coding is an important part of the study.

4.4 Proposal for using LDM with Unequal Error Protection in intravehicular networks

4.4.1 Application scenario

The scenario under study in this thesis is the wireless transmission of critical control data and non-critical multimedia data within trains. It is proposed to replace the usual TDM/FDM multiplexing transmission techniques by LDM, which has been proposed in other scenarios such as the next generation of digital terrestrial television (DTT) [Fay16]. In these type of scenarios the LDM system is used to send mobile services in the UL and fixed services in the LL. In DTT transmissions, Low Density Parity Checks (LDPC) codes are used for channel coding due the length of the transmitted frames. In an intra-vehicular transmission scenario the use of turbo codes may be a more suitable implementation due the short length of the transmitted frames. In this thesis, the capacity increase provided by an LDM system will be used to give extra protection to critical control data and increase throughput of the non critical data.

The scenario under study is a train car equipped with a wireless transmission system as can be seen in Figure 4.4. For simplicity, a downlink scenario is considered. The transmitter is located on the ceiling in the center of the car to ensure coverage throughout the car. Within the car there are two types of receivers: multimedia systems (MM), where the information transmitted to them is non-critical data such as passenger information, and control systems, where the transmitted data is information related to the train safety and therefore is critical information, such as brake, doors or traction system orders. Many of the control systems are usually located in places with difficult access and high interference such as the metallic box of the traction system or sensors and actuators located under the train chassis. On the other hand, the multimedia systems must be located in visible places to the passengers, so their location presents a high SNR. In the rest of the thesis, the term critical data will be used instead of control traffic, and non-critical data instead of multimedia traffic.

In a TDM system, the critical and non-critical data information share the same time slot as has been shown in Figure 4.2. In the considered system, critical data must be sent every T_a period with T_c length, ensuring error free transmission. Channel coding with code rate K_c^{TDM} and QoS systems at the upper layers are used to ensure this. The analysis of these QoS mechanisms are out of scope of this thesis. The hypothesis is that using LDM

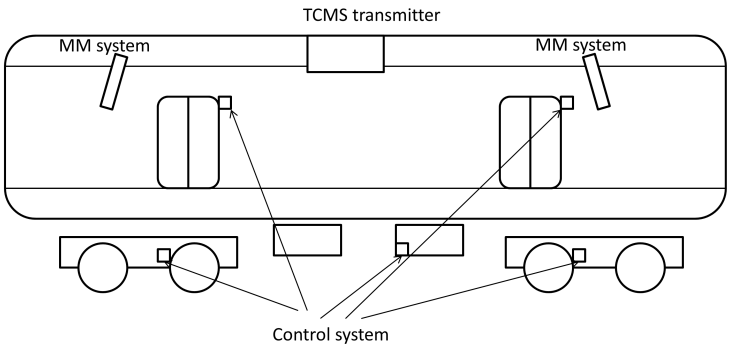

Figure 4.4: Example of a train scenario where the critical control systems are in hostile environments and non critical multimedia (MM) systems are located near the transmitter.

to send both critical and non-critical data in every time slot T_a, Unequal Error Protection (UEP) can be used to add reliability to the critical data while the non-critical data can have higher throughput or reliability depending of the application. The term UEP implies that resources available to protect data are not equally distributed among each bit stream, so each bit stream has different protection against noise.

In the case of LDM, in each time slot T_{a_n} critical and non-critical data share the same time slot as seen in Figure 4.5. Hence, critical data has the chance to use extra T_{nc} time to send more data and non-critical data has T_c time to send extra data. The critical data will be mapped in the UL who will have higher power allocation than LL but otherwise extra noise is added due the LL data. The extra T_{nc} time to send critical data will be used to obtain a lower code rate K_{UL}^{LDM} than TDM, i.e. $K_{UL}^{LDM} < K_c^{TDM}$. The hypothesis is that maintaining the maximum data rate of the critical data and using code rate K_{UL}^{LDM}, the total BER of critical data will lower than TDM. This K_{UL}^{LDM} must be able to correct the error introduced by the LL.

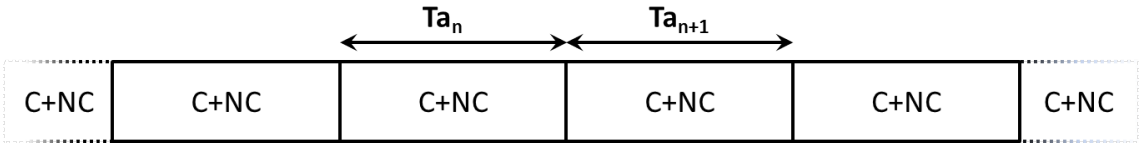

Figure 4.5: Time division using LDM.

4.4.2 Signal model and channel coding

To compare and validate the hypothesis that the proposed LDM sytem with UEP can outperform in terms of bit error rate probability (BER) and throughput a TDM or FDM system, the two multiplexing systems will be compared in a fair way. It is assumed that TDM will use all the available bandwidth. The bitrate in bps of critical data in TDM is given by Equation 4.13.

$$R_c^{TDM} = B \cdot N_c^{TDM} \cdot K_c^{TDM} \cdot \frac{T_c}{T_a}, \tag{4.13}$$

where B is the bandwidth, N_c^{TDM} is the modulation order, K_c^{TDM} is the coding ratio, T_c is the available time to send critical information and T_a the total time slot.

Non critical bitrate in a TDM system is given by Equation 4.14.

$$R_{nc}^{TDM} = B \cdot N_{nc}^{TDM} \cdot K_{nc}^{TDM} \cdot \left(\frac{1 - T_c}{T_a}\right), \tag{4.14}$$

where B is the bandwidth N_{nc}^{TDM} is the modulation order, K_{nc}^{TDM} is the used code rate, $(1 - T_c)$ is the available time to send data and T_a the total time slot.

As the LDM system uses all available time to transmit information the maximum ratio is defined as Equation 4.15.

$$R_{UL}^{LDM} = B \cdot N_{UL}^{LDM} \cdot K_{UL}^{LDM}, \tag{4.15}$$

and the LL bitrate is defined as Equation 4.16.

$$R_{LL}^{LDM} = B \cdot N_{LL}^{LDM} \cdot K_{LL}^{LDM}, \tag{4.16}$$

where B is the bandwidth, N_{UL} and N_{LL} are the UL and LL modulation orders respectively and K_{UL}^{LDM} and K_{LL}^{LDM} are the coding ratios of UL and LL.

Using LDM instead of TDM, the obtained extra bandwidth will be used to add reliability to critical data. The same bitrate used in TDM is maintained to send critical information in LDM, i.e., $R_c^{TDM} = R_{UL}^{LDM}$ and combining Equation 4.13 and 4.15:

$$B \cdot N_{UL}^{LDM} \cdot K_{UL}^{LDM} = B \cdot N_c^{TDM} \cdot K_c^{TDM} \cdot \frac{T_c}{T_a}, \tag{4.17}$$

and if the modulation order $N_{UL} = N_c$ keeps fixed, then Equation 4.18 is obtained from Equation 4.17.

$$K_{UL}^{LDM} = K_c^{TDM} \cdot \frac{T_c}{T_a}. \tag{4.18}$$

The coding ratio that can be used to send UL is now lower while the transmitted information rate keeps fixed. The obtained extra capacity using LDM will be used to obtain reliability of the critical data in order to reduce the BER of the data.

The LL is used to send non-critical data. In this case the obtained extra transmission time is not used to obtain more reliability of the data, but to increase the transmitted data rate in order to increase the throughput. If the obtained extra capacity in LL is used to increase reliability, the obtained extra redundancy would be negligible because $T_c \ll T_{nc}$. In this case if $N_{nc}^{TDM} = N_{LL}^{LDM}$ and $K_{LL}^{LDM} = K_{nc}^{TDM}$ are fixed, then

$$R_{LL}^{LDM} > R_{nc}^{TDM}. \tag{4.19}$$

4.4.3 Performance measurements

To demonstrate that the proposed LDM system improves the performance of current TDM systems in train carriage environments, BER of critical data will be obtained and compared to TDM and LDM. Throughput (Th) of the two systems will be also obtained using Equation 4.20. Throughput is defined as the information data rate that could be sent without errors.

$$Th = R \cdot (1 - P_b)\,, \tag{4.20}$$

where R is the total system bitrate and P_b is the resulting BER.

The goal of the simulations of Section 4.5 is to demonstrate that the proposed alternative method reduces the BER of critical data while it can increase throughput of both critical and non critical data.

In the simulations it is assumed that the critical receivers are located in low SNR locations (0 dB) and the non critical receivers are located in places with medium-high SNR, starting from 0 dB to 20 dB in steps of 5 dB .

4.5 Simulations and results

4.5.1 Simulation scenarios

The simulations were done assuming that the transmitted symbols x_{TDM} and x_{LDM}, using TDM and LDM respectively, have unit transmission power, i.e., $E[||x_{TDM}||^2] = E[||x_{LDM}||^2] = 1$.

In TDM system the fraction of time to transmit critical information (T_c) varies from 0.05 to 0.25 in steps of 0.05, and hence, the available time to transmit non-critical information varies from 0.95 to 0.75. The used coding ratio in TDM for both critical and non-critical data is $K_c^{TDM} = K_{nc}^{TDM} = 1/2$. The chosen modulation to transmit critical information is BPSK ($N_c^{TDM} = 1$) and the modulation used to send non-critical data is QPSK ($N_{nc}^{TDM} = 2$).

In the LDM system the UL uses the same BPSK modulation ($N_{UL}^{LDM} = 1$) and the coding ratio is defined by Equation 4.18 adding extra redundancy to the transmitted layer. For example, if the TDM system uses $T_c = 0.05$ to send critical data, the LDM system transmits the same information in the UL but reducing the coding rate to $1/20 \cdot K_c^{TDM}$, keeping the same bitrate of the critical data. In the case of using $T_c = 0.05$ and $K_c^{TDM} = 1/2$, the equivalent coding ratio used in the LDM scheme is $K_{UL}^{LDM} = K_c^{TDM} \cdot 1/20 = 1/40$. As

mentioned before, the use of turbo codes is proposed instead of the LDPC used in [Zhang14] for ATSC 3.0 due the short length of the transmitted frames.

The transmission scheme used to evaluate LDM in this chapter is a simplified transmission scheme as shown in Figure 4.6. This simplified scenario will be used to prove our first hypothesis, while in Chapter 5 a complete transmission scheme will be used to show final results. This simplified scenario is a baseband system where $x(t)$ symbols are transmitted through the channel to the receiver. The channel model used in the simulations follows a fast-fading Gaussian channel model with zero mean and variance one and the received symbol $y(t)$ is the convolution of $x(t)$ and $H(t)$, with additive gaussian noise.

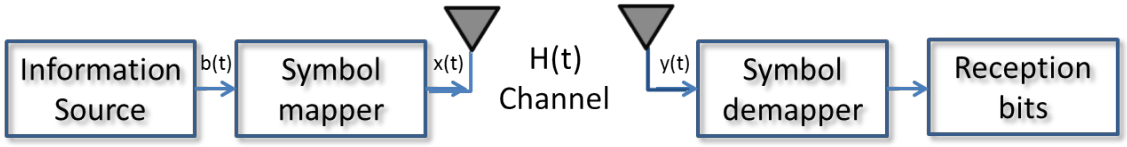

Figure 4.6: Simplified baseband transmission scheme used to evaluate LDM.

4.5.2 Simulation results

The simulations were done based on Monte Carlo simulations. Two types of data have been transmitted: critical data traffic using BPSK and non-critical data traffic using QPSK. In the train carriage scenario, T_c is fixed depending on the type of application and 6 different T_c values are considered, normalized with respect to T_a. Each T_c derives in a K_{UL}^{LDM} following Equation 4.18. Table 4.1 shows a summary of the equivalences between TDM and LDM parameters used in the simulations.

4.5.2.1 Critical data BER vs g

Critical data BER in LDM depends on the coding rate and the chosen injection level g. As described in Section 4.4.1, it is assumed that critical receivers are located in low SNR locations. BER simulation results in function of g and K_{UL}^{LDM} are shown in Figure 4.7. In the simulations it is assumed that the SNR of the critical receivers is 0 dB.

BER of critical data using TDM is plotted with discontinued lines using BPSK modulation. It can be seen that the BER is constant because TDM does not use layer injection; the critical data is transmitted at the assigned time slot T_c.

In Figure 4.7 four BER curves are plotted. The lower curve of the figure corresponds to a critical data transmission using LDM that corresponds in TDM to $T_c = 0.10$, that is, it uses 10% of the available time to send critical data in TDM. It could be observed that with lower T_c to transmit in TDM, there is more opportunity to add coding to the data in LDM, obtaining lower BER curves than TDM. BER of the TDM system is fixed at $2 \cdot 10^{-1}$, but

Data	TDM	LDM	Data	TDM	LDM
Critical	$T_c = 0.05$ $K_c^{TDM} = 1/2$ Bit Rate = 0.025	$T_a = 1$ $K_{UL}^{LDM} = 1/40$ Bit Rate = 0.025	Non-Critical	$T_{nc} = 0.95$ $K_{nc}^{TDM} = 1/2$ Bit Rate = 0.475	$T_a = 1$ $K_{LL}^{LDM} = 1/2$ Bit Rate = 0.5
	$T_c = 0.1$ $K_c^{TDM} = 1/2$ Bit Rate = 0.05	$T_a = 1$ $K_{UL}^{LDM} = 1/20$ Bit Rate = 0.05		$T_{nc} = 0.90$ $K_{nc}^{TDM} = 1/2$ Bit Rate = 0.45	$T_a = 1$ $K_{LL}^{LDM} = 1/2$ Bit Rate = 0.5
	$T_c = 0.15$ $K_c^{TDM} = 1/2$ Bit Rate = 0.075	$T_a = 1$ $K_{UL}^{LDM} = 3/40$ Bit Rate = 0.075		$T_{nc} = 0.85$ $K_{nc}^{TDM} = 1/2$ Bit Rate = 0.425	$T_a = 1$ $K_{LL}^{LDM} = 1/2$ Bit Rate = 0.5
	$T_c = 0.20$ $K_c^{TDM} = 1/2$ Bit Rate = 0.1	$T_a = 1$ $K_{UL}^{LDM} = 1/10$ Bit Rate = 0.1		$T_{nc} = 0.80$ $K_{nc}^{TDM} = 1/2$ Bit Rate = 0.40	$T_a = 1$ $K_{LL}^{LDM} = 1/2$ Bit Rate = 0.5
	$T_c = 0.25$ $K_c^{TDM} = 1/2$ Bit Rate = 0.125	$T_a = 1$ $K_{UL}^{LDM} = 5/40$ Bit Rate = 0.125		$T_{nc} = 0.75$ $K_{nc}^{TDM} = 1/2$ Bit Rate = 0.375	$T_a = 1$ $K_{LL}^{LDM} = 1/2$ Bit Rate = 0.5
	$T_c = 0.5$ $K_c^{TDM} = 1/2$ Bit Rate = 0.25	$T_a = 1$ $K_{UL}^{LDM} = 0.25$ Bit Rate = 0.25		$T_{nc} = 0.5$ $K_{nc}^{TDM} = 1/2$ Bit Rate = 0.25	$T_a = 1$ $K_{LL}^{LDM} = 1/2$ Bit Rate = 0.5

Table 4.1: Equivalence between TDM and LDM parameters used in simulations.

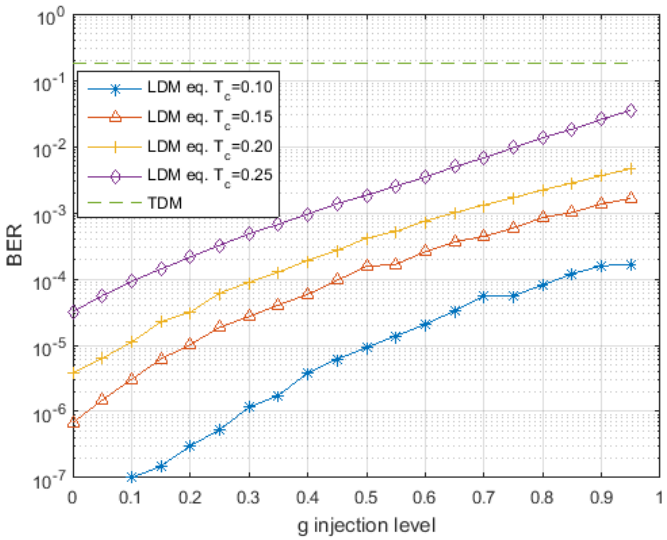

Figure 4.7: Critical data BER with SNR 0 dB vs g.

using LDM, BER below 10^{-7} can be obtained at the point where $g = 0$, i.e., at the point where LL information is not transmitted and BER $\simeq 10^{-4}$ in the opposite end ($g = 1$), where the critical data transmission power is identical to the non critical one.

4.5.2.2 Throughput of non critical data

Focusing on the analysis of non-critical data, its throughput, as defined in Equation 4.20 was simulated, whose results are shown in Figure 4.8.

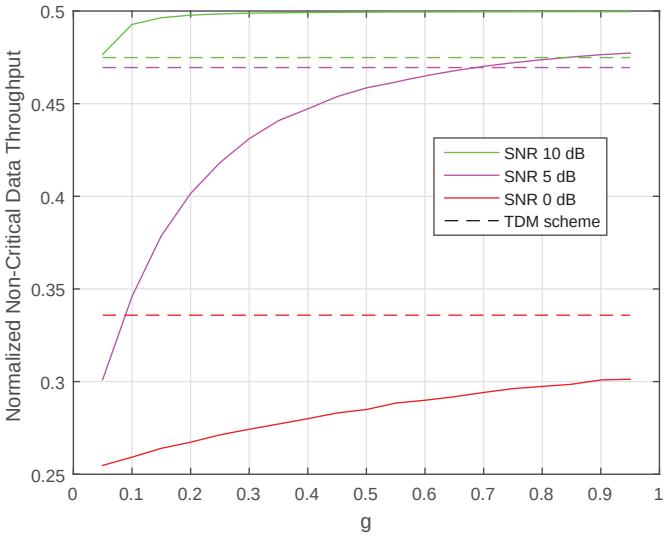

Figure 4.8: Normalized non-critical data throughput vs g with $T_c = 0.05$.

Simulations done in TDM have been represented as discontinuous lines in Figure 4.8 whereas the simulations in LDM are represented with solid lines. Different colors represent the different SNR in the non-critical receiver, varying from 0 dBs to 10 dBs in steps of 5 dBs. In Figure 4.8 it is observed that with SNR 0 dBs in the non-critical receiver, the normalized throughput in TDM is higher than the normalized throughput in LDM. It can be seen that the throughput increases as g increases, i.e., more power is allocated to non-critical LL data relative to the critical data UL. In the case of SNR = 0 dB, it can be seen that LDM throughput never outperforms TDM, so it is not a desirable case.

As the SNR of the non critical data receiver increases, there are cases where the throughput curve of the LDM system outperforms the TDM curve. Analyzing the 5 dB curve, it can be seen that in cases where $g > 0.7$, LDM throughput outperforms the TDM system. Below this $g = 0.7$ the TDM system is still preferable to an LDM system in terms of throughput. If the receiver SNR is increased to 10 dB, it can be observed that throughput of an LDM system is higher than TDM for every g so an LDM system is desirable to TDM.

Analyzing the results of the simulations of Section 4.5.2.1 and 4.5.2.2 it can be concluded that for critical data there are values and combinations of T_c, K_{UL}^{LDM} and g for whom BER of an LDM system is lower than TDM, and the throughput is higher. In order to analyze and obtain the cases where the selection of an LDM system is better than a TDM system, the normalized throughput curves of critical data versus non-critical data throughput are analyzed in next section.

4.5.2.3 Throughput comparison of critical and non critical data

For this simulation, the critical receiver stays in a hostile zone with SNR = 0 dB and $T_c = 0.25$ is fixed. The non critical receiver SNR varies from 0 dBs to 20 dBs. The obtained results can be seen in Figure 4.9.

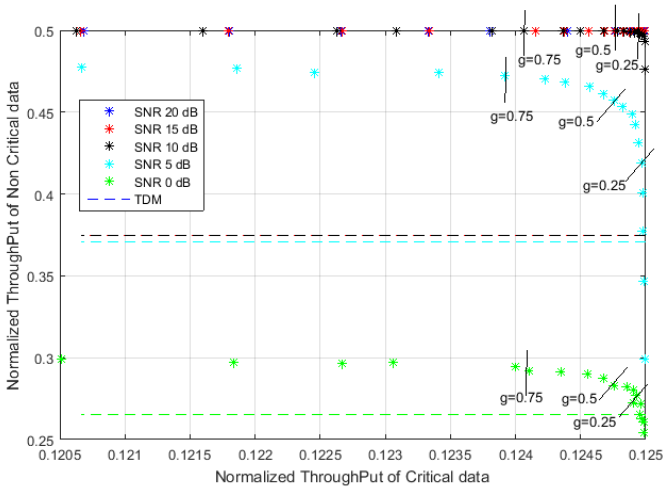

Figure 4.9: Critical data normalized throughput vs non critical data normalized throughput. Critical receiver SNR = 0 dB and $T_c = 0.25$.

$T_c = 0.25$ is equivalent to a $K_{UL}^{LDM} = 5/40$. The normalized throughput of the critical data in TDM is not plotted because it is out of scale, that is, all normalized throughput values of the critical data obtained in LDM are higher than normalized throughput of TDM. TDM throughput is represented by dashed lines, whose value does not vary with g. LDM throughput is represented using asterisks ($*$) and different colors represent the SNR of the non-critical receiver. Each asterisk in the graph represents a specific value of g, covering the complete range of g.

In Figure 4.9 the regions of $0 \leq g \leq 0.25$, $0.25 \leq g \leq 0.5$, $0.5 \leq g \leq 0.75$ and $0.75 \leq g \leq 1$ have been delimited. These regions are marked in Figure 4.9 for each of the different SNRs. As can be seen in the figure, the points where $g = 0$, since there is no LL, the normalized throughput of the non-critical information decreases. As g increases, throughput of non-critical information in LDM increases to become higher than TDM in some cases. If the case of SNR 0 dB in the non critical receiver is analyzed, it is observed that with values of g below 0.25 the LDM throughput does not outperform TDM. With $0.25 \leq g \leq 0.5$ it is observed that the throughput using LDM is higher than in TDM. Increasing g, it is shown that from $g = 0.75$ the throughput practically remains fixed. The conclusion of the analysis is that values of g higher than 0.25 should be chosen. Analyzing the 5 dB curve, practically the same situation is repeated. Below $g = 0.25$ the LDM throughput is not guaranteed to be higher than in TDM but with values of $g > 0.25$ any value of g makes LDM throughput higher than in TDM. In the case under study of $T_c = 0.25$ in the Figure 4.7 it is shown that

for values of $0.25 \leq g \leq 0.5$ the BER curve of the critical data in LDM goes from $3 \cdot 10^{-4}$ to $2 \cdot 10^{-3}$ keeping lower than $2 \cdot 10^{-1}$ of a TDM system. Looking to Figure 4.9 it shows that for values $0.25 \leq g \leq 0.5$ both critical and non-critical data throughput in LDM are above the TDM based system for all SNRs.

The main conclusion is that to maximize critical and non-critical throughput maintaining low BER, the injection level g must be fixed between 0.25 and 0.5 as shown in Figure 4.9.

4.5.2.4 Throughput comparison of TDM and LDM

To highlight the effect of T_c in the associated LDM coding rate and the non-critical data throughput, ΔTh_{nc} versus g is simulated and plotted where ΔTh_{nc} is defined as follows:

$$\Delta Th_{nc} = Th_{LL}^{LDM} - Th_{nc}^{TDM}, \tag{4.21}$$

where Th_{LL}^{LDM} is the LL data throughput using LDM and Th_{nc}^{TDM} is the non-critical data throughput using TDM. TDM curves using $T_c = 0.25$ are plotted with a cross (+) symbol and the equivalent code will be $K_{UL}^{LDM} = 5/40$. Curves using an asterisk ($*$) symbol are $T_c = 0.05$ curves so the equivalent coding rate in LDM will be $K_{UL}^{LDM} = 1/40$. Different colors represent SNR values of the non-critical receiver.

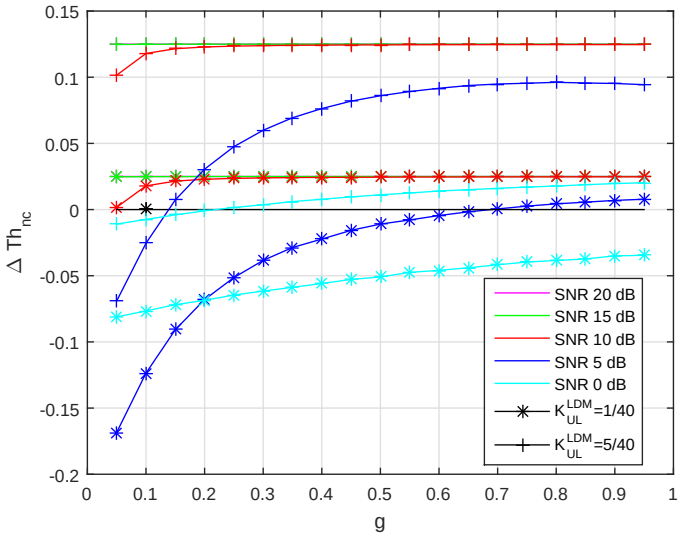

Figure 4.10: LDM throughput gain over TDM throughput.

It is shown that almost all values marked with a cross have a $\Delta Th_{nc} > 0$ which means that for $T_c = 0.25$ almost any value of g will satisfy that the LDM throughput is higher than TDM. Looking to the asterisk curves it is shown that not all values of SNR nor g make $\Delta Th_{nc} > 0$. There are SNR values below 5 dB that never satisfy that the LDM throughput is higher than the TDM. Increasing the SNR of the receiver, it can be observed that any

value of g satisfies that the LDM throughput is higher than the TDM throughput. In Figure 4.10 only the extreme values of simulated T_c-s have been plotted as examples.

4.5.2.5 BER and throughput curves over SNR

In order to show more representative curves, BER curves over SNR were simulated. To simulate and draw such curves T_c and g must be set. According to Figure 4.7 and 4.9, to maximize the throughput and keep the BER low, a value of g located in the upper right side of the curves in Figure 4.9 must be chosen, i.e., a value between $g = 0.25$ and $g = 0.5$. In the previous examples the extreme values of simulated T_c-s have been chosen. In this case, a value of $T_c = 0.15$ is chosen as an intermediate value to analyze its effect and g is fixed to 0.3. With these values, BER curves are plotted for both critical and non-critical data as function of SNR. The throughput of the critical and non-critical data are also represented as function of SNR.

In Figure 4.11, the BER of the critical data versus SNR is plotted. Using LDM and the extra protection that can be added to the system while maintaining the bitrate, BER is decreased. For example, with BER = 10^{-4} the LDM system has a gain of 8 dB over a TDM system.

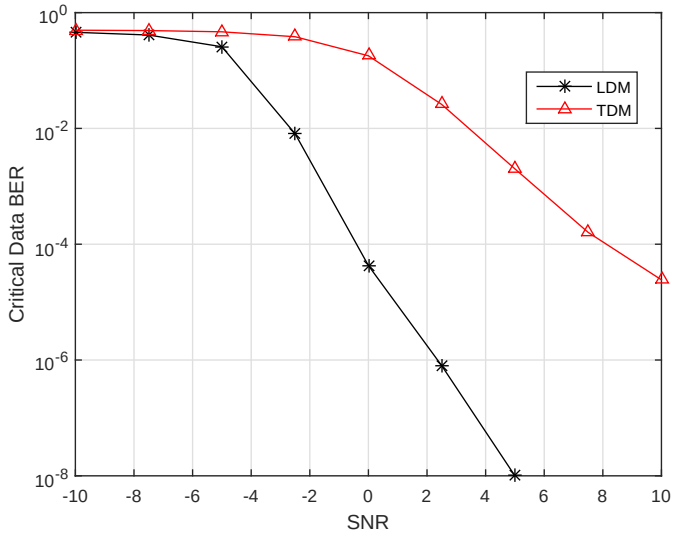

Figure 4.11: BER of critical data with $g = 0.3$ and $T_c = 0.15$.

Normalized throughput of the critical data versus SNR was simulated and plotted in Figure 4.12, where it can be seen that LDM always outperforms TDM in terms of throughput due the low BER of the critical data.

Non critical data BER and throughput were also simulated, where results are plotted in Figure 4.13, where BER of the LDM system always is higher than the TDM systems. Throughput of the non critical data is plotted in Figure 4.14. In this case, it can be seen

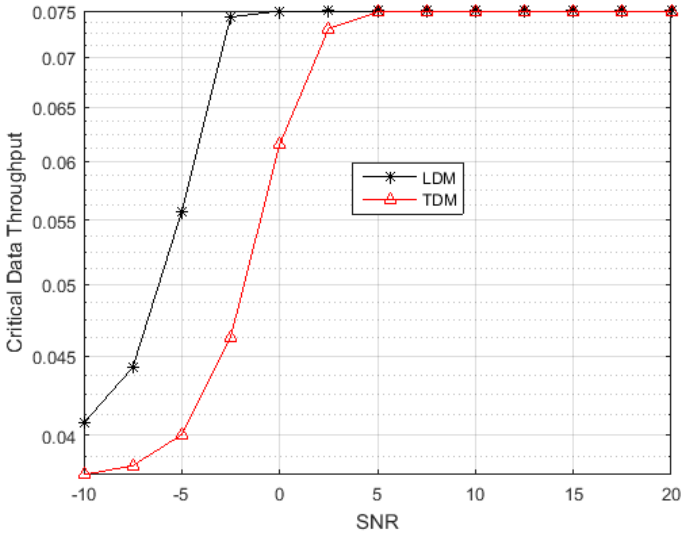

Figure 4.12: Normalized Throughput of Critical data with injection level $g = 0.3$ and $T_c = 0.15$.

that not always LDM throughput is higher than TDM. When the SNR of the non critical receiver is below 5 dB, TDM has higher throughput than LDM but above 5 dB, the LDM throughput is higher than TDM. Looking at Figure 4.8 (case $T_c = 0.05$), only SNR values higher than 10 dB make the non critical LDM throughput higher than TDM. In the case of $T_c = 0.25$ of Figure 4.9 all values of SNR makes the LDM non critical throughput higher than TDM, demonstrating that depending of T_c and SNR, non critical LDM throughput can outperform TDM.

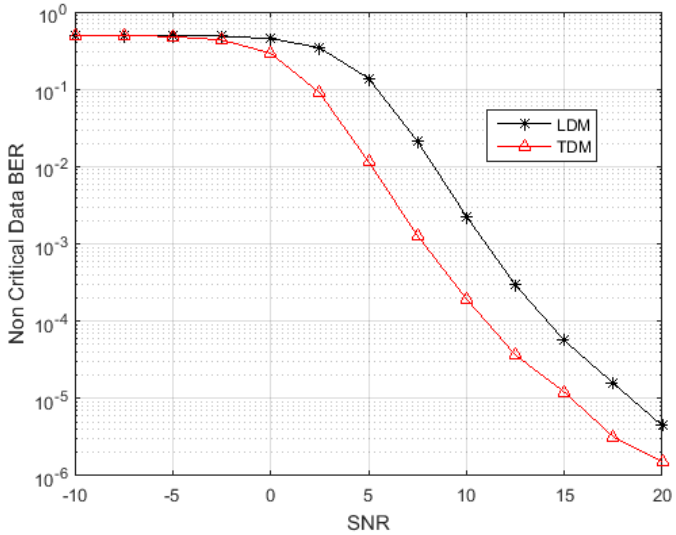

Figure 4.13: BER of Non Critical data with injection level $g = 0.3$ and $T_c = 0.15$.

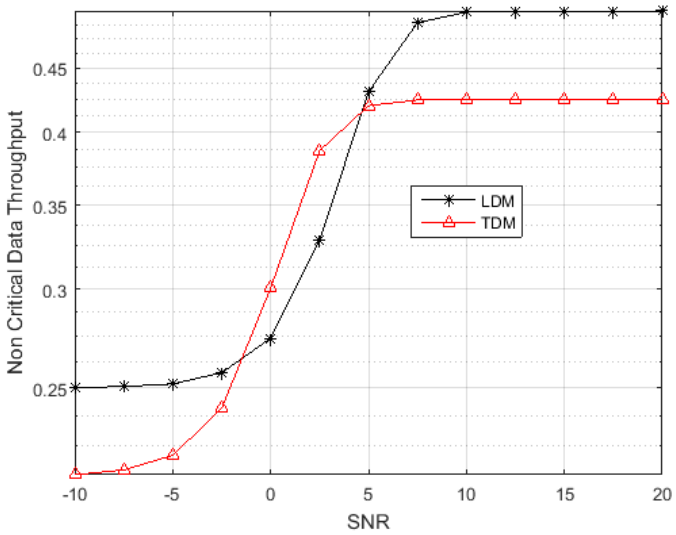

Figure 4.14: Normalized Throughput of Non Critical data with injection level $g = 0.3$ and $T_c = 0.15$.

4.6 Chapter summary

In this chapter, the use of LDM combined with UEP is proposed for intravehicular wireless networks replacing the traditional TDM/FDM schemes. The chapter starts with the fundamentals of LDM and an analysis of the theoretical capacity of an LDM system in comparison with a TDM system.

The proposed application scenario of LDM is an inside train carriage wireless system, where two types of data must coexist: critical and non critical data. The capacity gain that LDM systems can obtain is proposed in this chapter to use to increase reliability of critical data, giving priority against non critical data traffic. To prove the hypothesis, first simulations are carried out using a Gaussian channel and very simple baseband transmission scheme obtaining BER and throughput of both critical and non critical data.

The results show that an LDM scheme can outperform TDM in terms of BER and throughput, but injection level g and the application given critical data time slot (T_c) and non critical data time slot (T_{nc}) have a great impact depending on the SNR that the receivers expects.

With the proposed LDM system, reliability of the critical data is higher than TDM but throughput of the non critical data must be defined to select the correct parameters to fulfill the requirements of the system. The simulations carried out in this chapter demonstrate that a commitment rule is necessary between g, T_c, T_{nc} and the expected SNR.

The obtained results on this chapter were published in [Arruti17a] as a possible candidate to be used in an industrial wireless system with similar time constraints.

Chapter 5

System performance using SISO

5.1 Introduction

The goal of this chapter is to show the simulation results of combining the LDM scheme with UEP introduced in Chapter 4 and the Winner channel model presented in Chapter 3. The results in this chapter are novel, since LDM has never been used in this scenario and over a wireless train channel as the proposed in Chapter 3.

BER and throughput of critical data and non-critical data are simulated over different test scenarios to show the performance of LDM and are compared with TDM. The analyzed wireless channel is the Winner train channel proposed in Chapter 3 and its results are compared with HiperLAN 2 [ETSI02] A, B and C channel models described in Section 2.2.4.5 and a fast-fading channel. Furthermore, the transmission scheme used in these simulations is a more realistic system than the one used in Chapter 4, as shown in Figures 5.1 and 5.2.

The final objective of these simulations is to extend the conclusions from Chapter 4 to a realistic channel model and a complete wireless transceivers. The simulation results of this chapter are using SISO systems whereas the results of next section are using multiple-antenna configurations.

5.2 Simulator characteristics

The results provided in this and the next chapter have been obtained using simulator with the following parameters:

- Channel models: Inside train Winner channel model of Chapter 3, fast-fading channel and HiperLAN 2 A, B and C channel models.
- Possibility to use multiple transmission and reception antennas creating SISO, MISO, SIMO and MIMO systems.
- LDM or TDM transmission.

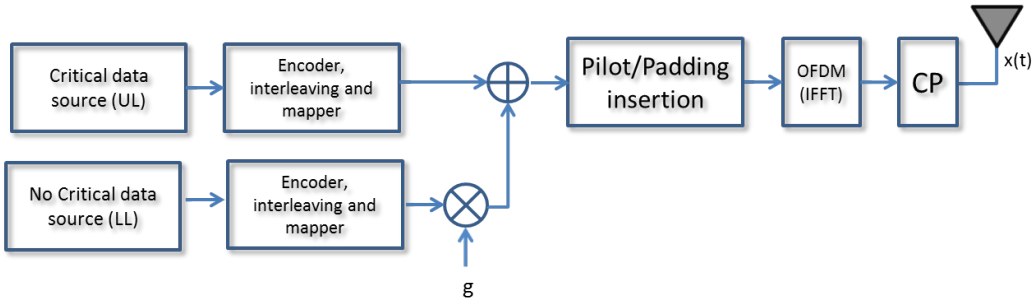

Figure 5.1: Two layer LDM transmitter block diagram.

- Different coding rates using turbo codes and Alamouti space time block coding.
- Orthogonal Frequency Division Multiplexing.

The transmitter is composed of information sources, where critical and non-critical data bits are generated and after encoding, interleaving and modulating, they are superposed to obtain LDM symbols. After pilot insertion, OFDM is used to send symbols $x(t)$ over the transmission channel $H(t)$. Perfect Channel State Information (CSI) is assumed in the receivers. There are two type of receivers:

- UL or critical data receivers, which receive the transmitted symbol $y(t)$ after channel convolution and noise addition, and performs a simple single-layer decoding obtaining the information in the UL.
- LL or non-critical receivers who do the same operation than UL receivers to obtain and regenerate UL. After that they estimate the LL symbol and perform a regular demodulation, decoding and deinterleaving to obtain LL data.

The transmitter and receiver block diagrams are shown in Figure 5.1 and Figure 5.2 respectively.

As described in the previous chapter, the critical data modulation used in these simulations is BPSK and non-critical data is modulated using QPSK. The simulation results of Sections 4.5.2.1 and 4.5.2.3 show that an injection level $g = 0.3$ obtains high critical data reliability results, maintaining high critical and non-critical data throughput levels, so in the simulator g is fixed to 0.3.

5.3 Test scenarios

11 test SISO scenarios are simulated in this chapter. The initial test scenarios are TDM and LDM scenarios with code rate 1 ($K_c^{TDM} = K_{nc}^{TDM} = K_{UL}^{LDM} = K_{LL}^{LDM} = 1$) and they are simulated as initial setup and for comparison purposes. After this initial setup, the rest of the test scenarios are simulated and compared to obtain results.

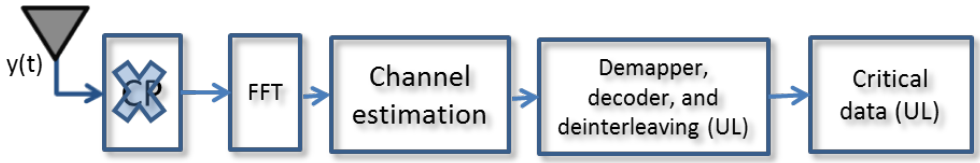

(a) Critical data receiver.

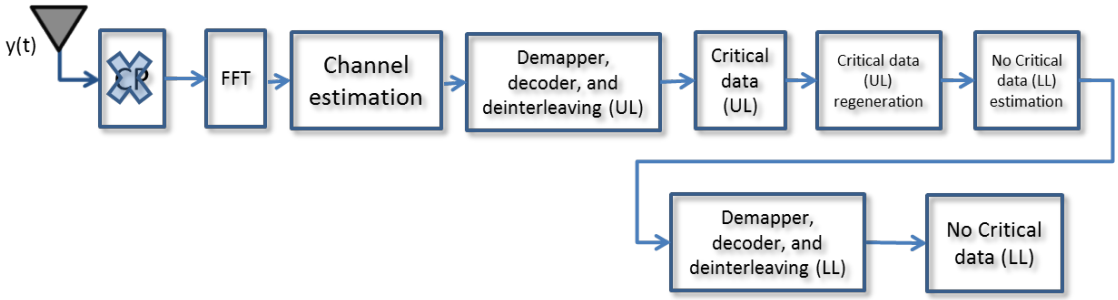

(b) Non-critical data receiver.

Figure 5.2: Two layers LDM receivers block diagrams.

The tested scenario are summarized in Table 5.1

Scenario	Mux	M_T	M_{R_c}	$M_{R_{nc}}$	T_c	T_{nc}	K_c	K_{nc}	$Max(Th_c)$	$Max(Th_{nc})$
1.1	TDM	1	1	1	1	0	1	x	1	0
1.2	TDM	1	1	1	0	1	x	1	0	1
1.3	LDM	1	1	1	1	1	1	1	1	1
2.1	TDM	1	1	1	0.5	0.5	0.5	0.5	0.25	0.25
2.2	LDM	1	1	1	1	1	0.5	0.5	0.5	0.5
3.1	TDM	1	1	1	0.25	0.75	0.5	0.5	5/40	0.375
3.2	LDM	1	1	1	1	1	5/40	0.5	5/40	0.5
3.3	TDM	1	1	1	0.15	0.85	0.5	0.5	3/40	0.425
3.4	LDM	1	1	1	1	1	3/40	0.5	3/40	0.5
3.5	TDM	1	1	1	0.05	0.95	0.5	0.5	1/40	0.475
3.6	LDM	1	1	1	1	1	1/40	0.5	1/40	0.5

Table 5.1: Tested scenario summary.

where Mux is the multiplexing technique used, T_c is the portion of time to send critical data in TDM, T_{nc} is the portion of time to send non-critical data, K_c is the code rate used to send critical data in TDM or in UL in LDM, K_{nc} is the code rate to send non-critical data in TDM or in LL in LDM, $Max(Th_c)$ is the maximum normalized throughput that the critical data will have and $Max(Th_{nc})$ is the maximum normalized throughput that the non-critical data will have. Throughput is defined in Equation 4.20.

5.4 Initial test scenarios

In this section the first three scenarios of Table 5.2 are simulated. The first two scenarios are TDM systems, where only one antenna is used to send and receive the critical and non-critical data transmission. In the first scenario, all available time is used to send critical data with a code rate of 1.

Scenario	Mux	M_T	M_{R_c}	$M_{R_{nc}}$	T_c	T_{nc}	K_c	K_{nc}	$Max(Th_c)$	$Max(Th_{nc})$
1.1	TDM	1	1	1	1	0	1	x	1	0
1.2	TDM	1	1	1	0	1	x	1	0	1
1.3	LDM	1	1	1	1	1	1	1	1	1

Table 5.2: Initial test scenarios.

If the channel behaviour is analyzed it can be seen that all TDM and LDM scenarios follow the same behaviour. Winner channel has always the lower BER, versus HiperLAN 2 channel A and fast fading channel. BER of scenario 1.1 can be as example in Figure 5.3.

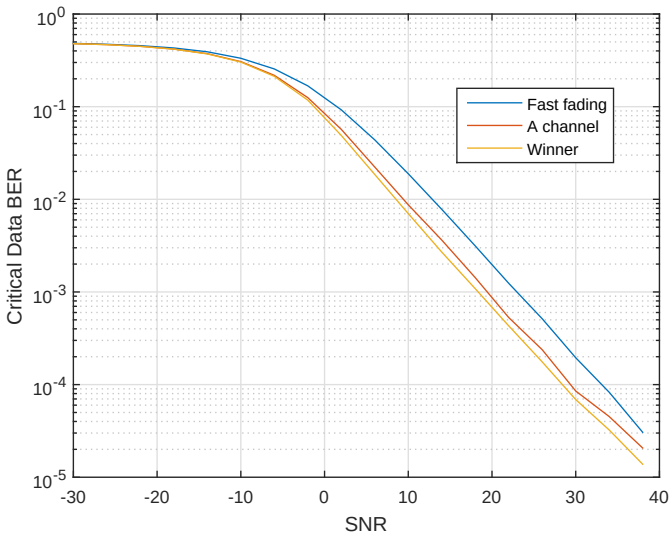

Figure 5.3: Critical data BER of scenario 1.1.

Focusing only on the Winner channel, critical data BER of scenario 1.1 and 1.3 are compared in Figure 5.4a and non-critical data BER of scenario 1.2 and 1.3 are compared in Figure 5.4b.

It could be concluded that in both cases, BER of the LDM system is higher than TDM when both systems are using the same code rate ($K_c = K_{nc} = 1$) and all available time to send data. In critical data transmission there is a difference of 3 dB between TDM and LDM. This is because in LDM, the LL adds an extra noise to the UL as seen in Equation 4.4. In the case of non-critical data the difference between TDM and LDM is 6 dB because the LL has lower power assignment than non-critical data in TDM.

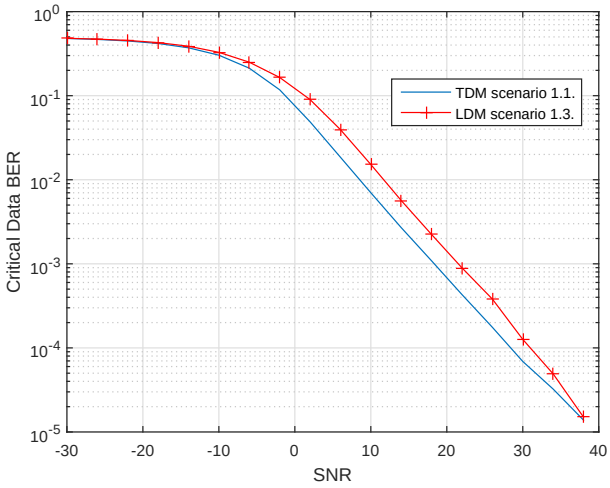

(a) Critical data BER comparison of Winner channel: scenario 1.1 vs scenario 1.3.

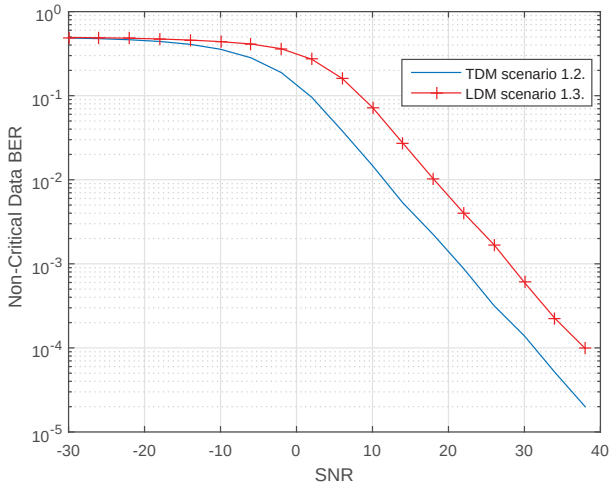

(b) Non-critical data BER comparison of Winner channel: scenario 1.2 vs scenario 1.3.

Figure 5.4: Simulation results of scenario 1.1, 1.2 and 1.3.

These cases are used to have an initial setup and a starting point to be used as comparative purposes.

5.5 SISO scenarios with same code rate K

Scenario	Mux	M_T	M_{R_c}	$M_{R_{nc}}$	T_c	T_{nc}	K_c	K_{nc}	$Max(Th_c)$	$Max(Th_{nc})$
2.1	TDM	1	1	1	0.5	0.5	0.5	0.5	0.25	0.25
2.2	LDM	1	1	1	1	1	0.5	0.5	0.5	0.5

Table 5.3: Tested scenarios 2.1 and 2.2.

In this section, TDM and LDM systems are compared maintaining the same code rate in both scenarios, that is, scenarios 2.1 and 2.2 are compared. In the TDM system, critical data and non-critical data share the available time to send data, with same time slot length ($T_c = T_{nc} = 0.5$). In this case, BER and throughput are simulated to compare two scenarios.

Focusing on BER curves of Figures 5.5a and 5.5b (scenario 2.1), it can be seen that both types of data take advantage of using a lower coding rate than the initial scenarios of Section 5.4. Fast fading channel take advantage of using code against A channel or Winner, obtaining a steeper slope. In scenario 2.1 at SNR higher than 5 dB in the critical data case or 10 dB in the non-critical data case, it can be seen that fast fading channel has lower BER than A or Winner channels. In scenario 2.2, similar behavior is observed with both types of data, but in this case SNR must be higher than 8 dB in the critical case and 16 dB in the case of non-critical data to obtain lower BER with a fast fading channel than A or Winner channel.

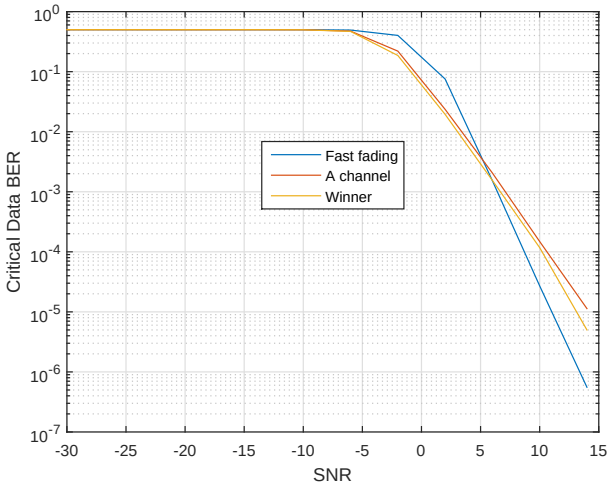

(a) Critical data BER of scenario 2.1.

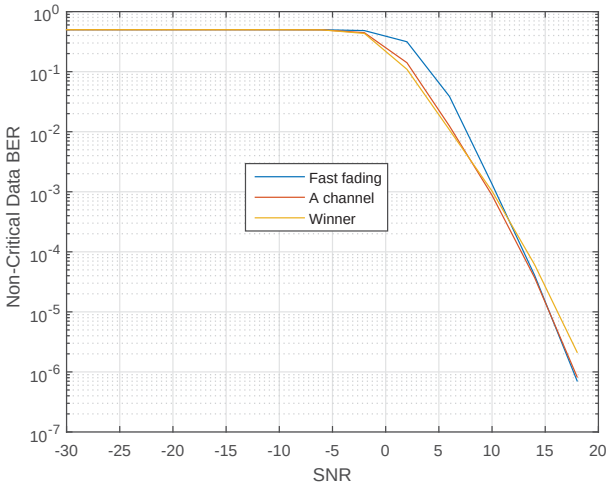

(b) Non-critical data BER of scenario 2.1.

Figure 5.5: Simulation results of scenario 2.1.

The throughput is defined by Equation 4.20 and in a TDM system is limited by the coding rate and the available time to send data. The maximum Th happens when $P_b = 0$, i.e, the maximum throughput in the critical case is 0.25. In the non-critical receiver the throughput is defined in the same way and the maximum throughput is 0.25. In the LDM case the same definition of throughput is used but in this case maximum throughput in both critical and non-critical data is 0.5, double than the TDM system. Equation 4.20 uses bit error rate to obtain throughput, but throughput definition using packet error rate instead of bit error rate is possible as defined in Equation 5.1:

$$Th_P = R \cdot (1 - P_P)\,, \tag{5.1}$$

where P_P is the packet error rate.

To compare both scenarios, BER and throughput of only Winner channel are plotted in Figure 5.6. It can be seen that using the same code rate, BER of the TDM system is lower than LDM in both critical and non-critical receivers. In the critical data transmission, TDM system has 3 dB gain against LDM and in the non-critical data case the gain is 6 dB. But, since LDM can use all available time, maximum throughput of LDM is higher than the TDM system; specifically LDM maximum throughput is double of TDM in both cases. This extra throughput using LDM can be exploited to add redundancy to the data with the aim of decreasing BER. Focusing on throughput using PER, critical and non-critical data are shown in Figure 5.6e and 5.6f respectively. It can be seen that LDM has higher throughput than TDM only when SNR is higher than 4 dB in critical case and 11 dB in non-critical case.

In next section, the extra available time that LDM gives to the transmission will be used

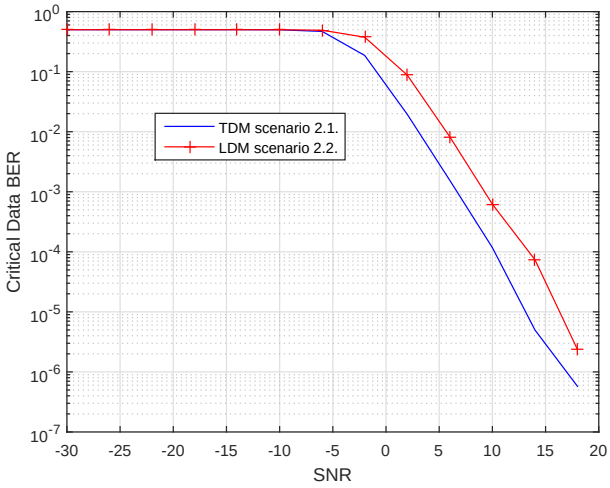

(a) Critical data BER of Winner channel.

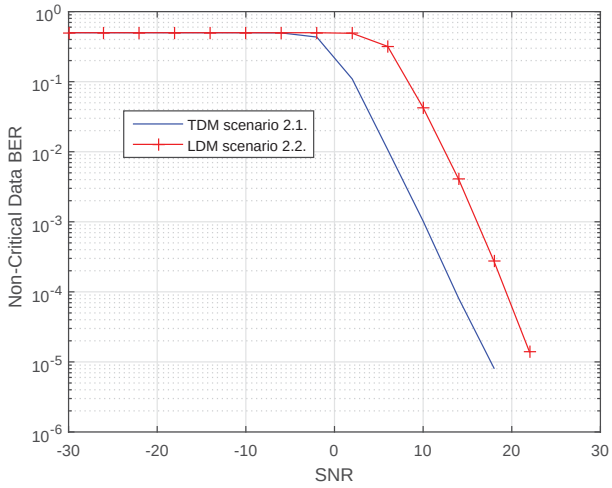

(b) Non-critical data BER of Winner channel.

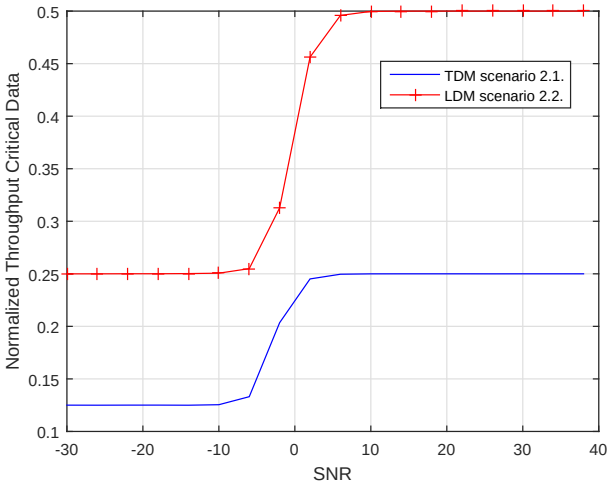

(c) Normalized critical data throughput using BER of Winner channel.

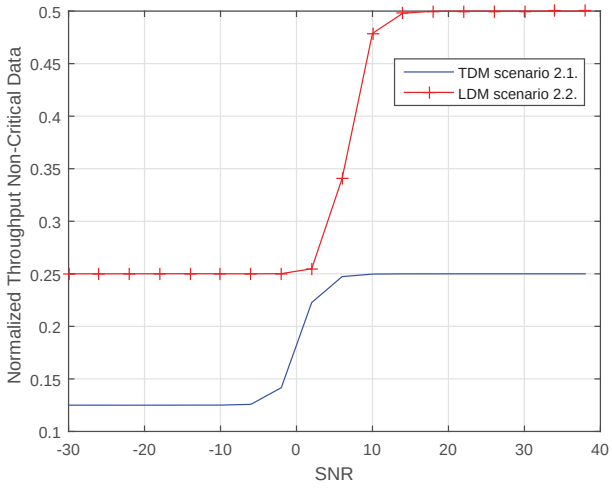

(d) Normalized non-critical data throughput using BER of Winner channel.

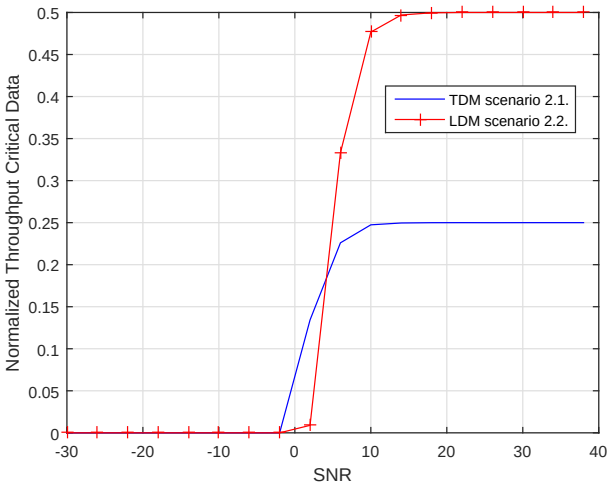

(e) Normalized critical data throughput using PER of Winner channel.

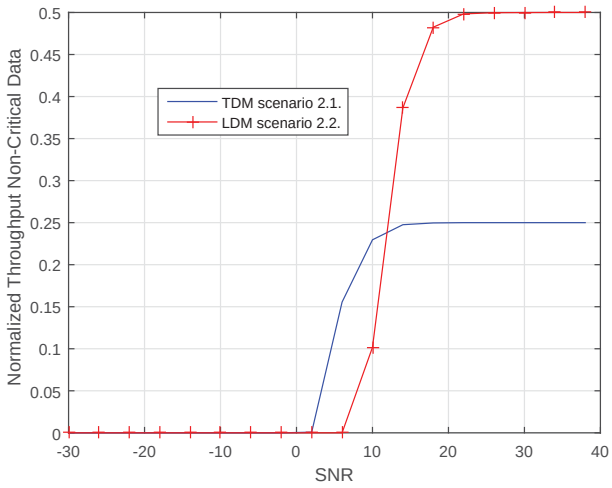

(f) Normalized non-critical data throughput using PER of Winner channel.

Figure 5.6: Winner channel simulation results: scenario 2.1 vs scenario 2.2.

to use different code rates with the objective of maintaining the same maximum bit rate in the critical data and obtain lower BER. In the case of non-critical data, it will not vary the code rate with the aim of increasing throughput instead of decreasing BER.

5.6 TDM vs LDM using different coding rates

In this section different scenarios were simulated to obtain results and evaluate the performance of the channel.

5.6.1 TDM and LDM scenario comparison with maximum critical throughput 5/40

Scenario	Mux	M_T	M_{R_c}	$M_{R_{nc}}$	T_c	T_{nc}	K_c	K_{nc}	$Max(Th_c)$	$Max(Th_{nc})$
3.1	TDM	1	1	1	0.25	0.75	0.5	0.5	5/40	0.375
3.2	LDM	1	1	1	1	1	5/40	0.5	5/40	0.5

Table 5.4: Tested scenarios 3.1 and 3.2.

As shown in the table 5.4 both scenarios 3.1 and 3.2 have maximum throughput of critical data of 5/40 in our simulator. Critical and non-critical data BER of scenario 3.1 show the same results than scenario 2.1 where the used code rate makes that fast fading channel has lower BER than channel A or Winner when SNR is higher than 5 dBs. But due to the low code rate that scenario 3.2 is using in the critical data, this effect does not happen and Winner and channel A have lower BER than fast fading channel as shown in Figure 5.7.

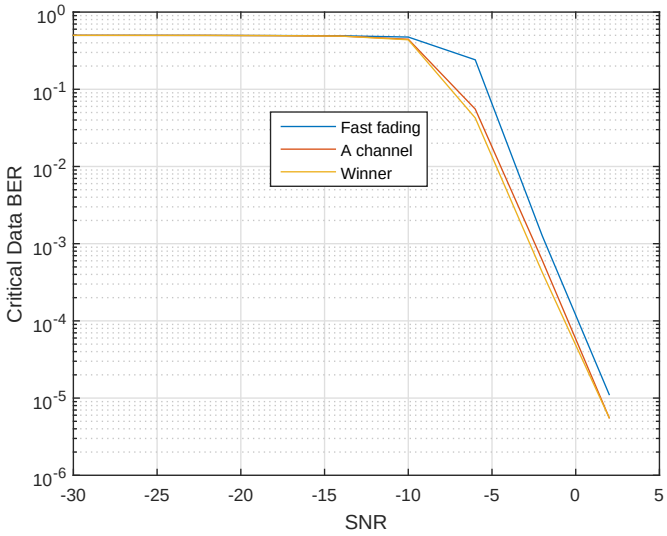

Figure 5.7: Critical data BER of scenario 3.2.

Analyzing non-critical BER simulations of both scenario 3.1 and 3.2, they have the same behaviour than scenario 2.1 and 2.2 because they are using the same code rate making that the fast fading channels has lower BER versus the rest of the channels when SNR is higher than 15 dB as seen in Figure 5.5b.

A comparison of both scenarios is plotted in Figure 5.8. In Figure 5.8a comparison of critical data BER is displayed. It can be seen that the LDM system with the same maximum bit rate than TDM has a lower BER. For example, with a SNR as low as -5 dB, LDM can achieve a BER of 10^{-2} while TDM system has a BER of $4 \cdot 10^{-1}$. With a SNR of 0 dB, LDM has achieved a SNR of $4 \cdot 10^{-5}$ and TDM a BER of $5 \cdot 10^{-2}$ having a difference of 3 order of magnitude. This lower BER affects in the critical data throughput, keeping the LDM throughput higher than in TDM (Figure 5.8c).

In Figure 5.8b non-critical BER of both scenarios is shown. In this case the code rate of 0.5 has kept in both cases so the BER of TDM system is lower than LDM, maintaining a 6 dB gain for all SNRs. This higher BER of LDM can be compensated with the extra available time to send non-critical data, as can be shown in Figure 5.8d. Maximum throughput of LDM is 0.5 while maximum throughput of TDM is 0.375. It can be seen that LDM can outperform TDM throughput in some cases. Focusing on throughput using BER of Figure 5.8d, with SNR higher than 6 dB, LDM throughput is higher than TDM and BER is $2 \cdot 10^{-1}$. Above this SNR the LDM system can obtain higher throughput than TDM. Throughput using PER of Figure 5.8f shows that with SNR higher than 13 dB LDM has higher throughput than TDM.

Another characteristic of LDM described in Chapter 4 and represented in Figure 4.3 is that the capacity of LDM increases with the difference between layers' SNR. Maximum capacity of LDM increases when the difference of SNR between layers increase, specifically when LL SNR is higher than UL. In the case where SNR of LL is equal or lower than UL SNR, the maximum capacity of LDM is the same capacity than TDM. In Figure 5.9 average BER of scenario 3.1 and 3.2 are plotted. Average BER (Av_{BER}) of the system is defined as Equation 5.2:

$$Av_{BER} = \frac{BER_c + BER_{nc}}{2}, \tag{5.2}$$

where BER_c is the critical data BER value and BER_{nc} is the non-critical data BER value. Av_{BER} is calculated for every pair of SNR (critical and non-critical) values. Figure 5.9a shows Av_{BER} of scenario 3.1 and Figure 5.9b shows Av_{BER} of scenario 3.2. Figure 5.9c is the top view of Figure 5.9a and it can be seen that in scenario 3.1 the critical data BER starts decreasing at 0 dB and the non-critical data BER starts at 4 dB. For scenario 3.2 top view of Figure 5.9b is the Figure 5.9d. In both figures it can be seen that critical data BER starts decreasing at -8 dB and that the non-critical case starts at 8 dB. The LDM system used in scenario 3.2 makes critical data BER lower than scenario 3.1 but non-critical data

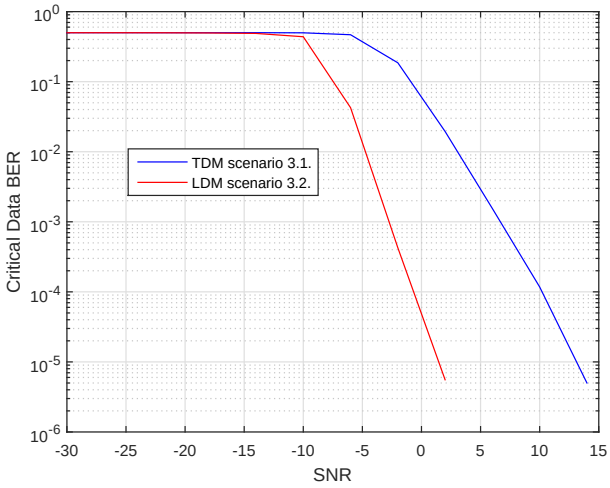

(a) Critical data BER scenario 3.1 vs scenario 3.2.

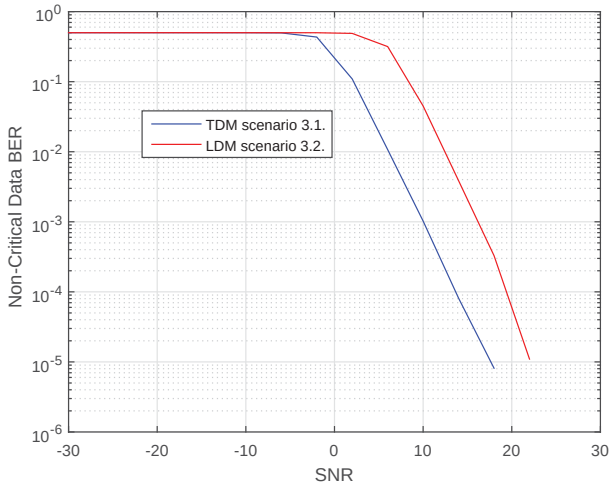

(b) Non-critical data BER scenario 3.1 vs scenario 3.2.

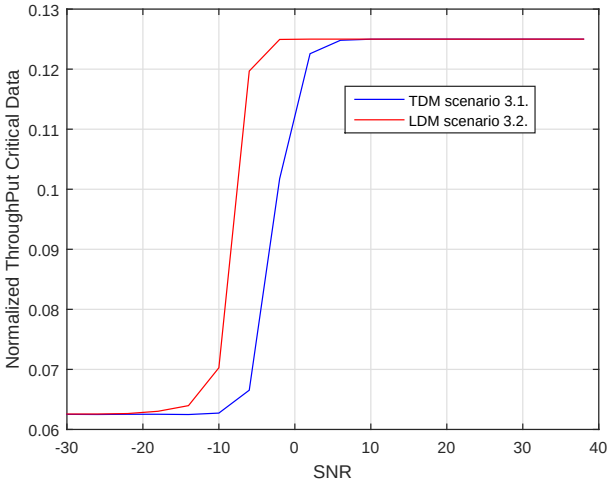

(c) Critical data throughput using BER of scenario 3.1 vs scenario 3.2.

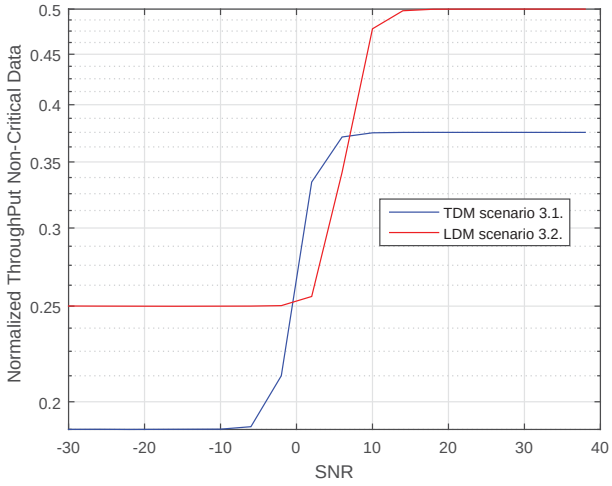

(d) Non-critical data throughput using BER of scenario 3.1 vs scenario 3.2.

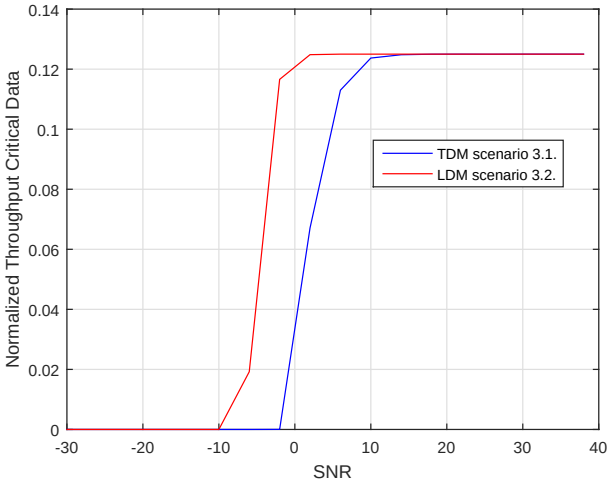

(e) Critical data throughput using PER of scenario 3.1 vs scenario 3.2.

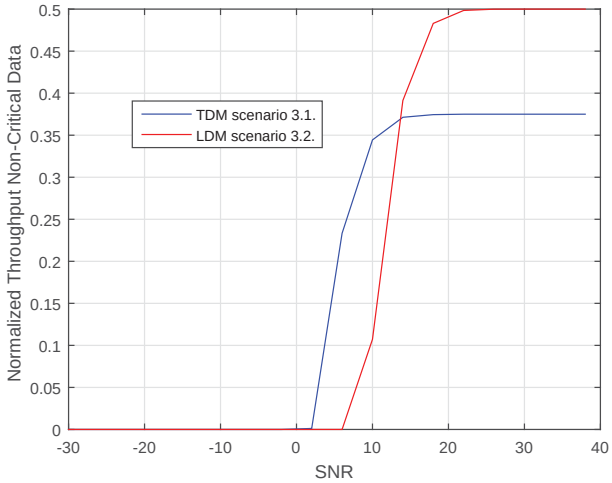

(f) Non-critical data throughput using PER of scenario 3.1. vs scenario 3.2.

Figure 5.8: Winner channel simulation results: scenario 3.1 vs scenario 3.2.

BER is penalized instead.

To prove that Av_{BER} of LDM system is lower than the TDM, the difference in Av_{BER}-s is calculated and displayed in Figure 5.10. Figure 5.10a is a 3-D view of these difference values. Positive values of Figure 5.10a means that $Av_{BER}^{LDM} < Av_{BER}^{TDM}$ while negative values means that $Av_{BER}^{LDM} > Av_{BER}^{TDM}$. Figure 5.10b is a top view of 5.10a where 4 zones can be identified. The fist zone in red is marked as the "invalid zone". This zone is where critical data SNR is so low that data can not be recovered, so this zone can not be used in transmission. The second zone in black is the "ineligible zone", where SNR of non-critical receiver is lower than critical data receiver. This situation needs to be avoided because LDM benefits happens when critical data SNR is lower than the non-critical. The third zone is the zone highlighted as the "positive values" zone. In this zone, LDM Av_{BER} is lower than TDM, making this zone as the optimum zone where the use of LDM is highly recommended. The remaining zone is where LDM's Av_{BER} is lower than TDM but the difference between them is not so high.

Bottom view of 5.10a is displayed in Figure 5.10c. In this figure the same zones of Figure 5.10b are highlighted but there is another one identified as "negative values" where Av_{BER} of TDM is lower than LDM. This means that in these values, the use of TDM is recommended instead of LDM, so this is a zone to avoid if there is using an LDM system.

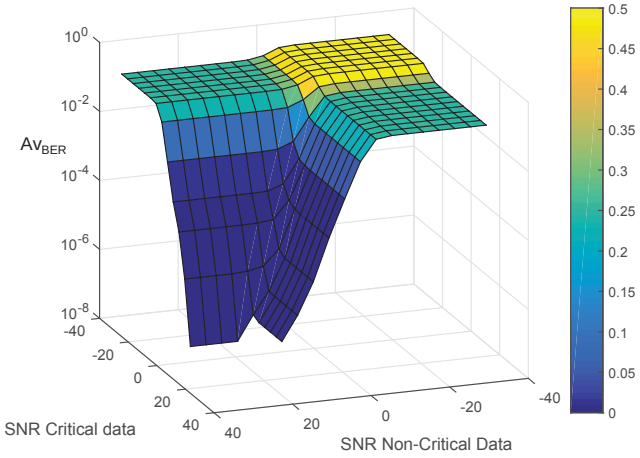

(a) Av_{BER} of TDM critical data vs non-critical data with different SNR values.

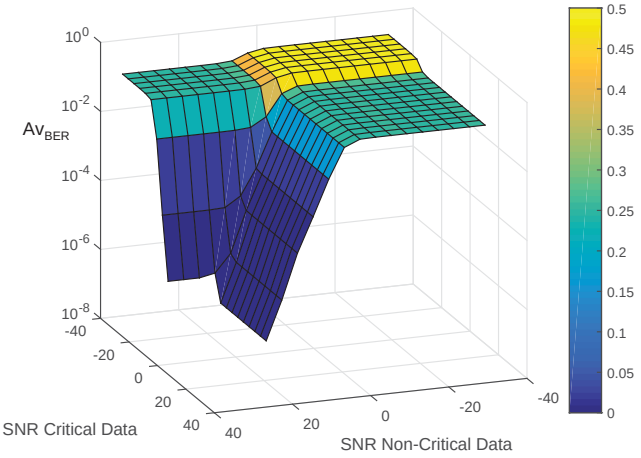

(b) Av_{BER} of LDM critical data vs non-critical data with different SNR values and $K_c^{LDM} = 5/40$.

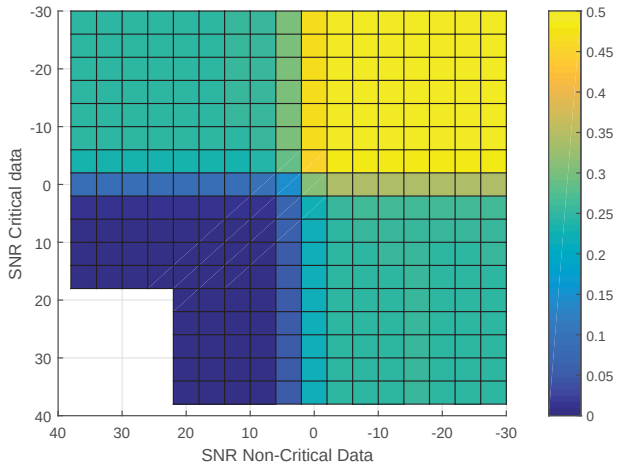

(c) Av_{BER} of TDM critical data vs non-critical data with different SNR values - top view.

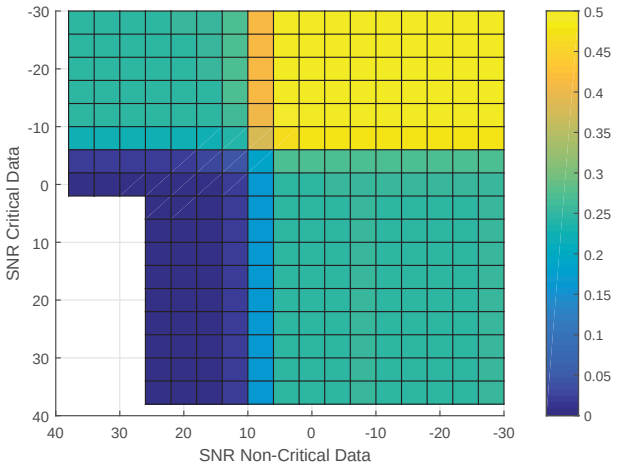

(d) Av_{BER} of LDM critical data vs non-critical data with different SNR values and $K_c^{LDM} = 5/40$ - top view.

Figure 5.9: Average BER simulation results of scenario 3.1 and 3.2.

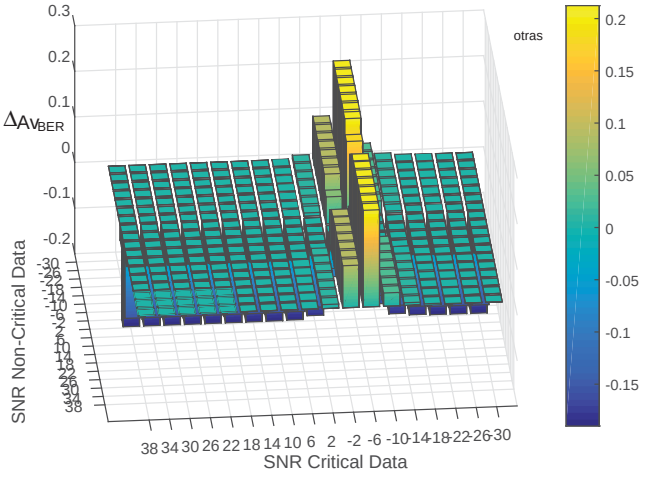

(a) BER difference between TDM and LDM. $K_{UL}^{LDM} = 5/40$.

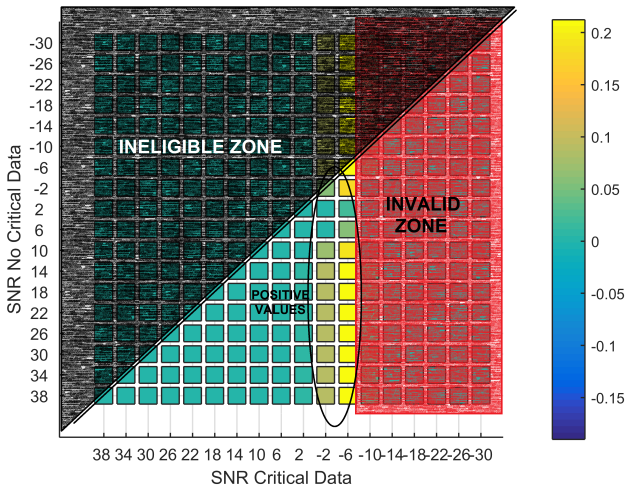

(b) Top view.

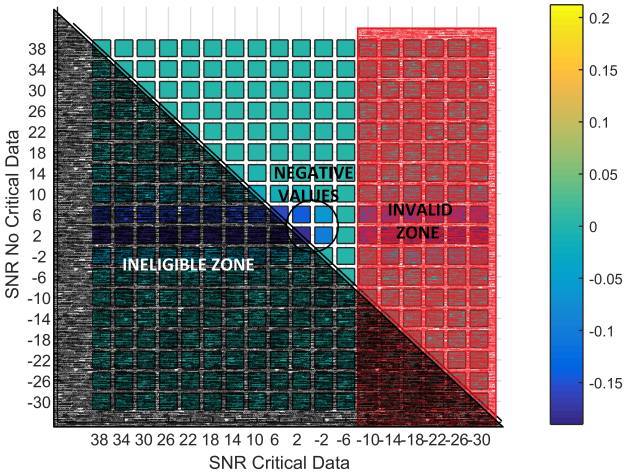

(c) Bottom view.

Figure 5.10: BER difference of scenario 3.1 and 3.2.

5.6.2 TDM and LDM scenario comparison with maximum critical throughput 3/40

Scenario	Mux	M_T	M_{R_c}	$M_{R_{nc}}$	T_c	T_{nc}	K_c	K_{nc}	$Max(Th_c)$	$Max(Th_{nc})$
3.3	TDM	1	1	1	0.15	0.85	0.5	0.5	3/40	0.425
3.4	LDM	1	1	1	1	1	3/40	0.5	3/40	0.5

Table 5.5: Tested scenarios 3.3 and 3.4.

In this section, scenarios 3.3 and 3.4 summarized in Table 5.5 are compared. Both scenarios have a maximum throughput of 3/40 on critical data. Simulation results of scenario 3.3 show same critical and non-critical data BER than scenario 3.1 as they use the same code rate. BER of critical data of scenario 3.4 has similar behaviour than scenario 3.2 where the BER of Winner channel is lower than A channel and fast fading for all SNR values as shown in Figure 5.11.

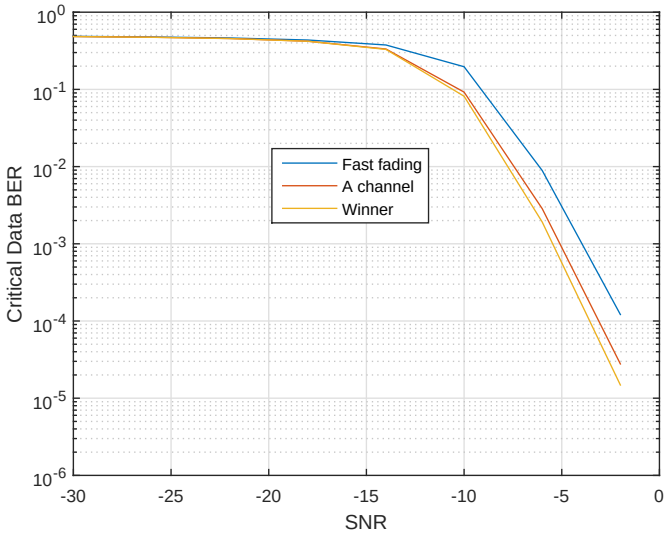

Figure 5.11: Critical data BER of scenario 3.4.

To see the differences between scenarios, a comparison is plotted in Figure 5.12. Comparing critical data BER, scenario 3.4 has lower BER than scenario 3.3 as seen in Figure 5.12a. For example a BER of $6 \cdot 10^{-4}$ is reached in the scenario 3.3 with a SNR of -5 dB versus a BER of $4 \cdot 10^{-1}$ in scenario 3.4. having a 3 order gain. With SNR 0 dB, BER of scenario 3.3 is $5 \cdot 10^{-2}$ versus $2 \cdot 10^{-6}$ BER of scenario 3.4, having a difference of 4 orders. This lower BER makes the throughput of scenario 3.3 represented in Figure 5.12c higher than scenario 3.4.

With non-critical data BER, the result is the same than scenario 3.1 of Section 5.6.1 because the coding is not changing but the maximum non-critical throughput now on scenario

3.3 is 0.425 versus 0.5 of the scenario 3.4. It can be seen in Figure 5.12d that for values of SNR higher than 9 dB, scenario 3.4 has higher throughput than scenario 3.3. In the case of throughput using PER of Figure 5.12f with SNR values higher than 15 dB, scenario 3.4 has higher throughput than scenario 3.3.

Analyzing the Av_{BER} as described in Chapter 5.6.1, the results are displayed in Figure 5.13. As the mentioned in previous chapter Figure 5.14a is a 3-D view of the Av_{BER} differences where positive values of Av_{BER} means that a scenario using LDM has lower average BER than a scenario using TDM. Figure 5.14b and 5.14c are the top and bottom view of Figure 5.14a where "ineligible zone" and "invalid zone" are highlighted in both top and bottom view. In this occasion the invalid zone starts at -16 dB and in the top view it can be seen that the positive values zone is wider than scenario 3.2. In the bottom view, where the negative values are highlighted, it can be seen that there are some values where a TDM scenario obtains lower BER than LDM, so these are values to avoid using an LDM scenario like scenario 3.4.

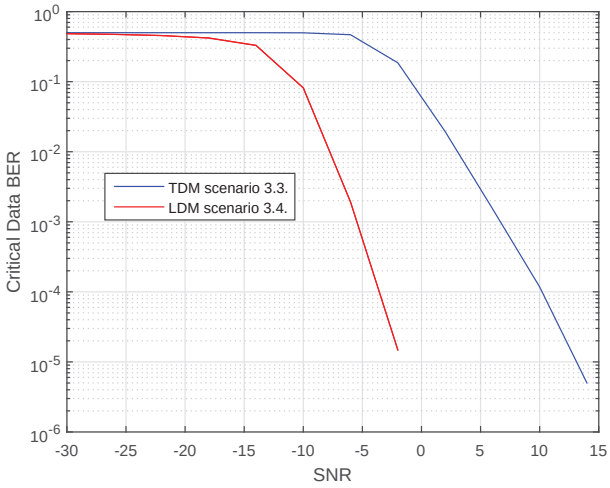

(a) Critical data BER scenario 3.3 vs scenario 3.4.

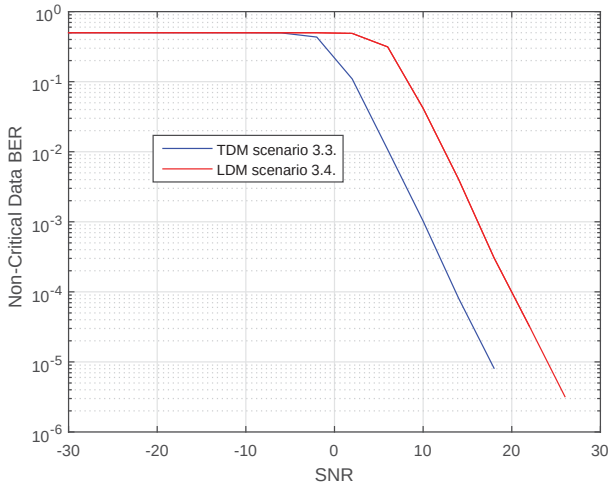

(b) Non-critical data BER of scenario 3.3 vs scenario 3.4.

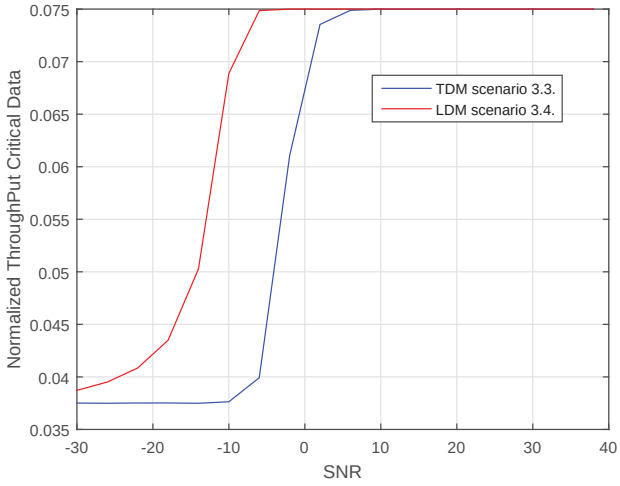

(c) Normalized critical data throughput using BER of scenario 3.3 vs scenario 3.4.

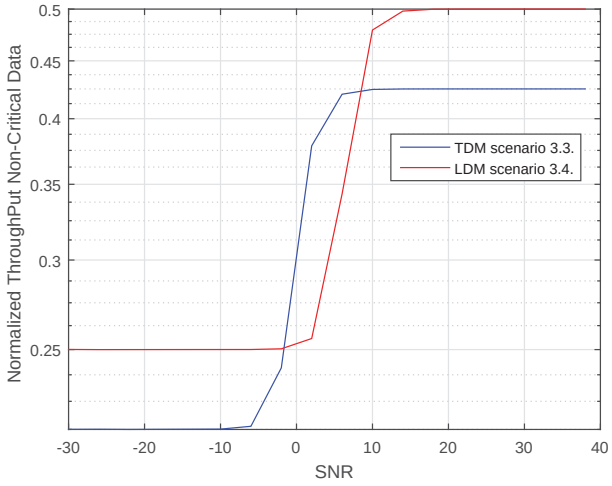

(d) Normalized non-critical data throughput using BER of scenario 3.3 vs scenario 3.4.

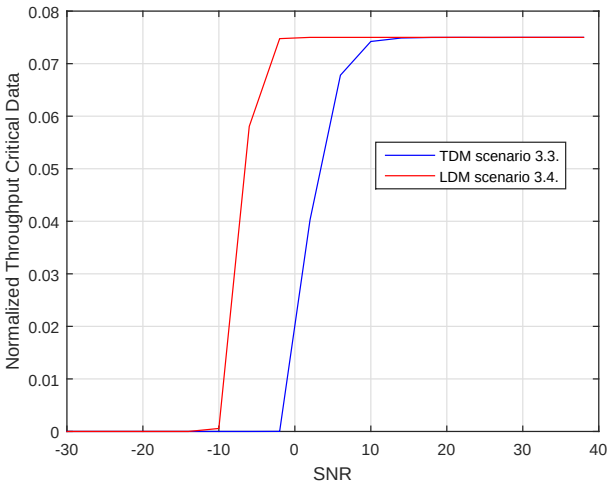

(e) Normalized critical data throughput using PER of scenario 3.3 vs scenario 3.4.

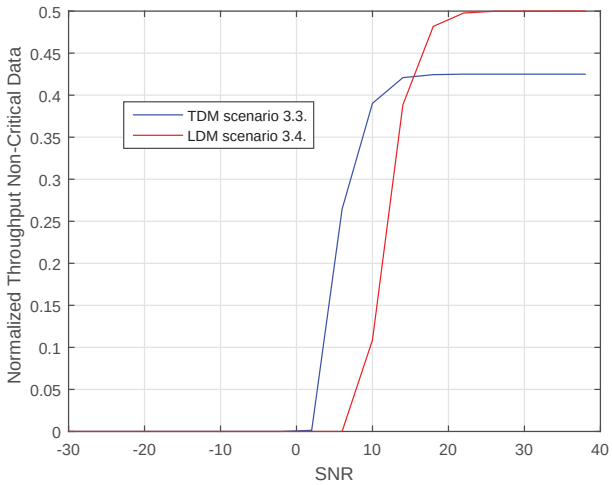

(f) Normalized non-critical data throughput using PER of scenario 3.3 vs scenario 3.4.

Figure 5.12: Comparison results of scenario 3.3 vs scenario 3.4.

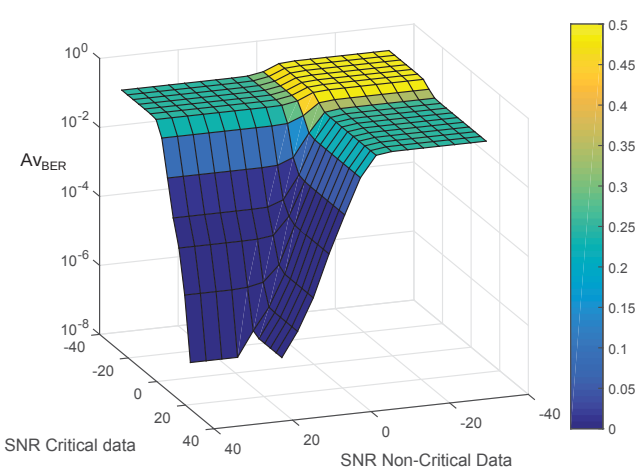

(a) Av_{BER} of TDM critical data vs non-critical data with different SNR values.

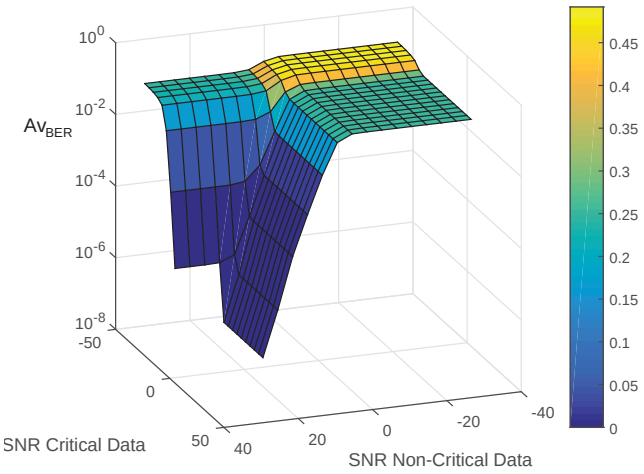

(b) Av_{BER} of LDM critical data vs non-critical data with different SNR values and $K_c^{LDM} = 3/40$.

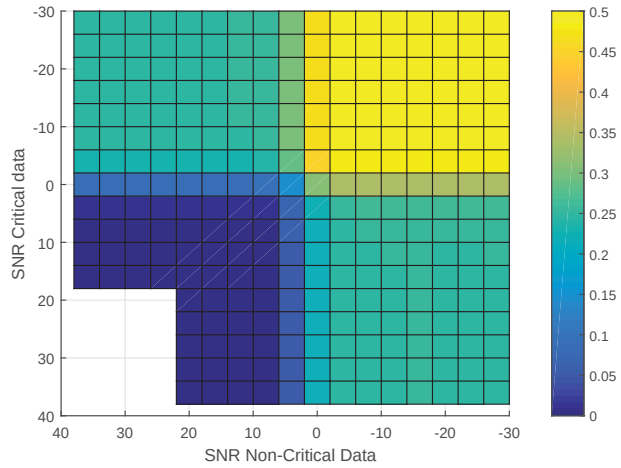

(c) Av_{BER} of TDM critical data vs non-critical data with different SNR values - top view.

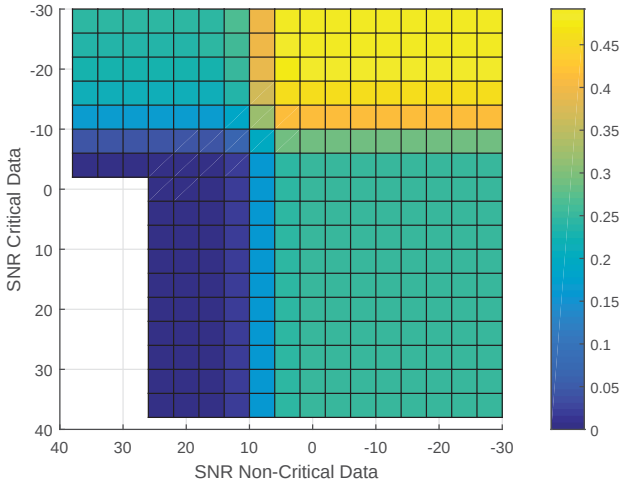

(d) Av_{BER} of LDM critical data vs non-critical data with different SNR values and $K_c^{LDM} = 3/40$ - top view.

Figure 5.13: Average BER simulation results TDM and LDM $K_{UL}^{LDM} = 3/40$.

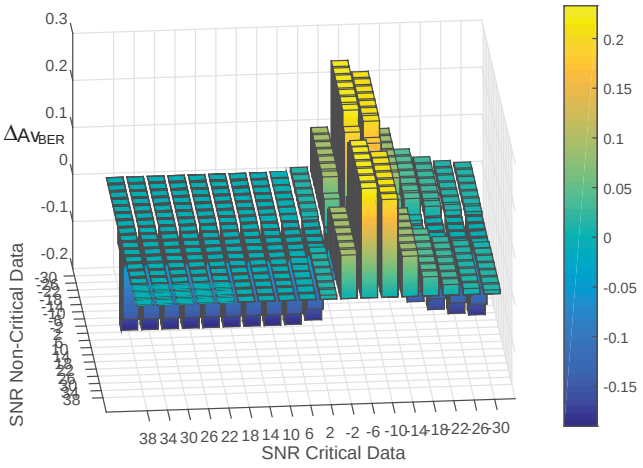

(a) BER difference between TDM and LDM. $K_{UL}^{LDM} = 3/40$.

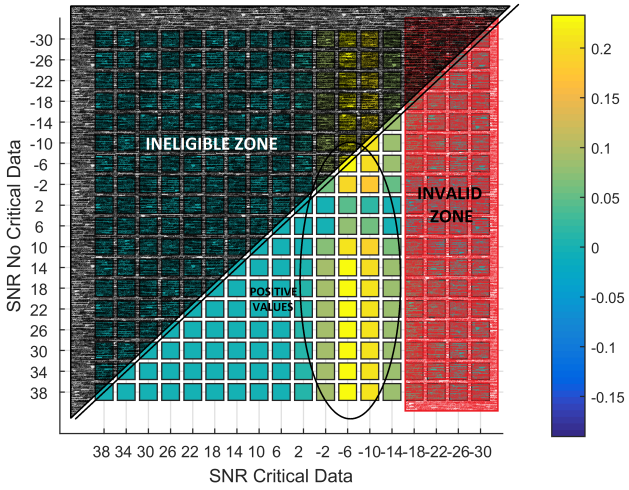

(b) Top view.

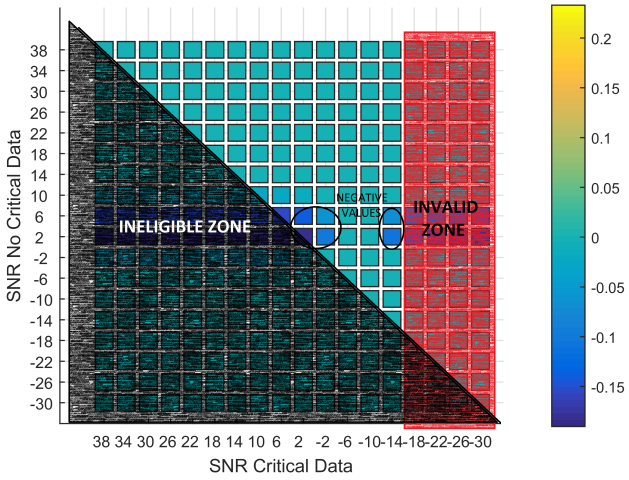

(c) Bottom view.

Figure 5.14: BER difference of scenarios 3.3 and 3.4.

5.6.3 TDM and LDM scenario comparison with maximum critical throughput 1/40

Scenario	Mux	M_T	M_{R_c}	$M_{R_{nc}}$	T_c	T_{nc}	K_c	K_{nc}	$Max(Th_c)$	$Max(Th_{nc})$
3.5	TDM	1	1	1	0.05	0.95	0.5	0.5	1/40	0.475
3.6	LDM	1	1	1	1	1	1/40	0.5	1/40	0.5

Table 5.6: Tested scenarios 3.5 and 3.6.

Scenarios 3.5 and 3.6 are compared now, with the characteristics summarized in Table 5.6, whose results are shown in Figure 5.15. Figure 5.15a shows that critical data BER can decrease considerably using LDM in scenario 3.6 using a code rate of 1/40. LDM obtains BER as low as $4 \cdot 10^{-4}$ with SNR -10 dB, in comparison with $5 \cdot 10^{-1}$ of TDM system. With SNR -5 dB, BER of $6 \cdot 10^{-6}$ with LDM is reached versus $4 \cdot 10^{-1}$ obtained with TDM. This low BER makes that critical data throughput of LDM is higher than TDM as shown in Figure 5.15c. In Figure 5.15b BER of non-critical data shows that it follows the same behaviour than previous scenarios 3.1 and 3.3 because it has the same characteristics. But analyzing non-critical data throughput of Figure 5.15d this time the point where LDM scenario throughput is higher than TDM is 10 dB, versus the 5 dB of scenario 3.2 or the 9 dB of scenario 3.4. In Figure 5.15f, throughput using PER shows similar behaviour than Figure 5.15d but SNR must be higher than 17 dB if you want higher throughput using LDM.

Regards the Av_{BER}, the simulation results are displayed in Figure 5.16 and the difference between average BER is displayed in Figure 5.17. In Figure 5.16d, critical data BER of scenario 3.6 starts decreasing at -20 dB and the non-critical data starts decreasing at 6 dB showing that critical data starts decreasing with lower SNR than scenario 3.5 (Figure 5.16c) but non-critical data starts decreasing with higher SNR.

The difference of Av_{BER} simulation results are displayed in Figure 5.17a in 3D and the top and bottom view in Figures 5.17b and 5.17c respectively. As previous scenarios, "ineligible zone" and "invalid zone" are highlighted. This time Figure 5.17b shows a wider positive value zone, where Av_{BER} of the LDM scenario is lower than TDM. However, analyzing Figure 5.17c it can be seen that in this occasion there is also negative values zone that it should be avoided.

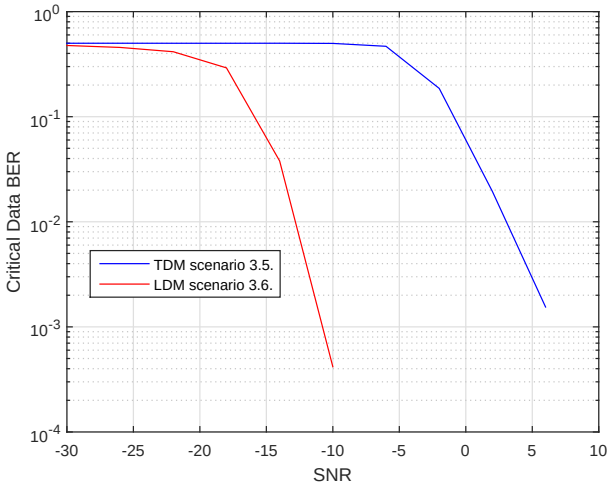

(a) Critical data BER scenario 3.5 vs scenario 3.6.

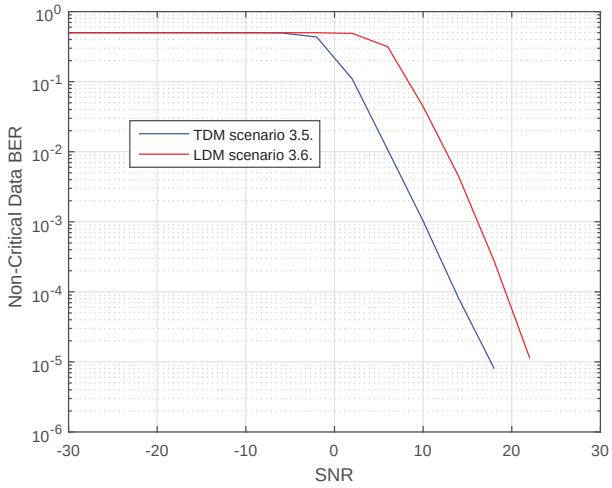

(b) Non-critical data BER of scenario 3.5 vs scenario 3.6.

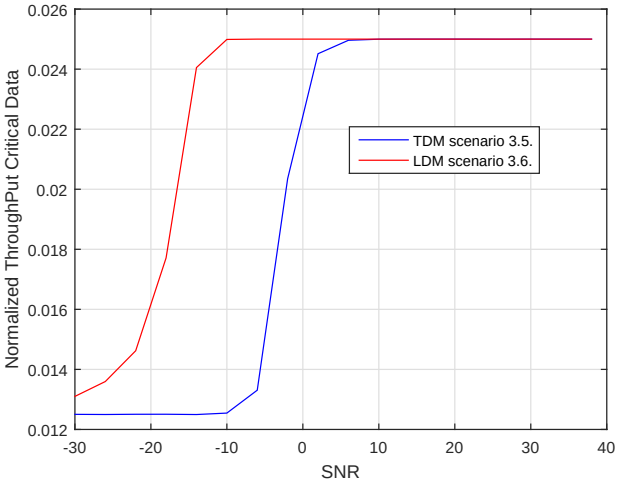

(c) Normalized critical data throughput using BER of scenario 3.5 vs scenario 3.6.

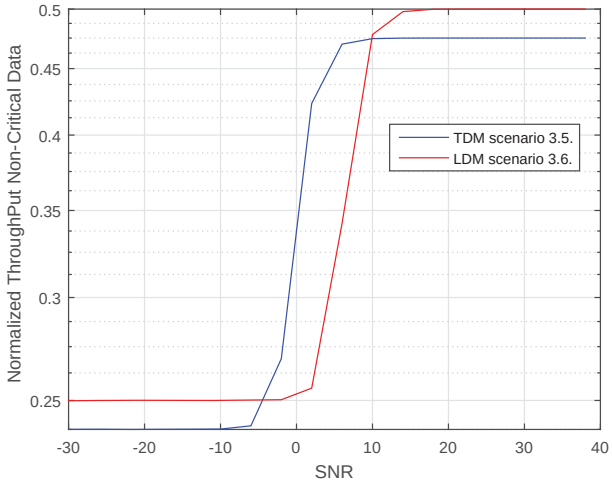

(d) Normalized non-critical data throughput using BER of scenario 3.5 vs scenario 3.6.

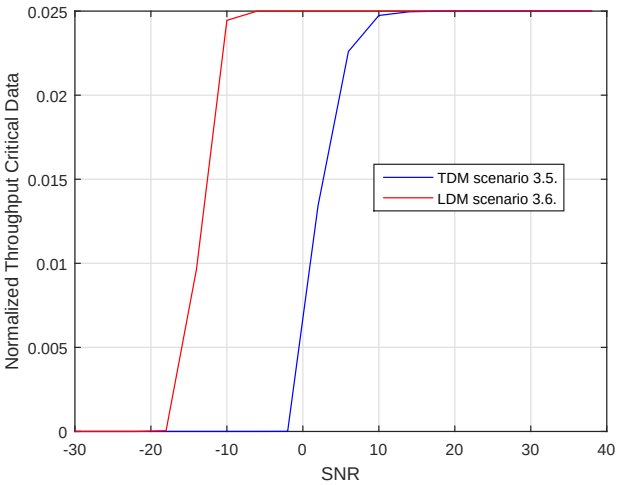

(e) Normalized critical data throughput using PER of scenario 3.5 vs scenario 3.6.

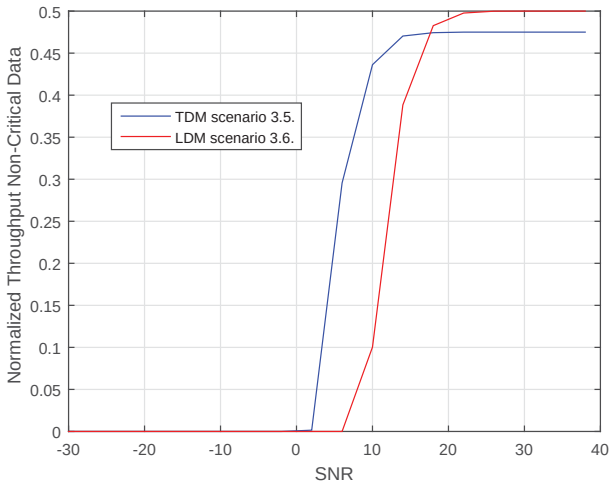

(f) Normalized non-critical data throughput using PER of scenario 3.5 vs scenario 3.6.

Figure 5.15: Comparison results of scenario 3.5 vs scenario 3.6.

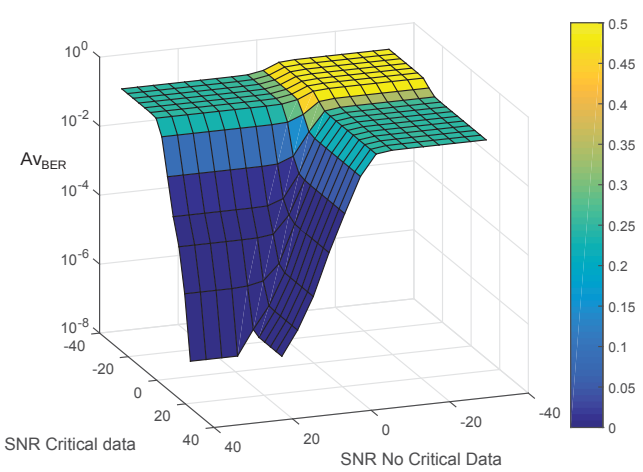

(a) Av_{BER} of TDM critical data vs non-critical data with different SNR values.

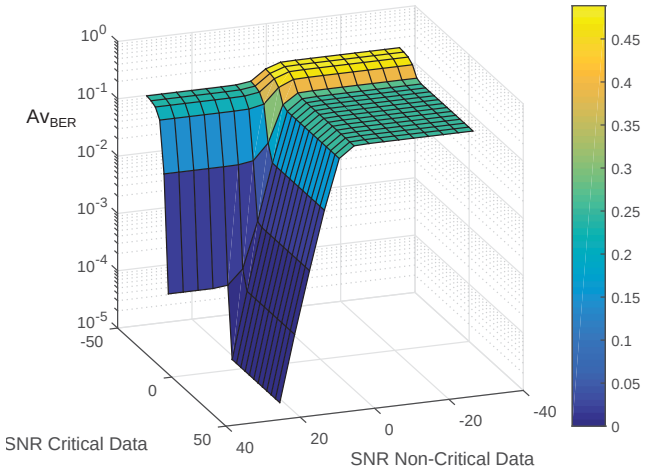

(b) Av_{BER} of LDM critical data vs non-critical data with different SNR values and $K_c^{LDM} = 1/40$.

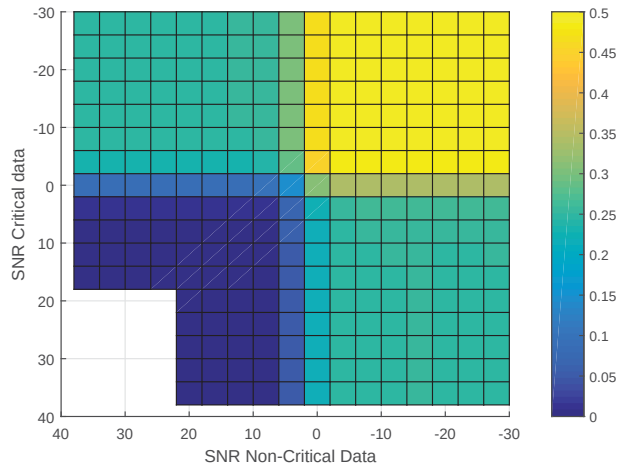

(c) Av_{BER} of TDM critical data vs non-critical data with different SNR values - top view.

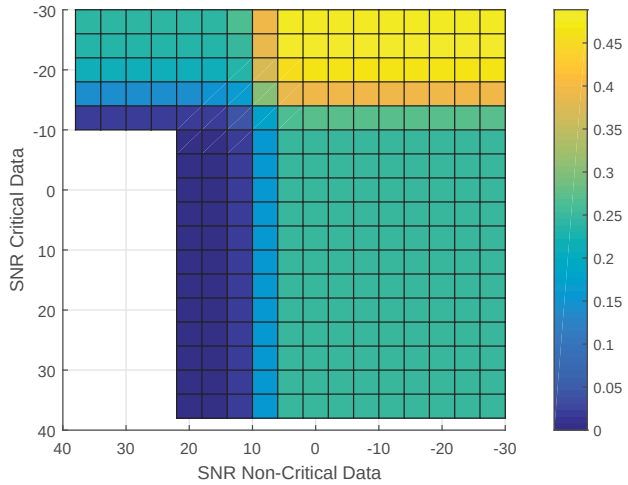

(d) Av_{BER} of LDM critical data vs non-critical data with different SNR values and $K_c^{LDM} = 1/40$ - top view.

Figure 5.16: Average BER simulation results TDM and LDM $K_{UL}^{LDM} = 1/40$.

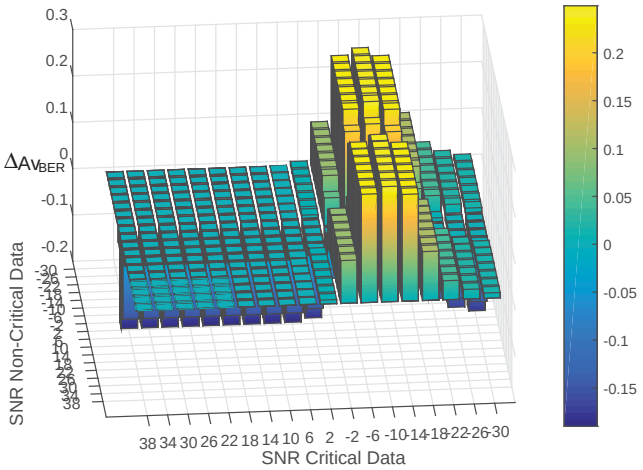

(a) BER difference between TDM and LDM. $K_{UL}^{LDM} = 1/40$.

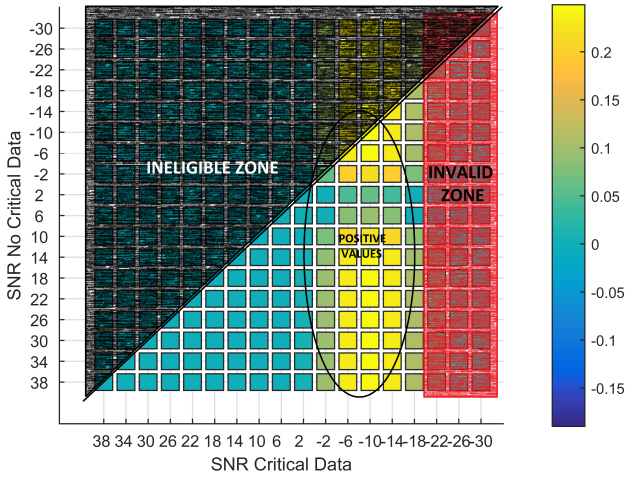

(b) Top view.

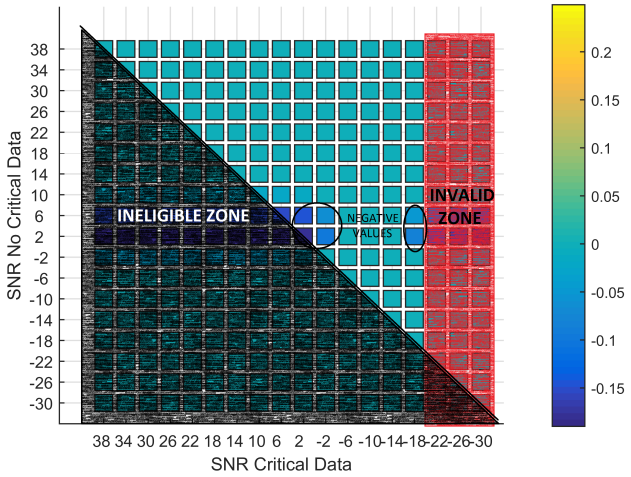

(c) Bottom view.

Figure 5.17: BER difference of scenarios 3.5 and 3.6.

5.6.4 Simulation results summary

This section summarizes the simulation results shown in Section 5.6. Significative simulation results are shown in Figure 5.18 where the most representative values are compared to extract conclusions.

In Figure 5.18a critical data BER of scenario 3.1, 3.2, 3.4 and 3.6 are shown corresponding to a TDM scenario with $K_c^{TDM} = 0.5$, LDM system with $K_{UL}^{LDM} = 5/40$, LDM system with $K_{UL}^{LDM} = 3/40$ and LDM system with $K_{UL}^{LDM} = 1/40$ respectively. Scenario 3.3 and 3.5 are not represented because they have the same result of scenario 3.1. It can be seen that exploiting the extra time provided by LDM, scenario 3.2, 3.4 and 3.6 can reduce BER depending of the available time to send critical data (T_c) of TDM. In systems where $T_c = 0.05$, a code rate of $K_{UL}^{LDM} = 1/40$ can be used, achieving very low BER with low SNR. Depending on T_c different K_{UL}^{LDM} could be used to decrease BER. Looking at Figure 5.18c it can be proven that with this coding critical throughput of LDM scenarios 3.2, 3.4 and 3.6 is always higher than the corresponding TDM scenarios.

Non-critical receiver BER simulation results are in Figure 5.18b. As the code rate does not change, BER results are the same in all TDM scenarios (3.1, 3.3 and 3.5) and the LDM scenarios (3.2, 3.4 and 3.6). But the available extra time that results of using LDM, is used to increase non-critical data throughput, as it can be seen in Figure 5.18d. Throughput of LDM scenarios (3.2, 3.4 and 3.6) stays fixed for three scenarios but throughput of TDM varies with the T_{nc} in scenario 3.1, 3.3 and 3.5, resulting that if a TDM scenario is using high T_{nc} with a low K_{UL}^{LDM}, the non-critical throughput difference between TDM and LDM decreases. For example, scenario 3.6 is using a very low code rate in the critical data ($K_{UL}^{LDM} = 1/40$) because in scenario 3.5 $T_c^{TDM} = 0.05$ is very low. It implies that $T_{nc}^{TDM} = 0.95$ and the extra time it gains using LDM is 0.05 so the throughput gain is very low. In Figure 5.18d scenario 3.5 is the scenario with $T_{nc}^{TDM} = 0.95$ and it must be compared with scenario 3.6, where LDM throughput curve is higher if SNR is higher than 10 dB. In the opposite side, comparing scenario 3.2 and 3.1, with a code rate in LDM of $K_{UL}^{LDM} = 5/40$, non-critical throughput difference is higher between scenarios, starting at 6 dB the zone where LDM throughput is higher than TDM.

With throughput using PER of Figures 5.18e and 5.18f, similar behaviour than throughput using BER of Figures 5.18c and 5.18d happens. In the critical data, LDM throughput is always higher than TDM but non-critical data throughput depends on T_{nc}. Analyzing Figure 5.18f, LDM scenario 3.2, scenario 3.4 and scenario 3.6 will have higher throughput than the corresponding TDM scenario when SNR is higher than 13, 15 and 17 dB respectively.

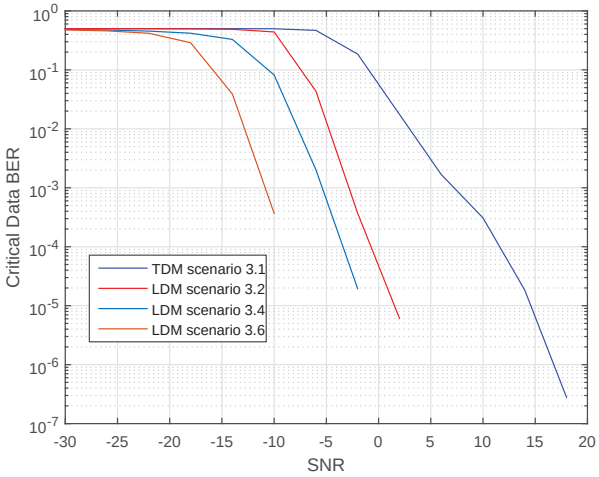

(a) Critical Data BER of scenarios 3.1, 3.2, 3.4 and 3.6.

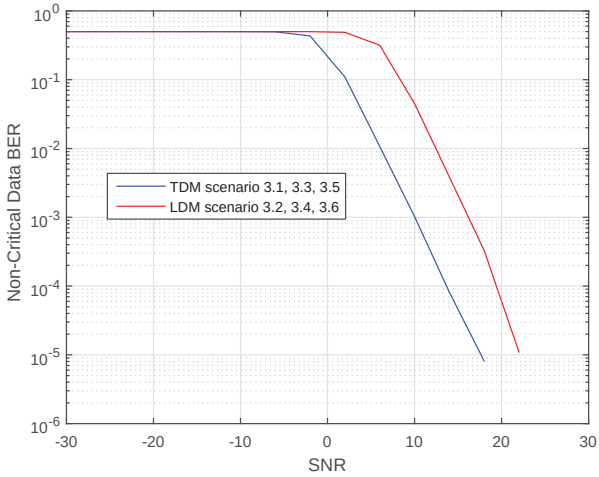

(b) Non-critical Data BER of scenarios 3.1, 3.2, 3.3, 3.4, 3.5 and 3.6.

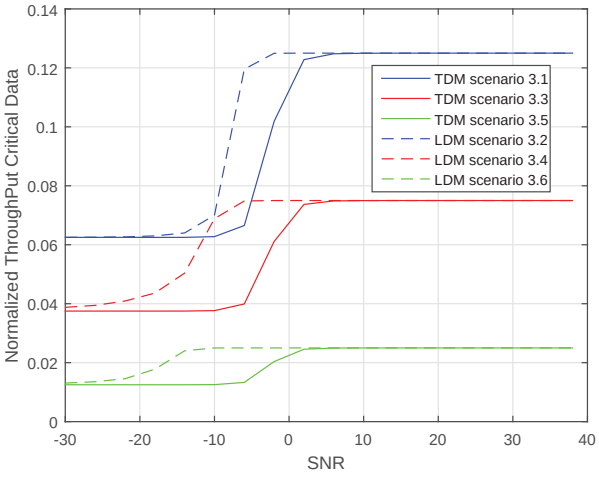

(c) Critical Data Throughput using BER of scenarios 3.1, 3.2, 3.3, 3.4, 3.5 and 3.6.

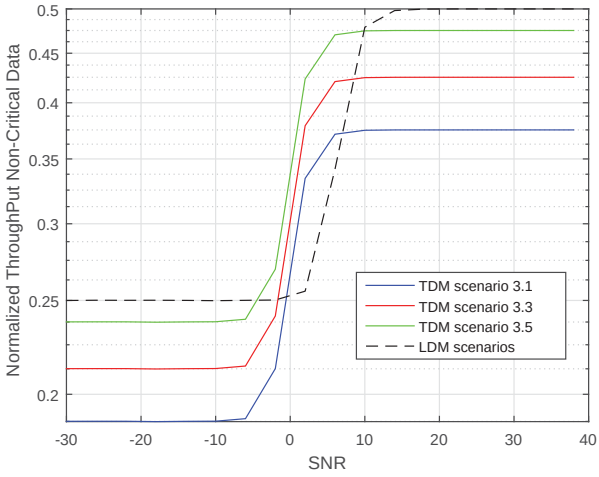

(d) Non-critical Data Throughput using BER of scenarios 3.1, 3.2, 3.3, 3.4, 3.5 and 3.6.

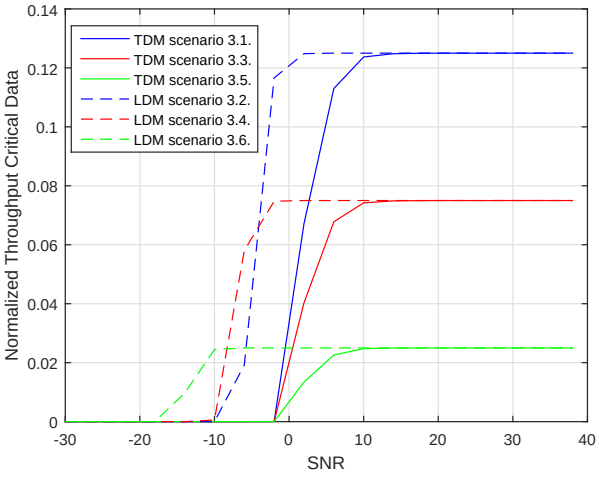

(e) Critical Data Throughput using PER of scenarios 3.1, 3.2., 3.3., 3.4., 3.5 and 3.6.

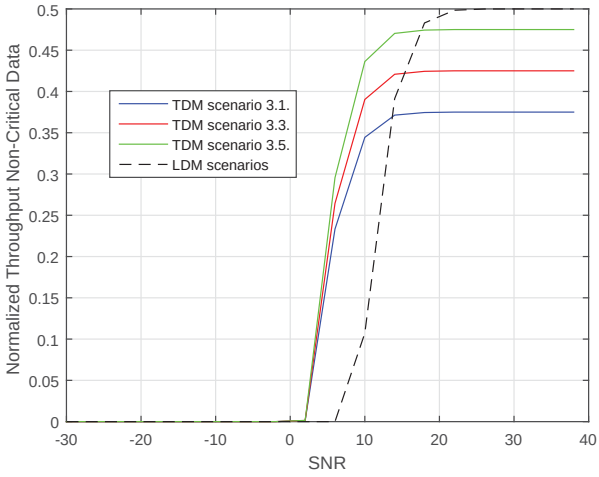

(f) Non-critical Data Throughput using PER of scenarios 3.1, 3.2, 3.3, 3.4, 3.5 and 3.6.

Figure 5.18: Comparison of tested scenarios.

5.7 Chapter summary

The main conclusion of this section is that a commitment rule is necessary to fulfill system requirements. Very low BER can be achieved using LDM and lower coding, but throughput of non-critical data will be compromised and a higher SNR will be necessary in the non-critical receiver to overcome TDM throughput. This could be done for example using directive antennas to obtain better SNR. The system design is very important and the system average SNR is a factor that affects to design criteria. LOS between non-critical receivers and the transmitter is desirable in such systems or the installation of directional gain antennas in the non-critical receivers.

This chapter has led to the publication [Arruti17b] where BER and throughput results of this chapter are published.

Chapter 6

Performance with multiantenna configurations

6.1 Introduction

In the previous chapter, simulated LDM and TDM systems have a single antenna at the transmitter and the receivers. In this chapter, scenarios with different antenna numbers are simulated. As the previous chapter, simulation results of combining the LDM scheme proposed in Chapter 4 and the Winner channel model presented in Chapter 3 are shown, enhancing the performance of the systems using multiantenna configurations.

6.2 Simulator characteristics

The simulations carried out in this chapter have the same parameters as in Chapter 5. When MISO and MIMO systems are used, which have been described in Section 2.3.1, a maximum likelihood (ML) detector [Jankiraman04] is used and perfect (CSI) is assumed in the receivers. When LDM is simulated, injection level $g = 0.3$ is fixed.

6.3 Test scenarios

15 MISO and MIMO systems are simulated in this chapter. The simulated scenarios are summarized in Table 6.1. $(\cdot)_{Alam}$ means that the transmitter will encode data over 2 antennas using Alamouti, instead of doubling the throughput through spatial multiplexing.

Scenario	Mux	M_T	M_{R_c}	$M_{R_{nc}}$	T_c	T_{nc}	K_c	K_{nc}	$Max(Th_c)$	$Max(Th_{nc})$
4.1	SDM	2	1	1	1	1	0.5	0.5	0.5	0.5
4.2	TDM	2	1	1	0.5	0.5	0.5	0.5	0.5	0.5
4.3	TDM	2	1	1	0.5	0.5	1_{Alam}	0.5	0.5	0.5
4.4	LDM	2	1	1	1	1	0.5_{Alam}	0.5_{Alam}	0.5	0.5
5.1	TDM	2	2	2	0.5	0.5	0.5	0.5	0.5	0.5
5.2	TDM	2	2	2	0.5	0.5	1_{Alam}	0.5	0.5	0.5
5.3	LDM	2	2	2	1	1	0.5_{Alam}	0.5	0.5	1
5.4	LDM	2	2	2	1	1	0.5_{Alam}	0.5_{Alam}	0.5	0.5
5.5	TDM	2	2	2	0.25	0.75	0.5_{Alam}	0.5	5/40	0.75
5.6	LDM	2	2	2	1	1	$5/40_{Alam}$	0.5	5/40	1
5.7	TDM	2	2	2	0.15	0.85	0.5_{Alam}	0.5	3/40	0.85
5.8	LDM	2	2	2	1	1	$3/40_{Alam}$	0.5	3/40	1
5.9	TDM	2	2	2	0.05	0.95	0.5_{Alam}	0.5	1/40	0.95
5.10	LDM	2	2	2	1	1	$1/40_{Alam}$	0.5	1/40	1

Table 6.1: Summary of tested multiantenna scenarios.

6.4 LDM SISO vs TDM MISO systems with same data bitrate 0.5

In this section LDM systems using SISO will be compared with TDM systems using MISO to evaluate their performance. MISO will be used in TDM to increase the transmitted maximum bit rate thanks to multiple antennas to make a fair comparison with SISO LDM systems. The main goal, as in previous sections, is to maintain the bitrate in the critical data transmission and try to maintain or increase the maximum throughput in non-critical receivers.

To do the comparison, scenario 2.2 (LDM) and 4.1, 4.2 and 4.3 (TDM) have been simulated. As it has been stated in the previous chapter, from this section onwards, only the behaviour of proposed Winner wireless channel will be analyzed. The main characteristics of each scenario are summarized in Table 6.2.

Scenario	Mux	M_T	M_{R_c}	$M_{R_{nc}}$	T_c	T_{nc}	K_c	K_{nc}	$Max(Th_c)$	$Max(Th_{nc})$
2.2	LDM	1	1	1	1	1	0.5	0.5	0.5	0.5
4.1	SDM	2	1	1	1	1	0.5	0.5	0.5	0.5
4.2	TDM	2	1	1	0.5	0.5	0.5	0.5	0.5	0.5
4.3	TDM	2	1	1	0.5	0.5	1_{Alam}	0.5	0.5	0.5

Table 6.2: Tested scenarios 2.2, 4.1, 4.2 and 4.3.

In the case of the analyzed MISO transmission (scenario 4.1), two antennas send simultaneously critical and non-critical data multiplexing in the spatial domain instead of through layers. This configuration is very similar to LDM, where the critical and non-critical infor-

mation are transmitting simultaneously during all the time. In this scenario, both antennas are being transmitted with same power levels, and the total transmitted power is normalized to be comparable with LDM.

Scenario 4.1 uses the same power allocation for both antennas. This is not fully comparable with the LDM scenario because LDM uses $\frac{1}{1+g}$ power to transmit critical data and $\frac{g}{1+g}$ to transmit non-critical data. To have a fair comparable scenario 4.1 with scenario 2.2, scenario 4.1b has been simulated, where the configuration is the same as scenario 4.1 but one antenna is transmitting critical data with $\frac{1}{1+g}$ power and the other antenna is transmitting non-critical data with power $\frac{g}{1+g}$.

Scenario 4.2 is very similar to scenario 4.1 but it loses the simultaneity of both types of information. In this case, critical and non-critical data do not share the same time slot thanks to spatial diversity. It uses different time slots to send different type of data; 50% of the time is transmitting critical data using MISO and Spatial Multiplexing and 50% of time is transmitting non-critical data in the same way.

Scenario 4.3 is a MISO system where the critical data uses Alamouti coding. Non-critical data does not use Alamouti but uses a 0.5 coding rate. Alamouti coding is a space time coding as it has been described in Chapter 2.3.2.1. Using Alamouti coding, two consecutive time slots and data from both antenna are considered to obtain two symbols, so the effective bit rate is 1. If 50% of the time is used to send critical data the resulting effective bit rate is 0.5. As it can be seen in Table 6.2, all scenarios have a maximum throughput of 0.5 in both type of data.

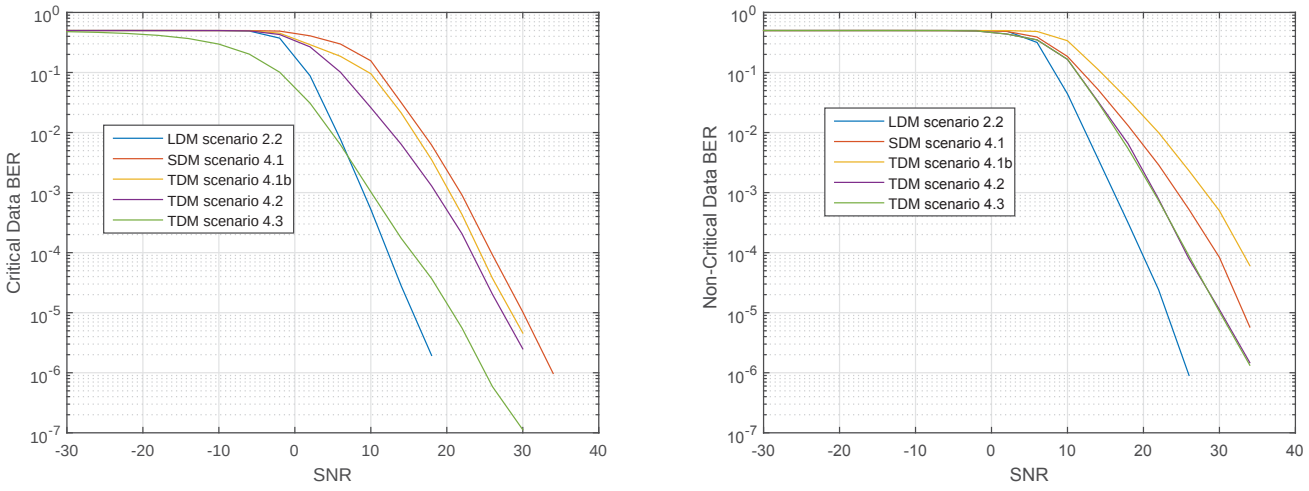

(a) Critical data BER, same data rate.

(b) Non-critical data BER, same data rate.

Figure 6.1: Simulation results of scenario 2.2 vs scenario 4.1, 4.2 and 4.3.

Simulation results are displayed in Figure 6.1. In Figure 6.1a the critical data BER is compared between all scenarios. It can be seen that only scenario 4.3 has lower BER than

scenario 2.2 based in LDM, if the SNR level is lower than 8 dB. All other scenarios have higher BER than LDM maintaining the data rate. In Figure 6.1b non-critical data BER is compared. In this case it can be seen that LDM based scenario 2.2 has lower BER than the rest of scenarios for all SNRs.

Another advantage of LDM compared with TDM/SDM scenarios is that TDM/SDM use 2 antennas against only the need of one antenna of the LDM scenario reducing the antenna complexity of the system.

6.5 LDM MISO vs TDM MISO systems with same critical data bitrate 0.5

In the previous section, LDM SISO and a TDM MISO have been compared. It can be seen that an LDM SISO system, with lower antenna number and complexity can have lower BER than a TDM MISO system depending on the SNR. In this section, LDM MISO will be compared with a TDM MISO system. Both systems have same number of transmit and receive antennas, and maximum throughput will be maintained to do a fair comparison. Scenarios 4.1, 4.2 and 4.3 described in section 6.4 are compared with scenario 4.4 based in LDM. A summary of compared scenarios is shown in Table 6.3.

Scenario	Mux	M_T	M_{R_c}	$M_{R_{nc}}$	T_c	T_{nc}	K_c	K_{nc}	$Max(Th_c)$	$Max(Th_{nc})$
4.1	SDM	2	1	1	1	1	0.5	0.5	0.5	0.5
4.2	TDM	2	1	1	0.5	0.5	0.5	0.5	0.5	0.5
4.3	TDM	2	1	1	0.5	0.5	1_{Alam}	0.5	0.5	0.5
4.4	LDM	2	1	1	1	1	0.5_{Alam}	0.5_{Alam}	0.5	0.5

Table 6.3: Tested scenarios 4.1, 4.2, 4.3 and 4.4.

Scenario 4.4 is an LDM system with 2 antennas to transmit and one to receive, and with a coding rate of 0.5 in both data type. It uses Alamouti space time block coding exploiting the spatial diversity of the 2 transmit antennas. With this Alamouti coding, the maximum rate is 0.5 in both type of data. The results of simulations are plotted in 6.2.

Results of simulation of critical data of Figure 6.2a show that scenario 4.4 based on LDM has lower BER than TDM when SNR is higher than 2 dB. If the SNR value is higher than 2 dB, LDM scenario has lower BER than all other scenarios. As the previous section, using gain antennas LDM can have lower BER than TDM for all SNR values. For example in this case to have lower BER than TDM at SNR -3 dB or higher, 2 dB gain antenna is necessary against the 4 dB antenna of the previous section to maintain the same BER level.

In the case of non-critical data, whose results are plotted in Figure 6.2b, it can be seen that scenario 4.2 and 4.3 have lower BER from SNR 0 dB to 3.5 dB than scenario 4.4, but above 3.5 dB, LDM based scenario has lower BER than TDM.

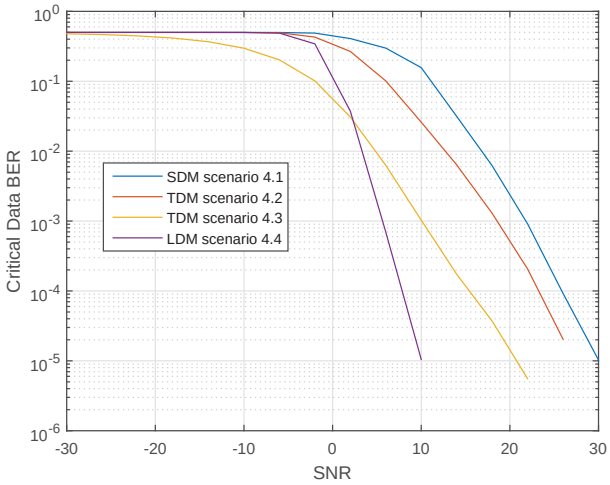

(a) Critical data BER, same data rate.

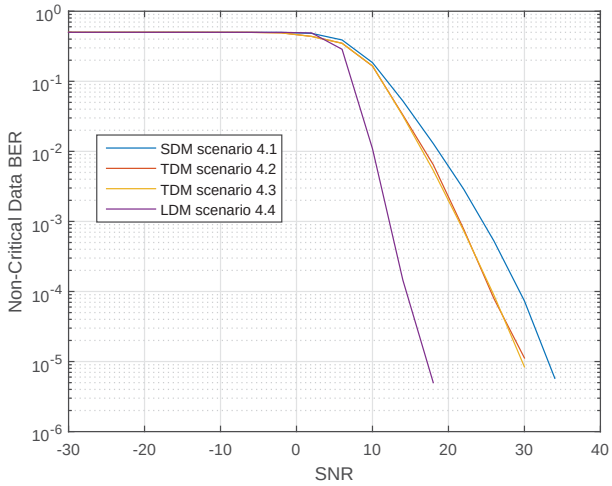

(b) Non-critical data BER, same data rate.

Figure 6.2: Simulation results of scenario 4.1, 4.2 and 4.3 vs scenario 4.4.

The conclusion is similar to previous section. Nevertheless, for the same 2x1 MISO configuration, using LDM and TDM, LDM has steeper slope than the SISO configuration. This allows to use antennas with lower gain to obtain lower BER than TDM maintaining the same bit rate in both cases. In non-critical data case, LDM has practically lower BER than TDM for nearly every SNR value.

6.6 MIMO scenarios with same critical data bitrate

LDM SISO and MISO scenarios were analyzed until now and compared with TDM SISO and MISO systems. In this section, MIMO systems using LDM and TDM will be analyzed and compared to evaluate their performance. MIMO scenarios are listed from scenario 5.1 to 5.10 in Table 6.1.

6.6.1 LDM vs TDM MIMO systems with critical data bitrate 0.5

Scenario	Mux	M_T	M_{R_c}	$M_{R_{nc}}$	T_c	T_{nc}	K_c	K_{nc}	$Max(Th_c)$	$Max(Th_{nc})$
5.1	TDM	2	2	2	0.5	0.5	0.5	0.5	0.5	0.5
5.2	TDM	2	2	2	0.5	0.5	1_{Alam}	0.5	0.5	0.5
5.3	LDM	2	2	2	1	1	0.5_{Alam}	0.5	0.5	1
5.4	LDM	2	2	2	1	1	0.5_{Alam}	0.5_{Alam}	0.5	0.5

Table 6.4: Tested scenarios 5.1, 5.2, 5.3 and 5.4.

The simulated systems are now MIMO systems. The simulated scenarios are summarized in Table 6.4, where the transmitter has 2 antennas and the receiver has also 2 antennas. The

simulation results of the scenarios are plotted in Figure 6.3.

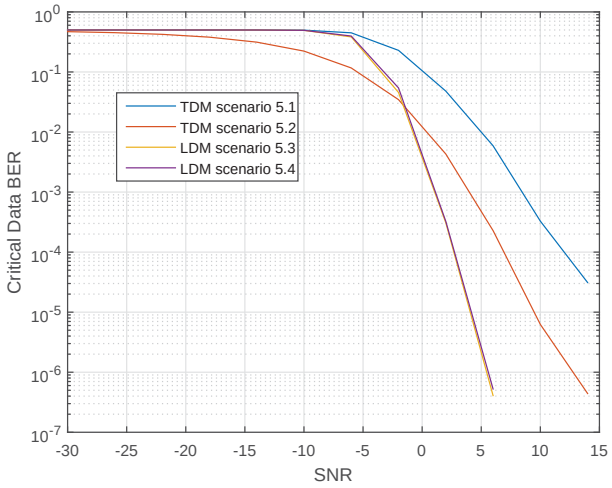

(a) Critical data BER scenario 5.1, 5.2, 5.3 and 5.4.

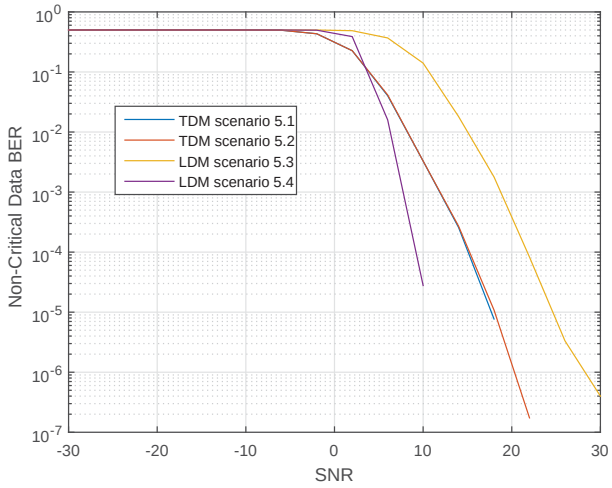

(b) Non-critical data BER of scenario 5.1, 5.2, 5.3 and 5.4.

Figure 6.3: Simulation results of scenario 5.1, 5.2, 5.3 and 5.4.

BER simulation results of critical data are in Figure 6.3a where a comparison between the simulated scenarios is shown. Scenarios 5.3 and 5.4, both of which use LDM with a code rate of 0.5 with Alamouti have lower BER than TDM scenario 5.1 for all SNR. But compared with scenario 5.2, which uses code rate 1 with Alamouti to maintain the same bit rate, LDM has lower BER when SNR is higher than -2 dB. Between -15 dB and -2 dB, TDM has lower BER than LDM, having a maximum difference from $1.5 \cdot 10^{-1}$ in TDM to $4 \cdot 10^{-3}$ in LDM when SNR is -6 dB.

In Figure 6.3b results for non-critical data are shown. The coding rate of scenario 5.3 is 0.5 without using Alamouti so the maximum throughput is 1. In this scenario BER is always higher than in scenarios 5.1 and 5.2 (TDM). But if the spatial diversity is exploited using Alamouti, as it does in scenario 5.3, the non-critical BER has a steeper slope. It can be seen that above a SNR of 4 dB, LDM system with Alamouti has lower BER than the other scenarios. Using Alamouti, the maximum throughput is reduced to 0.5 like the rest of the scenarios but BER is also reduced.

6.6.2 LDM vs TDM MIMO system with critical data bitrate 5/40

Scenario	Mux	M_T	M_{R_c}	$M_{R_{nc}}$	T_c	T_{nc}	K_c	K_{nc}	$Max(Th_c)$	$Max(Th_{nc})$
5.5	TDM	2	2	2	0.25	0.75	0.5_{Alam}	0.5	5/40	0.75
5.6	LDM	2	2	2	1	1	$5/40_{Alam}$	0.5	5/40	1

Table 6.5: Tested scenarios 5.5 and 5.6.

Scenario 5.5 is a TDM system that uses 2x2 MIMO and the critical data has 25% of the available time to send information, having a maximum throughput of 5/40. Scenario 5.6 is an LDM MIMO 2x2 system with same maximum throughput, but thanks to extra available time to send data, it uses a code rate of 5/40. Both scenarios use Alamouti to exploit space diversity.

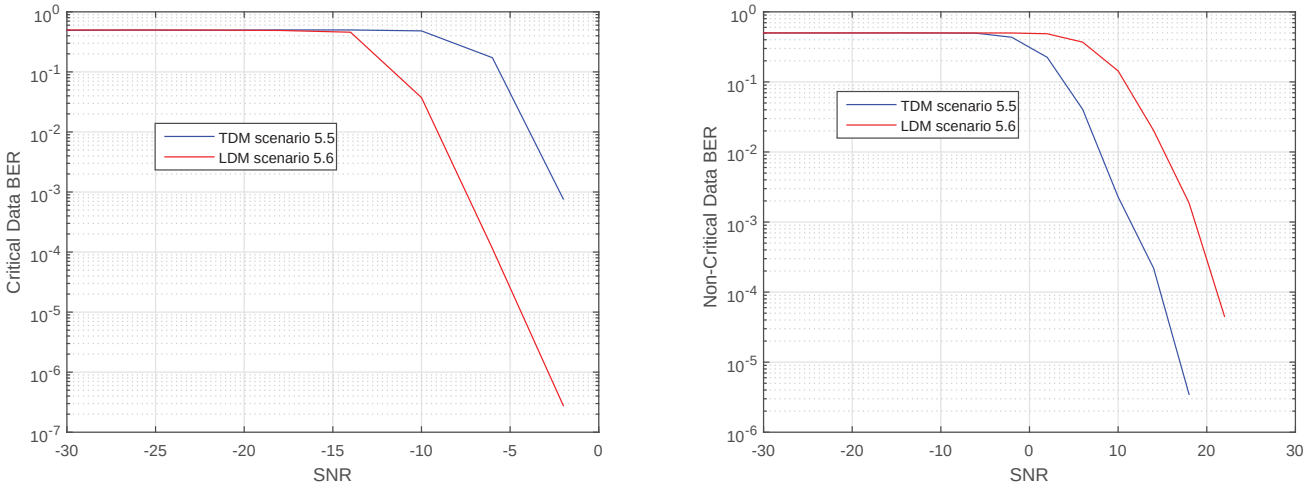

(a) Critical data BER scenario 5.5 and 5.6.

(b) Non-critical data BER of scenario 5.5 and 5.6.

Figure 6.4: Simulation results of scenario 5.5 and 5.6.

Results of simulations are shown in Figure 6.4 where in Figure 6.4a critical data simulations are compared. LDM has lower BER than TDM thanks to the lower code rate. In Figure 6.4b BER of non-critical data is shown, where it can be seen that TDM always has 6 dB gain over LDM. Using this configuration LDM has a maximum throughput of 1, 0.25 more than the TDM scenario.

6.6.3 LDM vs TDM MIMO system with critical data bitrate 3/40

Scenario	Mux	M_T	M_{R_c}	$M_{R_{nc}}$	T_c	T_{nc}	K_c	K_{nc}	$Max(Th_c)$	$Max(Th_{nc})$
5.7	TDM	2	2	2	0.15	0.85	0.5_{Alam}	0.5	3/40	0.85
5.8	LDM	2	2	2	1	1	$3/40_{Alam}$	0.5	3/40	1

Table 6.6: Tested scenarios 5.7 and 5.8.

Scenario 5.7 is a TDM system like scenario 5.5, i.e. it uses 2x2 MIMO, but the critical data has only 15% of the available time to send information. Critical data maximum throughput in this case is 3/40. Scenario 5.8 is an LDM MIMO 2x2 system with same critical maximum throughput and using a code rate of 3/40 and both scenarios use Alamouti to exploit space diversity. Figure 6.5a shows comparison of critical data simulations. Also in this case, LDM

has lower BER than TDM thanks to the lower code rate. In Figure 6.5b non-critical data BER is shown and the same behaviour as the previous section is observed, where TDM always has 6 dB gain over LDM. But in this case LDM has a maximum throughput of 1 now, only 0.15 more than TDM scenario. Hence, reduction of critical data BER carries a reduction of non-critical throughput while BER is maintained.

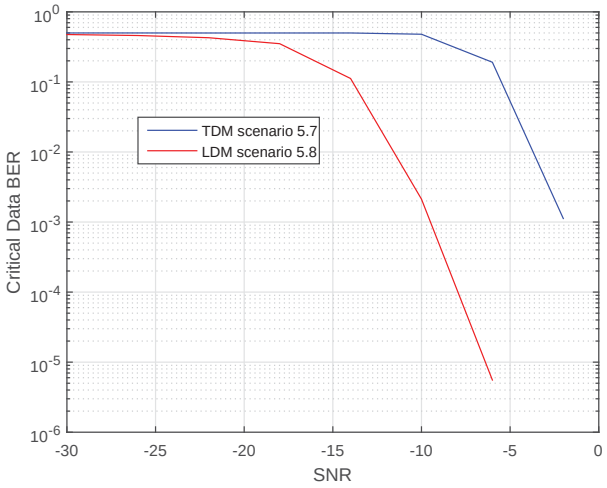

(a) Critical data BER scenario 5.7 and 5.8.

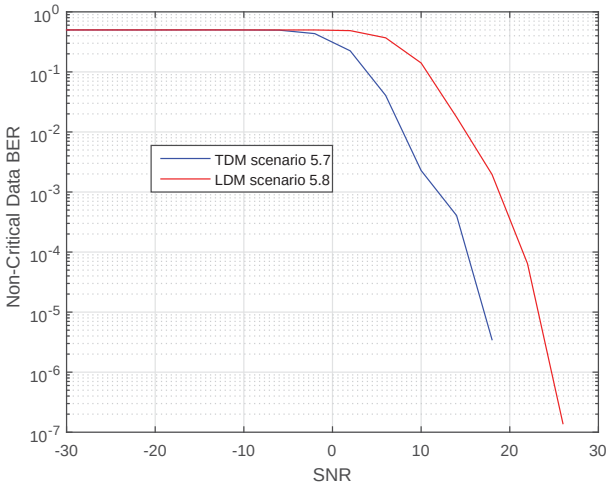

(b) Non-critical data BER of scenario 5.7 and 5.8.

Figure 6.5: Simulation results of scenario 5.7 and 5.8.

6.6.4 LDM vs TDM MIMO system with critical data bitrate 1/40

Scenario	Mux	M_T	M_{R_c}	$M_{R_{nc}}$	T_c	T_{nc}	K_c	K_{nc}	$Max(Th_c)$	$Max(Th_{nc})$
5.9	TDM	2	2	2	0.05	0.95	0.5_{Alam}	0.5	1/40	0.95
5.10	LDM	2	2	2	1	1	$1/40_{Alam}$	0.5	1/40	1

Table 6.7: Tested scenarios 5.9 and 5.10.

In this last comparison, where both scenarios are using 2x2 MIMO systems, critical data is using 5% of time to transmit data in TDM. This means that LDM can use a code rate of 1/40 to maintain the same throughput. In Figure 6.6a the comparison is shown, where it can be seen that such systems can obtain a BER as low as $2 \cdot 10^{-3}$ with a SNR of -15 dB, where TDM has a BER of $5 \cdot 10^{-1}$. In the non-critical data results of Figure 6.6b the same behaviour as the previous scenarios is observed where TDM has 6 dB gain over LDM, but maximum throughput of LDM is 0.05 higher than TDM.

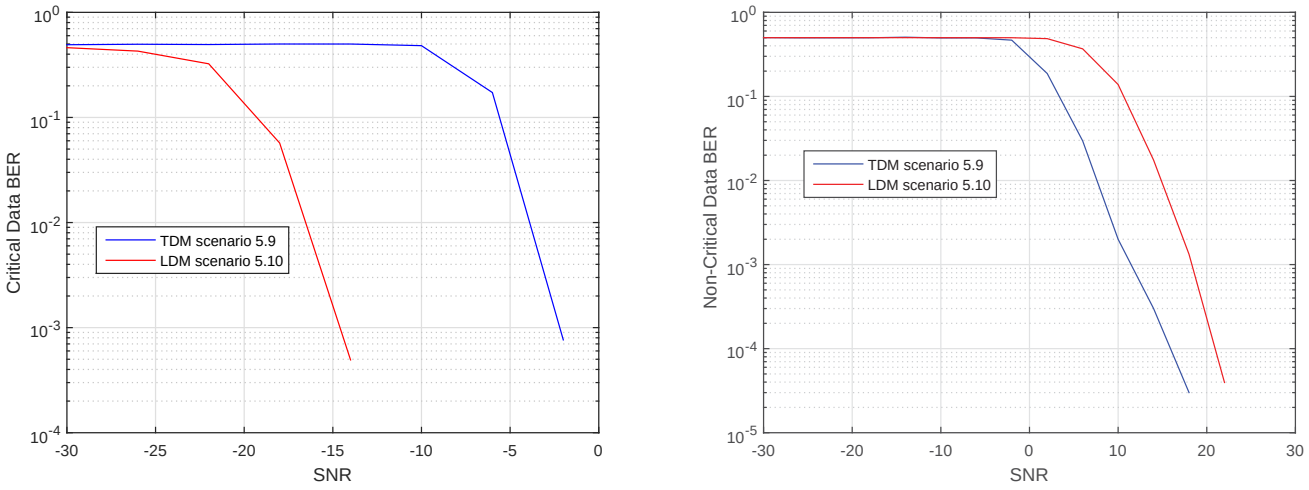

(a) Critical data BER scenario 5.9 and 5.10.

(b) Non-critical data BER of scenario 5.9 and 5.10.

Figure 6.6: Simulation results of scenario 5.9 and 5.10.

6.7 Summary of simulation results

6.7.1 MISO scenarios

In the case of MISO scenarios simulations it has been observed that LDM SISO scenario has lower BER in critical and non-critical data than simulated 2 TDM MISO scenarios but in one case, TDM MISO has lower BER than LDM if SNR is lower than 8 dB. Above 8 dB LDM has stepper slope, reaching $1 \cdot 10^{-6}$ BER with SNR 20 dB. In this case, if there is

opportunity to use antennas with gain, using 4 dB gain antenna, LDM will have lower BER than TDM above -3 dB SNR. With non-critical data, SISO LDM with the same code rate than MISO TDM has lower BER than TDM and extra antennas are not needed.

If an LDM MISO is compared versus a TDM MISO system with the same number of antennas and same maximum throughput, it can be concluded that an LDM MISO system has stepper slope than a TDM scenario but critical data BER is lower in LDM above a specific SNR. Below this SNR, one TDM scenario has lower BER than LDM. Depending of the requirements of the system TDM or LDM should be used or if there is opportunity to use directive antennas, use it to have lower BER in LDM critical receivers. Non-critical data BER is lower using LDM than TDM as described in section 6.5.

6.7.2 MIMO scenarios

As in the SISO case, TDM MIMO versus LDM MIMO with same maximum throughput are compared first, with a code rate of 0.5 in both critical and non-critical data using LDM and TDM. The conclusion is similar to SISO but the antenna gain needed by LDM to have lower BER than TDM is lower now. An LDM MIMO scenario has lower BER than a TDM MIMO scenario above SNR -2 dB. From -15 dB to -2 dB, only one TDM MIMO scenario has lower BER than LDM MIMO, but the BER difference is very low as described in section 6.6.1. Above SNR -2 dB, LDM MIMO has steeper slope reaching a BER of $3 \cdot 10^{-3}$ with SNR 0 dB. The non-critical data BER is lower than TDM above SNR 2 dB and has a steeper slope but below SNR 2 dB, TDM has lower BER for some scenarios.

Using the extra time of LDM to add redundancy to the critical data very low BER can be obtained. Following the same examples than SISO, $K_{UL}^{LDM} = 5/40$, $K_{UL}^{LDM} = 3/40$ and $K_{UL}^{LDM} = 1/40$ are used. Now, thanks to the use of multiple antennas and Alamouti coding, BER of the data is decreased. With $K_{UL}^{LDM} = 1/40$ and Alamouti, BER of 10^{-3} is obtained with only SNR -15 dB versus 0.5 that have the TDM system. In the non-critical data, TDM has always lower BER than LDM. With our simulation conditions, TDM is always 6 dB over LDM system. To avoid this difference 6 dB gain antennas could be used in non-critical receivers for example. Using directive antennas, non-critical receivers will have same BER than TDM but higher throughput than TDM.

6.8 Chapter summary

In this chapter, the LDM system proposed in Chapter 5 is extended with MIMO and MISO configurations. Several scenarios have been tested to know the performance of using LDM instead of TDM using multiantenna systems.

The main conclusion is that an LDM-SISO could have lower critical and non-critical

data BER than a TDM-MISO under some SNR conditions reducing antenna complexity. In the LDM-MISO case, having the same antenna number than TDM-MISO the critical and non-critical data could be lower than the previous case.

Comparing LDM-MIMO with TDM-MIMO with same bitrate, it could be observed that LDM-MIMO can outperform TDM-MIMO in terms of BER and throughput in both critical and non-critical data, when system SNR is above a threshold. Using UEP to protect critical data, it is observed that LDM-MIMO outperforms TDM-MIMO in critical data BER while non-critical data BER is penalized, but throughput increased. Depending of the system requirements and characteristics, the more suitable scenario must be chosen.

The results of this chapter have been submitted to "Vehicular Communications" journal of Elsevier editorial.

Chapter 7
Conclusion and Further Research

This chapter summarizes the work done, the main contributions and further research.

7.1 Summary

The aim of this PhD thesis has been to propose a reliable method to transmit data over a wireless channel, focusing on inside train wireless transmission. This type of channel is very interesting because new train communication systems are using a relying system to receive information using external antennas and transmit the information inside the train. Additionally, one of the goals of recent research works is to replace wired control systems by wireless systems, which allows to have more flexible and easy to deploy systems and lighten the weight of the train.

The first step to design a reliable wireless system is to know the target wireless channel. After carrying out a deep literature review, a new Winner model has been proposed in this thesis. To obtain the parameters of the Winner model, Ray Tracing techniques have been used. Based in the physical layout of the analyzed train scenario a ray tracing model has been generated and the more significant parameters have been extracted to obtain a mathematical model.

Train systems use a Train Control and Monitoring System (TCMS) where the transmitted information data can be classified as control data, which are considered critical, and monitoring data, whose priority is not so high and are considered non-critical. To ensure the reliability of the critical data over the non-critical one, Layered Division Multiplexing (LDM) with UEP is proposed transmission method. LDM is proposed to add reliability to critical data and increase or maintain the throughput of the non-critical data. The theoretical capacity gain has been analyzed and using a simple simulator with a gaussian channel, the possibility to reduce BER has been proved.

Finally, a more complete simulator has been developed that includes the proposed novel wireless channel, HiperLAN based channels, multiplexing techniques as LDM, TDM and FDM, and multiantenna systems as SISO, MISO and MIMO. Combining different techniques developed in the simulator, several different scenarios have been tested to obtain BER and

throughput and extract conclusions. It can be seen that LDM obtains lower BER than TDM and FDM in most of the considered setups. Depending of the scenarios and the available resources (number of antennas, antenna gain, computing power...) LDM can be a good alternative to TDM or FDM.

7.2 Thesis Contribution

The main contribution of this research work are the following:

- **Chapter 3:** A novel inside train wireless channel is proposed based in the Winner standard. Based on Ray Tracing simulations and the train layout, the main parameters to generate a Winner model are extracted and compared with measurement campaigns in the literature. The new model is compared with the measurements campaign done inside trains and checked that they match. This novel inside train wireless channel is presented in [Arruti13].

- **Chapter 4:** LDM combined with UEP is analyzed and proposed to be the multiplexing technique to be used over the wireless channel. LDM combined with UEP adds reliability of critical data while coexists with non-critical. To prove that BER can be reduced compared with TDM or FDM, first simulations are done using a simple gaussian channel with one antenna to send and receive. The simulation results confirm the hypothesis and they are published in [Arruti17a] as a possible candidate to be used in industrial environments too.

- **Chapter 5:** The proposed LDM system is tested in complete simulator with different channel models, including the proposed in Chapter 3. In this chapter, only SISO simulations are done obtaining system performance results. Several scenarios have been simulated to obtain BER and throughput results with the aim of analyzing when an LDM system should be used instead of TDM or FDM systems. Part of the simulation results are published in [Arruti17b].

- **Chapter 6:** In the last chapter, multiantenna configurations are tested using LDM system and compared with TDM/FDM systems. BER and throughput simulation results of multiantenna configurations have been submitted to "Vehicular Communications" journal of Elsevier editorial.

7.3 Suggestions for Further Research

The work described in this PhD dissertation can be improved and extended in many ways. Here are some suggestions for further research:

- The proposed model does not include the effect of travelers moving inside the train car. The literature proposes to model these travellers as circular cylinders [Ghaddar04] moving inside the train following a behaviour model. The model can be improved inserting spurious noise that affects the wireless channel randomly.

- The proposed model needs to be adjusted. A future work will be to create a laboratory scenario similar to a train carriage in order to replicate our scenarios in a controlled way. A more realistic approach is to perform intensive channel sounding tests in a real train to adjust the model parameters.

- LDM system is implemented only in the simulator. Another interesting future research is the implementation of LDM over laboratory Software Define Radio (SDR) systems to have a realistic system. With this realistic system, wireless transmission tests can be done to obtain BER results.

- The simulations assume that the receiver has perfect Channel State Information (CSI). But in the real world this assumption is not true and the receivers can work with partial CSI. A further research about the effect of this partial CSI over LDM systems may be interesting.

Appendix A
Publications

The following publications have been published or submitted for publication by the author of this thesis in refereed journal and conference proceedings.

Journal papers:

- E. Arruti, M. Mendicute, M. Barrenechea, "Performance analysis of inside train wireless system using LDM and Unequal Error Protection", submitted to *Vehicular Communications*, Elsevier editorial.

International conference papers:

- E. Arruti, M. Mendicute, M. Barrenechea, "Unequal error protection with LDM in inside carriage wireless communications", in *International Conference on Intelligent Transport Systems (ITS) Telecommunications. ITST 2017*, Warsaw, 29-31 May 2017.
- E. Arruti, M. Mendicute, M. Barrenechea, "QoS in industrial wireless networks using LDM", in *International Workshop of Electronics, Control, Measurement, Signals and their application to Mechatronics. ECMSM2017*, San Sebastian, 24-26 May, 2017.
- E. Arruti, M. Mendicute, J. Thompson, "A Novel WINNER Based Model for Wireless Communications Inside Train Carriages", in *7th European Modelling Symposium on Mathematical Modelling and Computer Simulation (EMS)*, Manchester. 20-22 November, 2013. Pp. 584-589.

The author also has contributed to these publications during the period of the thesis:

Journal papers:

- F. Casado, A. Arriola, E. Arruti, I. Ortego, J.I. Sancho, "Frequency estimation for compact microstrip antennas", in *Electronics Letters*, Vol. 51. Nº 7. Pp. 546-548. 02 April, 2015.

- F. Casado, A. Arriola, E. Arruti, I. Ortego, J.I. Sancho, "Pin diodes and their impact on reconfigurable compact microstrip antennas with high frequency ratio", in *Microwave and Optical Technology Letters*, Vol. 56. Nº 11. Pp. 2676-2681. November,. 2014.

- M. Barrenechea, M. Mendicute, E. Arruti, "Fully pipelined implementation of tree-search algorithms for vector precoding", in *International Journal of Reconfigurable Computing*,Vol. 2013, Article ID 496013, 12 p. 2013.

International conference papers:

- I. Jiménez, M. Barrenechea, M. Mendicute, E. Arruti, "Iterative joint MMSE design of relaying MIMO downlink schemes with nonlinearly precoded transmission", in *IEEE International Workshop on Signal Processing Advances in Wireless Communications (SPAWC).*, Cesme, Turkey. 17 - 20 June, 2012. Pp. 424-428.

- F. Casado, A. Arriola, E. Arruti, J. Parrón, I. Ortego, I. Sancho, "2.45 GHz Printed IFA on Metallic Environments: Clearance Distance and Retuning Considerations", in *6th European Conference on Antennas and Propagation (EuCAP)*, Prague. 26-30 March, 2012. Pp. 921-924.

- I. Jiménez, M. Barrenechea, M. Mendicute and E. Arruti, "Non-linear precoding approaches for non-regenerative multiuser MIMO relay systems", in *Proceedings of the 20th European Signal Processing Conference (EUSIPCO)*, Bucharest. 27-31 August, 2012. Pp. 1399-1403.

- F. Casado, A. Arriola, J. Parron, E. Arruti, I. Ortego, J.I. Sancho,, "Reconfigurable Matching Network for 2.45 GHz printed IFA on metallic environments", in *: Antennas and Propagation Conference (LAPC) 2012*, Loughborough. 12-13 November, 2012. Pp. 1-4.

- M. Barrenechea, M. Mendicute, I.Jimenez, E. Arruti, "Implementation of complex enumeration for multiuser MIMO vector precoding", in *Proceedings of the 19th EURASIP European Signal Processing Conference EUSIPCO*,Barcelona 29 August-2 September, 2011.

- M. Barrenechea, L. Barbero, I. Jiménez, E. Arruti, M. Mendicute, "High-throughput implementation of tree search algorithms for vector precoding", in *36th International Conference on Acustics, Speech and Signal Processing, ICASSP*, Praga, 22-27 May, 2011 Pp. 1689-1692.

National conference papers:

- S. Irastorza, G. Sasiain, A. Arriola, E. Arruti, and D. Valderas, "Antenas embebidas para redes de área corporal a 2.45 GHz", in *Jornadas Telecom I+D.*, Madrid. 24-26 November, 2009.

- M. Barrenechea, M. Mendicute, E. Arruti, "Vector precoding de complejidad fija para el canal MIMO Multiusuario", in *XXIV Simposium Nacional de la Unión Científica Internacional de Radio (URSI 2009)*, Santander. 16-18 September, 2009.

References

[3GPP03] 3GPP, "Spatial Channel Model for Multiple Input Multiple Output (MIMO) Simulations", 2003.

[3GPPBS12] 3GPPBS, "Base Station (BS) radio transmission and reception", 2012.

[3GPPUE12] 3GPPUE, "User Equipment (UE) radio transmission and reception", 2012.

[Ai12] B. Ai, R. He, Z. Zhong, K. Guan, B. Chen, P. Liu, and Y. Li, "Radio Wave Propagation Scene Partitioning for High-Speed Rails", 2012.

[Akki86] A. Akki and F. Haber, "A statistical model of mobile-to-mobile land communication channel", *Vehicular Technology, IEEE Transactions on*, vol. 35, no. 1, 2 – 7, feb 1986.

[Alamouti98] S. Alamouti, "A simple transmit diversity technique for wireless applications", *IEEE Journal on Selected Areas on Communications*, vol. 16, no. 8, 1451–1458, 1998.

[Arruti13] E. Arruti, M. Mendicute, and J. Thompson, "A Novel WINNER Based Model for Wireless Communications inside Train Carriages", in *2013 European Modelling Symposium*, pp. 584–589, Nov 2013.

[Arruti17a] E. Arruti, M. Mendicute, and M. Barrenechea, "QoS in industrial wireless networks using LDM", *International Workshop of Electronics, Control, Measurement, Signals and their application to Mechatronics. IEEE*, 2017.

[Arruti17b] E. Arruti, M. Mendicute, and M. Barrenechea, "Unequal error protection with LDM in inside carriage wireless communications", in *International Conference on Intelligent Transport Systems (ITS) Telecommunications*, May 2017.

[Barazzetta16] M. Barazzetta, D. Michel, R. Diamanti, L. Bastianelli, F. Moglie, and V. M. Primiani, "Optimization of 4G wireless access network features by using reverberation chambers: Application to high-speed train LTE users", in *2016 46th European Microwave Conference (EuMC)*, pp. 719–722, Oct 2016.

[Baum05] e. a. Baum, Hassan El-Sallabi, "Final Report on Link Level and System Level Channel Models", *D5.4 v. 1.4*, 2005.

[Bergmans74] P. Bergmans and T. Cover, "Cooperative broadcasting", *IEEE Transactions on Information Theory*, vol. 20, no. 3, 317–324, May 1974.

[Berisha16] T. Berisha, P. Svoboda, S. Ojak, and C. F. Mecklenbrauker, "Cellular network quality improvements for high speed train passengers by on-board amplify-and-forward relays", in *2016 International Symposium on Wireless Communication Systems (ISWCS)*, pp. 325–329, Sept 2016.

[Biglieri98] E. Biglieri, J. Proakis, and S. Shamai, "Fading channels: Information-theoretic and communications aspects", *IEEE Transactions on Information Theory*, vol. 44, no. 6, 2619–2692, Oct. 1998.

[Chiu10] S. Chiu and D. Michelson, "Effect of Human Presence on UWB Radiowave Propagation Within the Passenger Cabin of a Midsize Airliner", *Antennas and Propagation, IEEE Transactions on*, vol. 58, no. 3, 917 –926, march 2010.

[Chizhik00] D. Chizhik, F. Rashid-Farrokhi, J. Ling, and A. Lozano, "Effect of antenna separation on the capacity of BLAST in correlated channels", *Communications Letters, IEEE*, vol. 4, no. 11, 337 –339, nov. 2000.

[Chuah98] C.-N. Chuah, J. Kahn, and D. Tse, "Capacity of multi-antenna array systems in indoor wireless environment", in *Global Telecommunications Conference, 1998. GLOBECOM 1998. The Bridge to Global Integration. IEEE*, vol. 4, pp. 1894 –1899 vol.4, 1998.

[Cichon95] D. Cichon, T. Zwick, and W. Wiesbeck, "Radio link simulations in high-speed railway tunnels", in *Antennas and Propagation, 1995., Ninth International Conference on (Conf. Publ. No. 407)*, vol. 2, pp. 216 –219 vol.2, apr 1995.

[Cichon96] D. Cichon, T. Zwick, and W. Wiesbeck, "Ray optical modeling of wireless communications in high-speed railway tunnels", in *Vehicular*

Technology Conference, 1996. Mobile Technology for the Human Race., IEEE 46th, vol. 1, pp. 546 –550 vol.1, apr-1 may 1996.

[Dong10] W. Dong, G. Liu, L. Yu, H. Ding, and J. Zhang, "Channel Properties of indoor part for high-speed train based on wideband channel measurement", in *Communications and Networking in China (CHINACOM), 2010 5th International ICST Conference on*, pp. 1 –4, aug. 2010.

[El-Sallabi06] H. El-Sallabi, D. Baum, P. Zetterberg, P. Kyosti, T. Rautiainen, and C. Schneider, "Wideband Spatial Channel Model for MIMO Systems at 5 GHz in Indoor and Outdoor Environments", in *Vehicular Technology Conference, 2006. VTC 2006-Spring. IEEE 63rd*, vol. 6, pp. 2916 – 2921, may 2006.

[Emag17] Emag, "RT EM.CUBE Emag Technologies", *http://www.emagtech.com/content/emcube*, 2017.

[Erceg09] L. S. Erceg, "TGn Channel Models", *IEEE P802.11 Wireless LANs, Tech Rep. May 2004*, 2009.

[ETSI02] ETSI, "Broadband Radio Access Networks (BRAN); HIPERLAN Type 2; Physical (PHY) layer", *TS 101 475*, 2002.

[Fay16] L. Fay, L. Michael, D. Gómez-Barquero, N. Ammar, and M. W. Caldwell, "An Overview of the ATSC 3.0 Physical Layer Specification", *IEEE Transactions on Broadcasting*, vol. 62, no. 1, 159–171, March 2016.

[Foschini98] M. J. G. Foschini, "On limits of wireless communications in a fading environment when using multiple antennas", *Wireless Personal Communications*, vol. 6, 1998.

[Gadkari99] S. Gadkari and K. Rose, "Time-division versus superposition coded modulation schemes for unequal error protection", *IEEE Transactions on Communications*, vol. 47, no. 3, 370–379, Mar 1999.

[Gao10] L. Gao, Z. Zhong, B. Ai, and L. Xiong, "Estimation of the Ricean factor in K the high speed railway scenarios", in *Communications and Networking in China (CHINACOM), 2010 5th International ICST Conference on*, pp. 1 –5, aug. 2010.

[Garcia08] C. Garcia, A. Lehner, T. Strang, and K. Frank, "Channel Model for Train to Train Communication Using the 400 MHz Band", in *Vehicular*

Technology Conference, 2008. VTC Spring 2008. IEEE, pp. 3082 – 3086, may 2008.

[Ghaddar04] M. Ghaddar, L. Talbi, and T. A. Denidni, "Human body modelling for prediction of effect of people on indoor propagation channel", *Electronics Letters*, vol. 40, no. 25, 1592–1594, Dec 2004.

[Gómez-Barquero15] D. Gómez-Barquero and O. Simeone, "LDM Versus FDM/TDM for Unequal Error Protection in Terrestrial Broadcasting Systems: An Information-Theoretic View", *IEEE Transactions on Broadcasting*, vol. 61, no. 4, 571–579, Dec 2015.

[Haider02] K. Haider and H. S. Al-Raweshidy, "HiperLAN/2 performance effect under different channel environments and variable resource allocation", *London Communications Symposium*, 2002.

[He11] R. He, Z. Zhong, B. Ai, and J. Ding, "An Empirical Path Loss Model and Fading Analysis for High-Speed Railway Viaduct Scenarios", *Antennas and Wireless Propagation Letters, IEEE*, vol. 10, 808 –812, 2011.

[Hoppe07] R. Hoppe, J. Ramuh, H. Buddendick, O. Stabler, and G. Wolfle, "Comparison of MIMO Channel Characteristics Computed by 3D Ray Tracing and Statistical Models", in *Antennas and Propagation, 2007. EuCAP 2007. The Second European Conference on*, pp. 1 –5, nov. 2007.

[IEEE10] IEEE, "IEEE Standard for Information technology– Local and metropolitan area networks– Specific requirements– Part 11: Wireless LAN Medium Access Control (MAC) and Physical Layer (PHY) Specifications Amendment 6: Wireless Access in Vehicular Environments", *IEEE Std 802.11p-2010 (Amendment to IEEE Std 802.11-2007 as amended by IEEE Std 802.11k-2008, IEEE Std 802.11r-2008, IEEE Std 802.11y-2008, IEEE Std 802.11n-2009, and IEEE Std 802.11w-2009)*, pp. 1 –51, 15 2010.

[IEEE13] IEEE, "IEEE Std 802.11ac-2013 part 11: Wireless LAN medium access control (MAC) and physical layer (PHY) specifications", Jun. 2013.

[ITU-R07] ITU-R, *ITU-R Recommendation P.1238-5, "Propagation data and prediction methods for the planning of indoor radio communications systems and radio local area networks in the frequency range 900 MHz to 100 GHz"*, International Telecommuncation Union, 2007.

[Jankiraman04] M. Jankiraman, *Space-time codes and MIMO systems*, Artech House, 2004.

[Karedal07] J. Karedal, S. Wyne, P. Almers, F. Tufvesson, and A. F. Molisch, "A Measurement-Based Statistical Model for Industrial Ultra-Wideband Channels", *IEEE Transactions on Wireless Communications*, vol. 6, no. 8, 3028–3037, August 2007.

[Kermoal02] J. Kermoal, L. Schumacher, K. Pedersen, P. Mogensen, and F. Frederiksen, "A stochastic MIMO radio channel model with experimental validation", *Selected Areas in Communications, IEEE Journal on*, vol. 20, no. 6, 1211 – 1226, aug 2002.

[King14] C. King, "Fundamentals of wireless communications", in *2014 IEEE-IAS/PCA Cement Industry Technical Conference*, pp. 1–7, April 2014.

[Kita09] N. Kita, T. Ito, S. Yokoyama, M.-C. Tseng, Y. Sagawa, M. Ogasawara, and M. Nakatsugawa, "Experimental study of propagation characteristics for wireless communications in high-speed train cars", in *Antennas and Propagation, 2009. EuCAP 2009. 3rd European Conference on*, pp. 897 –901, march 2009.

[Li08] Y. H. Li, *Wireless Channel Model Analysis For GSM-R System*, Ph.D. thesis, 2008.

[Liu12] L. Liu, C. Tao, J. Qiu, H. Chen, L. Yu, W. Dong, and Y. Yuan, "Position-Based Modeling for Wireless Channel on High-Speed Railway under a Viaduct at 2.35 GHz", *Selected Areas in Communications, IEEE Journal on*, vol. 30, no. 4, 834 –845, may 2012.

[Maurer08] Maurer, "A Ray-Optical Channel Model for Mobile to Mobile Communications", *4th MCM COST 2100*, 2008.

[Medav08] Medav, "RUSK Measurement Campaigns Overview", 2008.

[Medbo98a] J. Medbo and P. Schramm, "Channel Models for HIPERLAN/2", *ETSI Tech Rep.*, 1998.

[Medbo98b] J. Medbo and P. Schramm, "Channel models for HIPERLAN/2 in different indoor scenarios, EP BRAN 3ERI085B, ETSI", 1998.

[Medbo99] J. Medbo and J.-E. Berg, "measured radiowave propagation characteristics at 5 GHz for typical hiperlan/2 scenarios", *ETSI Tech Rep.*, 1999.

[Molisch05] A. F. Molisch, *Wireless Communications*, IEE Press-Wiley, 2005.

[Ouyang08] W. J. C. Ouyang, "Wireless Propagation Analysis and Measurement in Enclosed Reflective Structures", 2008.

[Ozcelik04] H. Ozcelik, *Indoor MIMO Channel Models*, Master's thesis, Institut fur Nachrichtentechnik und Hochfrequenztechnik, University of Technology, Vienna, 2004.

[Parviainen08] R. Parviainen and Pekka, "Results of High Speed Train Channel Measurements", *European Cooperation in the Field of Scientific and Technical Research*, 2008.

[Paulraj03] A. Paulraj, R. Nabar, and D. Gore, *Introduction to Space-Time Wireless Communications*, Cambridge University Press, Cambridge, UK, 2003.

[Pekka07a] J. M. Pekka, "WINNER II Channel Models: Part I Channel Models", 2007.

[Pekka07b] K. Pekka, "WINNER II Channel Models part II Radio Cahannel Measurement and Analysis Results", 2007.

[Pellegrini06] F. D. Pellegrini, D. Miorandi, S. Vitturi, and A. Zanella, "On the use of wireless networks at low level of factory automation systems", *IEEE Transactions on Industrial Informatics*, vol. 2, no. 2, 129–143, May 2006.

[Prasad09] M. Prasad and P. Dalela, "Some experimental investigation of the effect of railway tunnels on mobile communications in Western India", *annals of telecommunications - annales des teleccommunications*, vol. 64, 247–257, 2009.

[Prasad10] M. Prasad, K. Ratnamla, and P. Dalela, "Mobile Communication Measurements Along Railroads and Model Evaluations Over Eastern-Indian Rural Regions", *Antennas and Propagation Magazine, IEEE*, vol. 52, no. 5, 131 –141, oct. 2010.

[Saleh87] A. Saleh and R. Valenzuela, "A Statistical Model for Indoor Multipath Propagation", *Selected Areas in Communications, IEEE Journal on*, vol. 5, no. 2, 128 –137, february 1987.

[SATURN] SATURN, "Smart Antenna Technology in Universal bRoadband wireless Networks", .

[Sayeed02] A. Sayeed, “Deconstructing multiantenna fading channels”, *Signal Processing, IEEE Transactions on*, vol. 50, no. 10, 2563 – 2579, oct 2002.

[Shannon48] C. Shannon, “A mathematical theory of communication”, *Bell Labs Technical Journal*, vol. 27, 379–423, 1948.

[Shiu00] D. Shiu, G. Foschini, M. Gans, and J. Kahn, “Fading correlation and its effect on the capacity of multielement antenna systems”, *Communications, IEEE Transactions on*, vol. 48, no. 3, 502 –513, mar 2000.

[Spencer00] Q. Spencer, B. Jeffs, M. Jensen, and A. Swindlehurst, “Modeling the statistical time and angle of arrival characteristics of an indoor multipath channel”, *Selected Areas in Communications, IEEE Journal on*, vol. 18, 347 –360, 2000.

[Steinbauer98] M. Steinbauer, “A comprehensive transmission and channel model for directional radio channel”, *COST 259 TD (98) 027*, 1998.

[Steinbauer00] D. H. Steinbauer and G. Sommerkorn, “Array measurement of the double-directional mobile radio channel,”, *Proceedings of the 51st IEEE Vehicular Technology Conference (VTC ’00)*, 2000.

[Steinbauer01] M. Steinbauer, A. F. Molisch, and E. Bonek, “The double-directional radio channel”, *IEEE Antennas and Propagation Magazine*, vol. 43, no. 4, 51–63, Aug 2001.

[Telatar99] I. E. Telatar, “Capacity of multi-antenna gaussian channels”, *European Transactions on Telecommunications*, vol. 10, no. 6, 585–595, Nov. 1999.

[Unterhuber16] P. Unterhuber and S. P. et al., “A Survey of Channel Measurements and Models for Current and Future Railway Communication Systems”, *Mobile Information Systems*, 2016.

[Wallace02] J. Wallace and M. Jensen, “Modeling the indoor MIMO wireless channel”, *Antennas and Propagation, IEEE Transactions on*, vol. 50, no. 5, 591 –599, may 2002.

[Wang09] C. Wang, X. Cheng, and D. Laurenson, “Vehicle-to-vehicle channel modeling and measurements: recent advances and future challenges”, *Communications Magazine, IEEE*, vol. 47, no. 11, 96 –103, november 2009.

[Wei10] H. Wei, Z. Zhong, K. Guan, and B. Ai, "Path loss models in viaduct and plain scenarios of the High-speed Railway", in *Communications and Networking in China (CHINACOM), 2010 5th International ICST Conference on*, pp. 1 –5, aug. 2010.

[Weichselberger03] W. Weichselberger, *Spatial Structure of Multiple Antenna radio Channels*, Master's thesis, Institut fur Nachrichtentechnik und Hochfrequenztechnik, Vienna, 2003.

[Yannick04] C. Yannick, P. Yannis, and V. Rodolphe, "A spatio-temporal radio channel characterization with a 3D ray tracing propagation model in urban environment", in *Personal, Indoor and Mobile Radio Communications, 2004. PIMRC 2004. 15th IEEE International Symposium on*, vol. 4, pp. 2341 – 2345 Vol.4, sept. 2004.

[Zhang14] W. Zhang, Y. Wu, N. Hur, T. Ikeda, and P. Xia, "FOBTV: Worldwide Efforts in Developing Next-Generation Broadcasting System", *IEEE Transactions on Broadcasting*, vol. 60, no. 2, 154–159, June 2014.

[Zhang16] L. Zhang, W. Li, Y. Wu, X. Wang, S. I. Park, H. M. Kim, J. Y. Lee, P. Angueira, and J. Montalban, "Layered-Division-Multiplexing: Theory and Practice", *IEEE Transactions on Broadcasting*, vol. 62, no. 1, 216–232, March 2016.

[Zwick02] T. Zwick, C. Fischer, and W. Wiesbeck, "A stochastic multipath channel model including path directions for indoor environments", *Selected Areas in Communications, IEEE Journal on*, vol. 20, no. 6, 1178 – 1192, aug 2002.